Molecular Characterisation of the *SNAKESKIN* mutation in *Arabidopsis*

By Cathlene M. Eland B.Sc. (hons)

Thesis submitted to the
University of Nottingham
for the degree of
Doctor of Philosophy,
November 2003.

1.0 ABSTRACT **3**

2.0 INTRODUCTION **4**

2.1 THE PLANT CUTICLE AND EPIDERMAL LAYER 4
2.1.1 The Plant cuticle *4*
2.1.2 Development and Differentiation of Epidermal Cells *5*
2.2 INTERACTIONS BETWEEN THE CYTOSKELETON, CELL SHAPE AND CELL WALL 7
2.3 THE PLANT CELL WALL 10
2.3.1 Structure of the Plant Cell Wall *10*
2.3.2 Cell Wall Expansion *11*
2.3.3 Cell–to-Cell Adhesion and Separation *13*

3.0 THE *SKS* MUTANT EXHIBITS DEFECTIVE EPIDERMAL DEVELOPMENT **15**

3.1 INTRODUCTION 15
3.1.1 The Plant Cuticle *15*
3.1.2 Pavement Epidermal Cells *16*
3.2 MATERIALS AND METHODS 21
3.2.1 Seed Stocks *21*
3.2.2 Plant Growth Conditions *21*
3.2.3 Crossing *21*
3.2.4 Confocal Microscopy *22*
3.2.5 Cryo-Scanning Electron Microscopy *23*
3.2.6 Temperature and Light Dependent Hypocotyl and Root Elongation *24*
3.2.7 β-Glucuronidase Assays *24*
3.3 RESULTS 27
3.3.1 General sks Mutant Morphology *27*
3.3.2 The sks Mutant Exhibits Defects in Cotyledon Epidermis *32*
3.3.3 The sks Mutation Disrupts Root Epidermal Development *38*
3.3.4 The sks Mutant Exhibits Defects in Newly Formed Leaf Primordium *42*
3.3.5 The sks Hypocotyl exhibits Post-Embyronic Cell Division Events *46*
3.3.6 Mutant Hypocotyl Tissues Exhibit a Finite Capacity for Elongation *48*
3.4 DISCUSSION 52
3.4.1 sks has Defects in Epidermal Integrity due to Possible Cell Wall Alterations *52*
3.4.2 The sks Mutation Results in Reduced Cell Expansion and Increased Division *53*
3.4.3 Conclusions *55*

4.0 THE *SKS* MUTANT EXHIBITS ALTERED CELL WALL COMPOSITION **56**

4.1 INTRODUCTION 56
4.1.1 Structure of the Primary Cell Wall *56*
4.1.2 Cell Wall Maturation and Secondary Cell Wall Formation *60*
4.1.5 Generation of Intracellular Spaces *62*
4.2 METHODS 63
4.2.1 Fourier Transform Infrared Spectroscopy *63*
4.2.2 TEM and Immunogold Labelling *63*
4.2.3 Cell Wall Neutral Sugar Analysis *64*

4.3 RESULTS 67
4.3.1 FT-IR Analysis of sks 67
4.3.2 Immunogold Labelling of sks and Wild Type Cell Walls 70
4.3.3 Neutral Sugar Analysis of sks 75
4.4 DISCUSSION 79
4.4.1 Conclusions 81

5.0 MAP-BASED CLONING OF THE *SKS* MUTATION 82

5.1 INTRODUCTION 82
5.1.1 Forward Genetics and Map Based Cloning 82
5.1.2 Reverse Genetics and Insertional Mutants of Arabidopsis 84
5.2 METHODS 86
5.2.1 Generation of a Mapping Population 86
5.2.2 DNA Extraction 86
5.2.3 DNA Extraction for 96-samples 87
5.2.4 Mapping using SSLP and INDEL Markers 88
5.2.5 Localisation of the sks Mutation using SNPs 89
5.2.6 Primers Used in Mapping and Cloning the sks Mutation 91
5.2.7 SALK Lines 96
5.3 RESULTS 97
5. 3.1 Sequencing of Quasimodo and Initiation of sks Mapping 97
5.3.2 Rough Mapping of sks and Sequencing of At1g77130 97
5.3.4 Further Mapping of the sks mutation using InDELs 103
5.3.5 Fine Mapping of the sks Mutation using SNPs 106
5.4 DISCUSSION 110
5.4.1 Conclusions 112

6.0 CONCLUSIONS AND FUTURE PROSPECTS 113

7.0 ACKNOWLEDGEMENTS 117

8.0 BIBLOGRAPHY 118

1.0 ABSTRACT

Screening of an *En* element population of *Arabidopsis thaliana* resulted in the identification of a mutant known as *snakeskin* (*sks*) in which the epidermal cell-cell linkages appear to be significantly perturbed (Marchant and Bennett, unpublished results). As a result of the breakdown of epidermal cell-to-cell linkages there are changes in epidermal cell architecture and distribution. These include alterations in pavement epidermal cell shape, stomatal distribution and trichome morphology.

The defect in epidermal cell-to-cell adhesion may be a consequence of reduced cell expansion resulting in increased cell division as a compensation mechanism. This results in altered stomatal index and density and reduced root and hypocotyl elongation. A change in the ability of a cell to expand may be attributed to defects in cell wall composition or to the cytoskeleton that determines where the cell wall components are localised during expansion. The *sks* mutant was found to have changes in its cellulose, xyloglucan and pectin fractions of the cell wall resulting in defects in cell wall adhesion, strength and expansion.

To gain a greater understanding of the *sks* mutation the molecular basis of the *SKS* gene map based cloning was undertaken employing a combination of SSLPs, InDels and SNP markers. The *SKS* gene was found to be located on the bottom arm of chromosome 1 on BAC clone T11I11. SALK insert lines have been utilised in a candidate gene approach in addition to fine mapping the mutation with SNP markers.

2.0 INTRODUCTION

2.1 The Plant Cuticle and Epidermal Layer

2.1.1 The Plant cuticle

The development of the cuticle represents the first major adaptation of plants to surviving in a terrestrial environment. Fossil records of plant remains from 460 million years ago reveal spores surrounded by a tough membrane, sheets of cuticle and small tubes composed of sporopollenin (Freeman, 2002). The aerial surfaces of modern land plants are almost entirely covered with a waxy cuticle that serves as a permeability barrier, limits water loss, provides a mechanical barrier and acts as a medium for plant signals perceived by insects and microbes as well as a reflective surface for attenuating radiation (Kerstiens, 1996). The cuticle and its constituents are synthesised by epidermal cells during the growth period of the shoot. Immature, unexpanded leaves are covered with a procuticle that is composed of nonlamellate waxes (Bird and Gray, 2003). As the leaf expands the cuticle thickens and pectin lamellae appear as more constituents are added. Lamellation of the procuticle occurs as cutin and polysaccharides like pectin are laid down in layers between the epidermal cell wall and cuticular membrane to form the cuticle proper (Heredia, 2003).

Above this cuticle proper, waxes are deposited and form the epicuticular wax layer. As more wax is deposited in the epicuticular wax layer, wax crystals are formed above a thin amorphous layer of waxes (Bird and Gray, 2003). Beneath the epicuticular wax layer and the cuticle proper, two thick cutin layers are deposited known as the internal and external cuticular layers (Bird and Gray, 2003). As the cuticle develops the primary cell wall becomes incorporated into the proper cuticle and a secondary cell wall may develop. This secondary cell wall is more fibrous than the primary cell wall and contains cellulose and lipophillic globules may be visible (Bird and Gray, 2003). The cuticle matures alongside the leaf with continued wax deposition and cuticle development. Once the leaf has finished expanding the cuticle is no longer added to, unless it is damaged by wounding (Bird and Gray, 2003).

In organs that undergo very rapid expansion, the cuticle may initially be very loose and wrinkled with very pronounced folds (Jeffree, 1996). As growth continues, the cuticle flattens out and the wrinkles disappear. Although the surface area of the wrinkled cuticle is not enough to allow maximum cell expansion, wrinkling may help to

prevent cuticle splitting during the most rapid period of cell expansion (Jeffree, 1996). This phenomenon of cuticle loosening is of fundamental importance to understanding the rate-limitation of plant growth by the outer epidermal cell wall, of which the cuticle is an integral part (Jeffree, 1996).

2.1.2 Development and Differentiation of Epidermal Cells

Epidermal cells of the shoot apical meristem can differentiate into trichomes, stomatal guard cells or epidermal pavement cells. Pavement epidermal cells make up most of the surface area of a mature epidermis. These cells are thin, flattened structures with lobes along their lateral margins that interlock with neighbouring cells (Frank and Smith, 2002). It is this distinctive shape that gives the leaf mechanical strength and allows cell expansion in all directions within the plane of the leaf (Glover, 2000). The convoluted jigsaw puzzle appearance of some epidermal cells has been associated with localised stretching due to the underlying tissues. However, it has also been suggested that the waviness represents an expansion reserve of wall substance that disappears as the leaf grows (Dale, 1988).

Epidermal cells commence expansion earlier than other cell types and it has been suggested that the epidermis may govern leaf expansion. The epidermal cells in early leaf primordia are square in outline and develop their irregular morphology as they increase in size (Pyke and Lopez-Juez, 1999). Work involving epidermal cells of the stem has found that although the inner tissues of the stem have a role in stem elongation, it is the epidermis that primarily contributes to auxin-induced elongation of stem tissue. Stem elongation and therefore steady growth, involves the co-ordinated actions of wall loosening in the epidermis and regeneration of tissue tensions by the inner tissues (Dale, 1988).

2.1.2.1 Stomatal Development

The pavement epidermal cells of the leaf are interspersed by many stomata and trichomes. Stomata allow controlled water loss and gas exchange between the photosynthesising tissue and the atmosphere that would otherwise be prevented by the impermeable waxy cuticle (Bird and Gray, 2003). The stoma consists of two guard cells that delimit a stomatal pore, the shape of the guard cells changes in response to turgor pressure and allows the stomatal pore to open and close (Serna and Fenoll, 2000a).

Changes in turgor pressure are brought about by bulk water and ion flow between guard cells and the neighbouring epidermal cells.

The series of cell divisions that differentiate the stomatal guard cells and their subsidiary cells occurs late in epidermal development as the pavement cells are undergoing cell expansion during leaf development (Wei *et al*, 1994). Stomatal production depends on the presence of division competent cells: epidermal pavement cells less than $400\mu M^2$ can either differentiate into large pavement epidermal cells, divide symmetrically to form two smaller pavement cells or can divide asymmetrically to initiate the development of stomatal complexes. These smaller epidermal cells become more restricted to existing stomatal complexes as leaf development progresses (Geisler *et al*, 2003).

The typical stomatal complex in *Arabidopsis* is the anisocytic complex that consists of a stoma surrounded by three unequally sized subsidiary cells (Berger and Altmann, 2000). However, this arrangement is only found in 40% of all stomatal complexes, the remaining complexes consist of complexes with between 2 to 6 neighbour cells (Geisler *et al*, 2000). In the formation of a primary anisocytic stomatal complex, three unequal cell divisions take place that are followed by an equal division (Serna and Fenoll, 2000a).

Stomata are not randomly distributed in normally developing leaves and they are rarely found directly adjacent to one another. Stomatal development begins with an unequal cell division of a protodermal cell that gives rise to the oldest neighbour cell and the first meristemoid. This meristemoid cell then divides unequally to give a new neighbour cell and a second meristemoid. The second meristemoid undergoes an unequal cell division to produce the youngest and final neighbour cell and a third meristemoid. The triangle shaped third meristemoid then acquires a rounded shape and assumes guard mother cell fate. This guard mother cell divides equally to give rise to the two guard cells that integrate the stoma and complete the formation of a primary complex (Serna and Fenoll, 2000a).

Some of the neighbour cells, usually those produced through the last unequal cell division can enter the stomatal pathway to form secondary anisocytic stomatal complexes. In this secondary pathway premature stomatal formation often occurs after the first or second unequal cell division. Some of the subsidiary cells from secondary stomatal complexes can go on to give tertiary stomatal complexes and premature stomatal formation (Serna and Fenoll, 2000a).

2.1.2.2 Trichome Development

As leaf development progresses, cell division patterns become less regular with islands of dividing cells known as protodermal cells among differentiated pavement epidermal cells. During trichome morphogenesis a protodermal cell ceases to divide and undergoes three rounds of endoreplication (Glover, 2000). After this the cell expands outwards from the leaf surface as a single cone and after another round of endoreplication (Glover, 2000) it begins to expand into a single cell that is composed of a stalk and two to four branches that reaches ~400μM in height (Szymanski *et al*, 2000). During trichome maturation the cell wall thickens to ~5μM and the trichome surface becomes covered with papillae (Marks, 1997).

As trichomes mature at the leaf tip, new trichomes emerge progressively towards the base. New trichomes also initiate in between developing trichomes that have been separated from one another by dividing epidermal cells (Marks, 1997). Trichome spacing has a distinct pattern but unlike stomata, the spacing of trichomes does not appear to rely on a cell lineage based pattern-generating mechanism. It is likely that interactions between developing epidermal cells determine which cells become committed to trichome development. These cells may then recruit a set of socket cells and inhibit neighbouring cells from adopting trichome fate (Glover, 2000).

2.2 Interactions Between the Cytoskeleton, Cell Shape and Cell Wall

The importance of the cytoskeleton in cell wall formation and cell shape cannot be forgotten. It has been suggested that the primary wall and the cytoskeleton are connected through membrane associated proteins although the nature of these proteins and the components they interact with have not been identified (Ridley *et al*, 2001). As plant cells are fixed spatially with respect to their neighbours; plant development relies on discrete and co-ordinate of changes in the cell wall to direct the final shape of each cell (Carpita *et al*, 2001). Plant cells can expand diffusely where wall extension and the incorporation of new wall material are distributed across the cell surface or by tip growth where wall extension and the incorporation of new wall material are focused at a single site on the cell surface (Smith, 2003).

Only pollen tubes and root hairs have been shown to rely on tip growth for their morphogenesis (Fu *et al*, 2002). Most cell types in plants are thought to expand by

diffuse growth that occurs preferentially along one axis due to the arrangement of the cellulose microfibrils. Cross-linked cellulose microfibrils restrict cell expansion and their alignment along one axis favours growth in the perpendicular axis (Smith, 2003). Cortical microtubules are closely associated with cellulose microfibrils and are generally aligned perpendicular to the major axis of cell expansion in diffusely growing cells (Smith, 2003). Cortical microtubules may also act to guide secretory vesicles containing other wall components to appropriate sites on the plasma membrane.

Actin microfilaments may also ensure the targeted delivery of vesicles that carry plasma membrane and cell wall components to the site of growth (Mathur et al, 2003a), however, this filamentous actin (F-actin) promotes cell expansion rather than controlling the pattern of expansion (Smith, 2003). Disrupted actin-filament growth in *wurm* and *distorted* mutants has been found to lead to altered epidermal cell morphology cell including unexpanded and unlobed pavement epidermal cells, distorted trichomes, and short, broad hypocotyl cells due to non-delivery of cell wall material to expanding cell ends (Mathur et al, 2003a).

The involvement of the cytoskeleton in the multidirectional cell expansion patterns that are involved in generating complex cell shapes has received increasing attention over the past few years (Smith, 2003). The morphogenesis of lobed epidermal pavement cells, like that of trichomes, involves multi-directional cell expansion that depends on both microtubules and F-actin. Shortly before the initiation of lobes, cortical microtubules become rearranged into U-shaped bands that are thought to direct localised cellulose deposition to form localised wall thickenings (Panteris *et al*, 1994). There is a strict alternate arrangement of microtubule bundles between neighbouring cells where every epidermal cells protrusion corresponds to a neighbours "constriction" (Panteris *et al*, 1993). The thinner regions of the wall between these thickenings are thought to extend more readily and as the cells expand under turgor pressure the formation of lobes occurs (Frank and Smith, 2002).

In both maize and *Arabidopsis*, local enrichments of cortical F-actin are found at the sites of lobe emergence, and these enrichments persist in the lobe tips as they elongate (Fu *et al*, 2002). The organisation of F-actin at lobe tips is similar to that seen in tip-growing cells except that the F-actin enrichment extends further into the apex of emerging lobes. The F-actin is thought to guide vesicle containing new cell wall materials to and/ or promotes vesicle fusion with the plasma membrane (Frank and Smith, 2002). Lobe formation therefore involves a tip growth-like process that occurs at

multiple sites along the cell margin in addition to a microtubule-dependent process that helps to localise growth to specific sites (Frank and Smith, 2002, Frank *et al*, 2003). Just prior to reaching the final cell shape and size the microtubule bands disintegrate and randomly orientated microtubules appear. These microtubules ensure that the thin walls of the bulges are reinforced and in fully differentiated cells the walls appear to be uniformly thick (Jung and Wernicke, 1990).

The importance of the role of the cytoskeleton in cell morphology is emphasised by various *Arabidopsis* and maize mutants, the *fra2* mutant lacks the microtubule severing katanin (AtKTN) and fails to form the lobes of epidermal cells (Burk *et al*, 2001). The *Arabidopsis spike1-1 (spk1-1)* mutant displays a phenotype very similar to the *sks* mutant with reduced epidermal cell expansion resulting in the loss of lobes from epidermal cells and gaps between adjacent epidermal cells (Qui *et al*, 2002). *SPK1* encodes a protein that may mediate the reorganisation of the cytoskeleton in response to extracellular signals (Qiu *et al*, 2002). In maize, the *brick* (*brk*) mutations results in the development of pavement epidermal cells that lack lobes (Frank *et al*, 2003). It was discovered that the *brk1* mutant failed to accumulate cortical F-actin at the sites of lobe emergence although cortical microtubule bands are normal (Frank and Smith, 2002).

The emergence of trichomes and trichome branches involves the organisation of microtubules into arrays with a net alignment transverse to the axis of elongation. During trichome branch elongation, actin filaments are arranged in longitudinal bundles with wall extension occurring along the length of the branch (Mathur and Chua, 2000). F-actin probably plays a similar role in elongating trichome branches to those that it plays in other diffusely growing cell types undergoing rapid elongation (Smith, 2003).

The *wurm* (*wrm)* and *distorted1* (*dis*) mutants encode actin related protein 2 (ARP2) and ARP3 respectively. The ARP2 and ARP3 proteins associate with five other subunits, the smallest of which ARPC5 has recently been identified (Mathur et al, 2003b), to form the ARP2/3 complex. This complex has a pivotal role in cellular morphogenesis through the role in the formation of a nucleation site for the growth of new actin filaments (Mathur *et al*, 2003a). It is thought that exocytotic vesicles carrying cell-building material are delivered to a cortical vesicle incorporation zone from the ends of fine actin filaments.

The *Arabidopsis* ZWICHEL (ZWI) gene is required for the normal elongation of trichome stalks and branches and encodes a kinesin. It is thought that ZWI functions to promote the formation of microtubule arrays that are critical for branch formation and

stalk elongation (Smith, 2003). The *ANGUSTIFOLIA* (*AN*) gene product promotes trichome branch formation and is also required for properly orientated growth of other cell types, indicating that *AN* could act directly at the level of microtubule organisation to promote normally polarised cell expansion (Kim *et al*, 2002 and Folkers *et al*, 2002).

2.3 The Plant Cell Wall

2.3.1 Structure of the Plant Cell Wall

Plant cells are surrounded by a cell wall that acts as an exoskeleton to give the plant cell its shape and allow high turgor pressures. The cell wall also participates in cell adhesion, cell-cell signalling, defence and many growth and differentiation processes (Cosgrove, 1997). Plant cell walls consist of complex carbohydrates, glycoproteins and phenolics. The main carbohydrate constituents of the cell wall are the polysaccharides homogalacturonan, rhamnogalacturonan I (RG-I), rhamnogalacturonan II (RG-II), gluconoarabinoxylan (GAX), xyloglucan (XG) and cellulose (Zablackis *et al*, 1995).

Cellulose is the main load bearing polysaccarhide and is composed of long, linear chains of β-1, 4-linked-D-glucopyranosyl residues and the orientation of the cellulose microfibrils determines the direction of cell expansion and therefore it is the major determinant of cell shape (Gardiner *et al*, 2003). Xyloglucan possesses a branched 4-linked β-D-glucan backbone with mono-, di- and tri-saccharide sidechains and is associated with cellulose by hydrogen bonding between glucose residues (Levy *et al*, 1997).

Homogalacturonan is a chain of unsubstituted 1,4-linked α-D-galactosyluronic acid residues that can be found in methyesterified and de-esterified forms. RG-I has a backbone of alternating galactosyl and rhamnosyl units and approximately half of the rhamnose units possess side-chains of arabinan and galactose with terminal fucose and glucosyluronic acids (Zablackis *et al*, 1995). RG-II has a backbone of nine α–D-1,4-linked galactosyluronic acid residues that possesses four different oligoglycosyl side chains containing xylose, fucose and apiose (Zablackis *et al*, 1995).

The general structure of the cell wall is thought to consist of a composite polymeric structure in which crystalline cellulose microfibrils are tethered together by long xyloglucan chains. Pectic polysaccharides and structural proteins are thought to be co-extensive but independent networks that physically entangle the cellulose-xyloglucan

network but are not covalently bonded to it (Cosgrove, 2001). Although this "sticky network" model is currently the most popular one, other models have been suggested.

A multicoat model has been proposed where each microfibril is coated by a series of progressively less-tightly bound polysaccharide layers and the linkage between microfibrils is made directly by the lateral non-covalent associations between these layers (Talbott and Ray, 1992). The "stratified wall" model proposed that pectic layers served as spacers between cellulose-hemicellulose lamellae. These pectic layers control wall thickness and allow easy slippage between the cellulose-hemicellulose layers that are thought to control wall extension (Ha *et al*, 1997).

Recently a new model has been proposed by Vinken *et al*, (2003) where the wall consists of a cellulose/xyloglucan framework, which is embedded in a matrix of interconnected modular pectins. This model assumes that pectin is deposited before the cellulose and that methylesterified HGA rich pectin are deposited in the cell plate of two daughter cells. Subsequent layers of pectin are deposited and HGA can be de-esterified by pectin methylesterases and associated with Ca^{2+} to strengthen the middle lamella (Vinken *et al*, 2003). Newly synthesised cell wall polymers such as pectin and XG are continuously being added on both sides of the Ca^{2+} gel that is pushed away from the cell membrane to form the middle lamella. Further layers of pectin are laid down and cellulose microfibrils are synthesised at the cell membrane and extruded into the extracellular matrix where they are crosslinked by XGs until the desired thickness of the primary cell wall has been reached (Vinken *et al*, 2003).

2.3.2 Cell Wall Expansion

The orientation and extent of an individual cell's expansion are key in determining its final size and shape yet cell expansion is poorly understood at the molecular level (Schindelman *et al*, 2001). Biophysical studies point to a central regulatory role for the cell wall in the expansion process, but it is not known what molecular machinery is involved in cell wall extension, nor how developmental and environmental signals modulate this process (Gendreau *et al*, 1997). Cell expansion patterns may be highly localised as in tip growing cells or more evenly distributed over the wall surface.

During cell wall expansion new material is deposited along the entire expanding wall. The interlacing molecules are cleaved enzymatically and internal osmotic pressure pushes the fibrillar components apart. New microfibrils and associated polymers are

laid down on the innermost surface of the wall; forming a highly stratified and cross-linked fabric (Carpita and Gibeaut, 1993). The cell wall accommodates this enormous expansion without losing mechanical integrity and generally without becoming thinner. This implies that there is an effective means of integrating new polymers into the wall without destabilising the load-bearing network (Cosgrove, 1997).

The walls of growing plant cells are characterised by high rates of synthesis and selective turnover of wall polysaccharides and by a form of stress relaxation that allows the wall to expand. Wall expansion is generally well co-ordinated with wall polymer synthesis and secretion; however wall thinning may occur in growing cells under unusual conditions. Growing cells are generally found to be more pliant than walls from non-growing cells (Cosgrove, 1997) and during rapid cell elongation their cell walls become more extensible as the new cellulose microfibrils are laid down in the same helical fashion, almost transverse to the axis of elongation (Carpita and Gibeaut, 1993).

The basis for wall expansion is probably a combination of biochemical loosening of the wall to permit turgor driven extensibility of the wall polymer network and the incorporation of new cell wall polysaccharides to reinforce the newly extended wall. Wall stress relaxation is the means by which plant cells reduce their turgor and water potential and so enables them to absorb water and to expand (McQueen-Mason, 1995). Without stress relaxation, wall synthesis would only thicken the wall and not expand it. Expansins have also been implicated in cell wall expansion as they are involved in the disruption of non-covalent bonds between cellulose and xyloglucan allowing incorporation of new cell wall materials and cell wall extension (McQueen-Mason, 1995).

The processes involved in determining the final shape of plant cells and the subsequent secondary cell wall formation must be well controlled as the processes that modify cell walls after growth has stopped are irreversible (Cano-Delgado *et al*, 2000). Little is known about how cell expansion is integrated with secondary cell wall formation. The composition of secondary cell walls varies widely among different species and different cell types and are divided into lignified (woody) or non-lignified types (Turner *et al*, 2001). Lignified cell walls are composed of a complex mixture of lignin, cellulose, and non-cellulosic glycans like xyloglucan together with a variety of proteins and other minor components (Turner *et al*, 2001). While a number of cell types possess a thick secondary cell wall that does not contain lignin, only a few mutants

including the *trichome birefringence* mutant (Potikha and Delmer, 1995), have been shown to affect non-lignified secondary cell walls.

2.3.3 Cell–to-Cell Adhesion and Separation

Cell-to-cell adhesion combined with the mechanical properties of cell walls provides the basis for the mechanical strength of plant tissues and organs. Cell adhesion occurs during the later stages of cell division where a highly localised region of the parent cell wall is controllably degraded, this results in the loss of the connection of the middle lamellas between the daughter cells and the parent cells to form a tricellular junction (Parker *et al*, 2001). Small intercellular spaces can appear among epidermal cells on internal periclinal walls between lobes, but do not extend significantly. These epidermal intercellular spaces interconnect with the epidermal spaces between epidermal and sub-epidermal layers (Panteris *et al*, 1993).

Cell separation also occurs during abscission and dehiscence and it has been found that the cells that comprise the abscission or dehiscence zones are pre-programmed in a different way from adjacent non-separating cells. Abscission zones form where leaves, flowers and fruits detach from the plant during senescence or ripening and pod dehiscence results in the release of seeds. It has been found that most epidermal cells exhibit no separation. However, not all epidermal cells fall into this category and during the differentiation of a stomatal complex, a specific cell-to-cell interface must be degraded to enable the formation of a pore surrounded by two guard cells (Roberts *et al*, 2000). Another site where cell separation has been observed to take place is the outer layer of the root cap where the peripheral cells are sloughed off and release mucilage to facilitate the passage of the root through soil (Hawes and Lin, 1990).

The shedding of plant organs takes place at predetermined positions that are known as abscission zones. Cells that make up the abscission zone can be distinguished prior to cell separation; they comprise a few layers of cells that are smaller than adjacent cells and more densely cytoplasmic. However, certain cells in the mature plant body retain the ability to be converted into cells with the capability to differentiate into abscission cells. These secondary or adventitious zones are defined as functional abscission zones formed where one would not normally develop (Roberts *et al*, 2000).

Cross talk between auxin and ethylene plays an important role in dictating the site of cell separation where ethylene induces the formation of the zone, and auxin dictates

where it will be sited (McManus *et al*, 1998). There are two main classes of genes that are expressed during the cell separation process, the first class is involved in the mechanism of cell-to-cell separation while the second class comprise genes that are concerned with cellular protection. The primary site of cell wall breakdown within abscission zones is the middle lamella. It seems likely that cell separation involves many different enzymes including β-1,4-glucanase (cellulase), polygalacturonase and expansins that bring about the co-ordinated breakdown of the middle lamella and perhaps some of the cellulose microfibrils down (Roberts *et al*, 2000) and pathogenesis related proteins that are upreguated to preempt infection by micro-organisms (Roberts *et al*, 2002).

Pod dehiscence results in the premature shedding of seeds from siliques prior to and during harvest. *Arabidopsis* fruit consists of a bivalve silique where the fruit wall encloses two valves separated by a psuedoseptum and a replar region (Picart and Morgan, 1984). As silique maturation occurs the walls of the valve edge cells and the replum of the dehiscence zone become lignified and the cells of the dehiscence zone itself undergo cell wall degradation (Roberts *et al*, 2002). As the pod becomes desiccated during seed maturation, tensions in the fruit wall are created and the weakened dehiscence zone cells give way. This results in the pod shattering and releasing the seeds. As with abscission β-1,4-glucanases, polygalacturonase, proline rich proteins and dehydrogenases have been found to be up-regulated in dehiscence zones (Roberts *et al*, 2002).

3.0 The *sks* Mutant Exhibits Defective Epidermal Development

3.1 INTRODUCTION

Understanding the genetic factors that influence the cell wall properties of plants is of major importance for agriculture and food processing. Crop plants could be designed where the processing efficiency is improved as a result of the manipulation of the cell-cell separation properties of harvestable organs. Earlier screens of a transposon mutagenised population of *Arabidopsis thaliana* resulted in the identification of a mutant known as *snakeskin* (*sks*) (Marchant and Bennett, unpublished results). This chapter describes the characterisation of the *sks* mutant phenotype which has revealed significant perturbations in the epidermal cell-to-cell linkages in both the root and shoot tissues.

3.1.1 The Plant Cuticle

The aerial surfaces of plants are almost entirely covered with a waxy cuticle that has a layered structure and is fused to the epidermal cell wall. From the epidermal cell wall, there are the internal and external cuticular layers (Bird and Gray, 2003) and the cuticle proper (Heredia, 2003). Above this cuticle proper, waxes are deposited and form the epicuticular wax layer where wax crystals develop (Bird and Gray, 2003). Cutin and cutan are the two main structural polymers of the cuticular layers and may occur in any ratio depending on the stage of cuticle development (Jeffree, 1996). Cutin is a polar, cross-linked polymer that consists of oxygenated C_{16} and C_{18} fatty acids cross-linked with ester bonds and are encrusted with epicuticular waxes (Heredia, 2003). The structure of cutan has not yet been confirmed but it is thought to consist of cutin monomers, n-alkanes, alkenes and α,ω-alkidienes (Jeffree, 1996), held together with nonester bonds (Heredia, 2003).

Polysaccharide microfibrils including pectin, cellulose and hemicelluloses including xylan and xyloglucan are also embedded in the cuticular layer (Jeffree, 1996). This polysaccharide-rich polymer matrix may absorb mechanical strain caused by flexure and serve as a buffer zone between the cell wall and the outer region of the cuticle (Grace and van Gardingen, 1996).

Cuticular wax is a general term to describe complex mixtures of homologous series of long-chain aliphatics like alkanes, alcohols, aldehydes, fatty acids and esters with the addition of varying proportions of cyclic compounds like triterpenoids and hydrocinnamic acid derivatives that are embedded within the cuticle and in the crystalline epicuticular wax layer (Heredia, 2003). Trace amounts of polysaccharides and amino acids may also be present in the plant cuticle (Heredia, 2003).

Long chain hydrocarbons are produced from $C_{16:1}$ and $C_{18:1}$ fatty acid precursors produced in the plastids. These fatty acids are elongated extraplastidially by malonyl-CoA to produce very long chain fatty acids (VLCFAs) (Bird and Gray, 2003). VLCFAs are modified by reduction to aldehydes, then by decarbonylation to give alkanes, two oxidation reactions produce secondary alcohols and ketones, acyl reduction produces aldehydes and reduction gives primary alcohols (Bird and Gray, 2003).

Signals from the cuticle may affect stomatal development and epidermal cell fate (Bird and Gray, 2003). The *abnormal leaf shape 1-1* (*ale1-1*) mutation encodes a subtilisin-like serine protease and results in the incomplete formation of a cuticle leading to deformed epidermal pavement cells, reduced trichome number and leaf fusion (Tanaka *et al*, 2001). The *Arabidopsis fiddlehead* (*fdh*) mutant has a very similar phenotype to *ale1-1* with the epidermal cells of the shoot and inflorescence adhering to one another. The *fdh* gene encodes a β-ketoacyl-CoA synthase or fatty acid elongase involved in lipid metabolism (Yephremov *et al*, 1999), and may also be involved in cuticle formation.

3.1.2 Pavement Epidermal Cells

The development of epidermal pavement cells is predictable and depends on the position of a cell along the longitudinal axis of the leaf. Stage I cells are localised at the base of the leaf and have just commenced expansion (Fu *et al*, 2002). These stage I cells are mostly square, rectangular or pentagonal; a few cells in this region have expanded and are bordered by several smaller cells. These larger cells are the transition between stage I and stage II cells.

Stage II cells are found around the midpoint of the leaf, have a slightly wavy appearance as lobe expansion has been initiated and have established their long axis of expansion (Fu *et al*, 2002). After stage II, cell expansion occurs primarily in the lobes

and leads to the formation of stage III cells. Stage III cells are localised at the tip of the leaf and contain multiple extended lobes and very wavy cell outlines (Fu *et al*, 2002).

A variety of mutants with epidermal defects have been identified in *Arabidopsis*, the *korrigan* (*kor*) mutant shows a cell elongation defect in all cell types that results in highly irregular cell shapes (His *et al*, 2001). The *keule* mutant is cytokinesis defective and has multinucleate cells that are enlarged, bloated and have a rough surface (Assad *et al*, 2001) similar to the epidermal cells of *quasimodo1* (Bouton *et al*, 2002). The maize mutant *crinkly4* (*cr4*) affects the differentiation of epidermis and results in enlarged, irregularly shaped epidermal cells (Jin *et al*, 2000).

3.1.2.1 Stomatal Patterning

It has been deduced that 99.4% of the stomata present on the leaves of *Arabidopsis* plants are surrounded by a stomata free region of at least one pavement cell (Geisler *et al*, 1998). This characteristic spacing of stoma may occur to prevent the diffusion shells of each stoma overlapping and so allow maximum gas exchange with the fewest stomata (Bird and Gray, 2003). Having at least one pavement epidermal cell between stomata also allows water and ion flow to the stomatal guard cells and so regulates the stomatal movements (Serna and Fenoll, 2000a).

The formation of a stomata free region around each stoma depends on the cell lineage associated with stomatal development, and the strict placement of secondary and tertiary meristemoids away from the previously formed stomata (Serna and Fenoll, 2000a). In addition, some protodermal cells do not enter the stomatal pathway but differentiate as pavement cells (Berger and Altmann, 2000). Neighbour cells are thought to receive positional cues by cell-cell signalling that are used to determine the plane of division (Geisler *et al*, 2003). These mechanisms may all contribute to the prevention of the formation of stomatal clusters.

It has also been noted that stomata and meristemoids are found over the junctions of palisade mesophyll cells and do not develop above the main vein (Serna and Fenoll, 2000b). The epidermis and mesophyll are derived form different cell layers of the meristem (L1 and L2) respectively and cellular interactions are necessary to establish specific cell patterns between these two layers (Serna *et al*, 2002). The meristemoid may signal the inner cells immediately below to divide and grow so that an airspace is produced, or the junction with the mesophyll cells may determine the position of the

meristemoid by governing the meristemoid mother cell division plane (Serna *et al*, 2002).

Very occasionally abnormal stomatal complexes can form in wild type plants and several mutants with abnormal stomatal patterning have been identified. In the *too many mouths (tmm), four lips* (*flp*) (Yang and Sack, 1995; Geisler *et al*, 1998) and *sdd1-1* (Berger and Altmann, 2000) mutants, the stomatal patterning and distribution is drastically affected to produce clusters of functional stomata. However, at this time no mutants with overall reduced numbers of stomata have yet been described (Glover, 2000).

The *SDD1* gene encodes a subtilisin-like serine protease involved in signal transduction and as a result the *sdd1-1* mutant shows an increase in the number of protodermal cells that enter the stomatal pathway to produce primary complexes. It has also been noted that in *sdd1-1* some of the unequal cell divisions occur so that the meristemoid is positioned adjacent to the pre-existing stomata and this results in the formation of stomatal clusters (Berger and Altmann, 2000).

The *tmm* and *flp* stomatal mutants both show alterations in stomatal patterning; the *flp* phenotype is characterised by the presence of two adjacent stomata. Another distinctive trait is the presence of a small percentage of unpaired guard cells, either single and isolated, or part of a small cluster. The *flp* mutation appears to affect the production of guard mother cells rather than meristemoid patterning or stomatal differentiation. (Geisler *et al*, 1998)

The *tmm* mutant has been found to encode leucine-rich repeat-containing receptor-like protein that may have a function in a position-dependent pathway that controls the patterning divisions of stomata (Nadeau and Sack, 2002). Many of the stomata of the *tmm* mutant of are in direct contact with one another and are arranged in clusters (Geisler *et al*, 1998). This abnormal stomatal patterning is a result of many of the satellite meristemoids forming in contact with pre-existing stomata or precursor cells. Stomatal clusters also result when adjacent meristemoids fail to divide away from each other or fail to develop into pavement cells (Geisler *et al*, 2000).

In many plant species the stomatal density is under genetic control but it is also modulated in response to many environmental factors that include humidity, temperature, CO_2 and light intensity. It has been reported that plants grown in reduced CO_2 levels have higher numbers of stomata than those grown in todays CO_2 concentrations (Brownlee, 2001).

As a result of research on the high carbon dioxide (*hic1*) (Gray *et al*, 2000) stomatal mutant in *Arabidopsis* it appears that the composition of the cuticle is fundamental to the movement of signals in the apoplast of the leaf epidermis. The *HIC* gene encodes a putative 3-ketoacyl coenzyme A synthase that is involved in wax biosynthesis. It has been found that plants with alterations in wax biosynthesis like *cer1* and *cer6* are also associated with aberrant stomatal densities (Gray *et al*, 2000), implying that the cell wall and cuticle plays a pivotal role as a channel for fate determining signals (Brownlee, 2001).

As a result of the discovery of the stomatal patterning mutants *hic*, *tmm*, *flp* and *sdd1-1* a combination of position dependent cell signalling and lineage based division mechanisms (Bird and Gray, 2003) are thought to regulate the orientation of asymmetric divisions and the fate of epidermal cells. Stomata are affected by, and have an effect on, their surrounding tissue but the exact signalling mechanisms are unknown (Geisler *et al*, 2000). Stomatal guard cells are known to lose their plasmodesmatal connections during early differentiation. However, guard cells are likely to signal to their neighboring epidermal cells via the cell wall through wall associated kinases (Bird and Gray, 2003).

3.1.2.2 Trichome Development

Trichomes are defined as hair-like structures that extend from the epidermis of aerial tissues and are present on the surface of most terrestrial plants. Plant trichomes comprise a diverse set of structures and many plants contain several types on a single leaf (Szymanski *et al*, 2000). The trichomes of *Arabidopsis* are 200-300μM in length, unicellular and consist of a stalk with two to four branches (Larkin *et al*, 1997) and have an elaborate cuticle (Glover, 2000).

Many genes have been isolated from *Arabidopsis* that have been found to have roles in trichome initiation, development and maturation. The pathway of trichome initiation and development has not been completely elucidated yet and there is new evidence emerging that is revealing the complex interactions that occur between genes involved in trichome initiation and spacing. Several mutants have been identified that are involved in trichome initiation and spacing including *REDUCED TRICHOME NUMBER (RTN)*, *TRASNPARENT TESTA GLABRA1 (TTG1)* and *(GLABROUS1) GL1* (Larkin *et al*, 1996).

Several mutations reduce trichome branching; leaf trichomes on the *stichel (sti)* mutant are long unbranched structures (Ilgenfritz *et al*, 2003). The trichomes on *stachel (sta)* mutants are defective in primary branching but not secondary branching and these trichomes have two branches on a long stalk. The trichomes of both the *zwichel (zwi)* and *angustifolia (an)* mutants are defective in secondary branching and so have two branches that develop from the trichome base (Marks, 1997).

Mutations that alter the final stages of trichome development include the *under developed trichome (udt)* mutation results in trichomes that are more slender than wild type and produce underdeveloped papillae towards the tips of their branches (Marks, 1997). Three other mutations, *chablis (cha), chardonnay (cdo)* and *retsina (rts)* result in trichomes that lack the rough papillate surface of wild type mature trichomes (Hulskamp *et al*, 1994).

The trichomes of *trichome birefringence (tbr)* mutant totally lack papillae and the ring of subsidiary cells at the base of the trichome appear deformed and the trichome base is swollen. The trichomes of *tbr* are thought to be completely impaired in their ability to synthesize secondary cell wall cellulose. The trichomes of *tbr* show extremely reduced birefringence. Birefringence is observed in most secondary cell walls of plant cells due to the presence of ordered cellulose microfibrils. In wild type plants, both the trichomes and papillae have been found to be birefringent (Potikha and Delmer, 1995).

3.2 MATERIALS AND METHODS

3.2.1 Seed Stocks

The mutant *snakeskin (sks)* was in the Columbia background and so the seed used in the majority of experiments was Columbia (wild type), Landsberg *erecta* and *sks*. All seed was donated by members of the Bennett laboratory, Plant Sciences, University of Nottingham, Sutton Bonington Campus, Leicestershire, LE12 5RD.

3.2.2 Plant Growth Conditions

Seeds were surface sterilised in 50% (v/v) sodium hypochloride for 6 minutes, and rinsed twice in 0.1% (v/v) triton-x solution, before being dried on Wattman filter paper after rinsing with 70% (v/v) ethanol. The seeds were sown on MS media and the petri dishes sealed with micropore tape. The growth medium consists of 1% (w/v) bacto-agar (Difco) and 1% (w/v) sucrose in 1x Murashige and Skoog medium, adjusted to pH 5.8 with 1M potassium hydroxide. The plates were then stratified at 4°C in the dark for 48 hours before being germinated vertically under constant light conditions of 50mol.m^2.sec^{-1} at 22°C.

Plants required for crossing or bulking up of seed were grown on MS plates for 14 days before being transferred to soil in the greenhouse. Seedlings were grown up in a 3:1 mix of compost (Levingtons, M3) and Vermiperil (Silvaperl, medium grade). Plants were covered using the Arasytem (Betatech) or plastic disposable sleeves (Zwapak, Holland) to prevent cross-pollination. The plants were grown at 24°C under constant light of 50mol.m^2.sec^{-1} in a glasshouse.

3.2.3 Crossing

Both the parent plants were grown up on soil for approximately a month or until both plants had well developed inflorescences. An inflorescence of the mother parent plant was chosen and the apical meristem was pinched out and all open flowers and siliques were removed with a pair of fine watchmakers forceps. Using a binocular dissecting microscope the sepals, petals and anthers were then removed from the unopened flowers of the mother plant.

An open flower was then removed from the father parent plant and used to pollinate the stigma of the prepared flowers of the mother plant. If crossing was successful then the carpel of the pollinated unopened flowers began to elongate and develop into a silique containing F1 seeds within 24 hours. When the F1 siliques have matured and dried, the seeds from each cross are collected separately, plated out and grown up to obtain F2 seed.

3.2.4 Confocal Microscopy

3.2.4.1 Imaging of Mature WT and *sks* Embyros

Mature seed of WT and *sks* was soaked for at least two hours in sterile distilled water to soften the seed coats. Embryos were then dissected out under a Zeiss Stemi SV6 binocular microscope with the aid of two size 5 syringe needles on moistened filter paper. The protocol as described by Bougourd *et al*, 2000 for aniline blue staining and clearing with chloral hydrate of *Arabidopsis* embryos was followed exactly. The only deviation from the protocol was the addition of two layers of insulation tape (Wilkinson Hardware, UK) to each end of the microscope slide before the cover slip was added to prevent the embryos being crushed. The slides were then left for at least one week before viewing as it was found that staining improved through time.

Optical sections were obtained with the help of Ranjan Swarup (Plant Sciences, University of Nottingham, Sutton Bonington Campus, Leicestershire, LE12 5RD) using a Leica TCS SP2 true confocal scanner (Leica Microsystems (UK) Ltd) and the 543-excitation line of 25mW argon ion laser. Images were taken through a 64x oil immersion lens with line averaging of 8 and Kalman averaging of 4. Images were processed using Leica Confocal Software (Leica Microsystems (UK) Ltd) and Adobe Photoshop (version 6).

3.4.2.2 Imaging of WT and *sks* Root Tissues

3, 5 and 7 day old WT and *sks* seedlings were stained in a 1:1000 dilution of *N*-(3-triethylammoniumpropyl)-4- (6-(4-(diethylamino)phenyl)hexatrienyl) pyridinium dibromide (FM® 4-64) in SDW for 15 minutes (Molecular Probes
Molecular Probes Europe BV, Netherlands). FM 4-64 is a lipophillic dye of vacuolar membranes displays that has an absorbance/emission spectra at 515/640 nm. The

seedlings were then rinsed in SDW before mounting on slides in SDW and covered with a coverslip.

Optical sections were obtained with the help of Ranjan Swarup (Plant Sciences, University of Nottingham, Sutton Bonington Campus, Leicestershire, LE12 5RD) using a Leica TCS SP2 true confocal scanner (Leica Microsystems (UK) Ltd) and the 543nm excitation line of 1.25mW He Ne laser. Series of images were taken through a 20x or 40x lens with line averaging of 4 and Kalman averaging of 8. Images were processed using Leica Confocal Software (Leica Microsystems (UK) Ltd) and Adobe Photoshop version 6 (Adobe Systems Inc., US)

3.2.5 Cryo-Scanning Electron Microscopy

Cryo-scanning electron microscopy (cryo-SEM) was undertaken on 3, 5, 7 and 9-day old *sks* and wild type Columbia plants. SEM work was undertaken with Tim Smith (Department of Life and Environmental Sciences, University of Nottingham, University Park, NG7 2RD) using a Jeol JSM -840 Scanning Electron Microscope incorporating a Polaron Cryotrans E7400. Tissue was frozen in slushed liquid nitrogen, sublimed at 85°C, sputter coated with gold and then examined at approximately –180°C at 10kV.

SEM work was also undertaken with Kim Findlay (Department of Cell Biology, John Innes Institute, Colney Lane, Norwich, NR4 7UH) using a Philips XL30 FEG scanning electron microscope fitted with an Oxford Turbotronik NTO and an Oxford CT100 Cryostation. Tissue was frozen in slushed liquid nitrogen, sublimed at - 95°C, sputter coated with gold and then examined at –160°C at 3kV.

3.2.5.1 Hypocotyl Cell Measurements

From scanning electron micrographs of 7 day-old wild type and *sks* hypocotyls, the hypocotyl cell length and the number of hypocotyl cells per 600μm were determined. The scanning electron micrographs of 7 day-old hypocotyl segments were taken in conjunction with Kim Findlay (Department of Cell Biology, John Innes Institute, Colney Lane, Norwich, NR4 7UH).

3.2.6 Temperature and Light Dependent Hypocotyl and Root Elongation

Wild type and *sks* seeds were sown on MS media on square petri dishes and stratified in the dark at 4°C for 48 hours. The square plates were then placed in a growth cabinet at 50mol.m^2.sec^{-1} light and grown at 20, 24 or 29°C for seven days or exposed to light for 1 day, then wrapped in 3 layers of silver foil for 6 days. After 7 days of growth the hypocotyl and root lengths of both WT and *sks* seedlings were measured

3.2.7 β-Glucuronidase Assays

3.2.7.1 *uidA* Marker Lines

The *uidA* (GUS) reporter gene expresses a soluble protein and unless the reporter protein is targeted to other compartments of the cell, the activity staining normally gives a strong water insoluble indigo dye in the cytoplasm (Hauser and Bauer, 2000). The GUS reporter gene has been fused to many genes of interest to create GUS marker lines in which the GUS protein is only expressed were the gene of interest is expressed within the plant.

Marker lines are invaluable tools in the characterisation of new mutants as they are specific to specialised cell types or hormones. The following *uidA* marker lines were crossed in to the *sks* background: NYU195 (End 195), NYU199 (End199) and NYU219 (CRC219) (Malamy and Benfey, 1997), *AtML1*::GUS (Sessions *et al*, 1999), Cyclin B1 and *AtPME15*. The resulting F1 seed was grown up on soil and the F2 seed harvested. The resulting F2 seed was germinated and when the seedlings reached the required age, homozygous GUS x *sks* seedlings were selected.

The NYU marker lines were created by Malamy and Benfey (1997) who created an enhancer trapping cassette by fusing the GUS coding sequence to the TATA region of the 35s promoter from CaMV. The minimal promoter GUS construct was cloned adjacent to the right border of PCV and introduced into *Arabidopsis* via *Agrobacterium* mediated root transformation. NYU195 and NYU199 lines only show GUS expression in the endodermal layer of the root although staining can be seen most clearly in cells of the meristematic zone. GUS expression in the NYU219 line only occurs in the columella root cap.

The *AtML1* construct was created by fusing the GUS reporter gene to 3.5kb of the *AtML1* promoter sequence with part of the first intron and cloning it into pBI101. This

construct was introduced into *Arabidopsis* using *Agrobacterium* mediated vacuum transformation (Sessions *et al*, 1999).

The *AtPME15* contruct was created and donated by Alan Marchant (Department of Forest Genetics and Plant Physiology, SLU, S 901 - 83 Umea, Sweden). This marker is fused the promoter of a pectin methyl esterase gene specific to stomatal guard cells. The *CyclinB1 uidA* marker is a mitotic marker in *Arabidopsis* (Casimiro *et al*, 2001) and the *CyclinB1* construct consists of *cyc1At* promoter upstream of the β-glucuronidase gene, *uidA* (Ferreira *et al*, 1994).

3.2.7.2 GUS Staining

The seedlings were incubated in staining solution at 37°C for several hours or overnight depending on the intensity of the stain required, before being cleared for microscopy with 70% (v/v) ethanol. The staining solution consists of 1X buffer (0.1M Tris pH 7.5, 2.9mg/ml NaCl and 0.66mg/ml K3Fe(CN)6), 20% (v/v) methanol and 0.5mg/ml 5-bromo-4-chloro-3-indolyl-β-d-glucoronide cyclohexylammonium salt (x-gluc).

3.2.7.3 Whole Mount Viewing

Seedlings were cleared for viewing by immersion in 70% (v/v) ethanol, changing the ethanol as required. The seedlings were then mounted on slides using a chloral hydrate solution (7:1:1 of water, chloral hydrate and glycerol) and sealed with clear nail varnish.

3.2.7.4 Sectioning of Plant Tissue

Seven day-old seedlings were GUS stained if needed and placed in fixation solution for 3 hours at room temperature. The fixation solution consists of 4% (v/v) glutaraldehyde, 10.8% (v/v) methanal, 10% (v/v) phosphate buffer (0.5 M Na_2HPO_4/ NaH_2PO_4 pH 7.2). The seedlings were then dehydrated by placing in an ethanol dilution series for ~1 hour at each step, 30%, 50%, 70%, 90% (v/v) and twice in absolute ethanol.

The seedlings were then embedded in Technovit 7100 resin (TAAB) according to the manufacturers instructions. The seedlings were first embedded in windows that were then placed in Beem capsules (TAAB) and filled with resin. The resin blocks containing the tissue were then attached to sectioning blocks using Technovit 3040-impression resin (TAAB).

Windows consisted of a strip of acetate film upon which two strips of double-sided tape (3M) were affixed back-to-back, sandwiching the acetate film. Rectangles were cut out of this strip, leaving a border of double-sided tape (3M) around each gap, one of the protective coverings of the double-sided tape was then removed and the windows were attached to another strip of acetate to form a well. The windows were then separated from one another, the last piece of protective covering of double-sided tape was removed, a seedlings root was placed in the well, filled with resin and then covered with a piece of acetate to allow polymerisation of the resin overnight. Once the resin has polymerised the resin "window" was cut out of the acetate and then embedded in a Beem capsule (TAAB).

Sections of 5μM were then cut using a Bright 3400 microtome and stained for 10 minutes with 0.05 % (w/v) ruthenium red; the sections were then rinsed with distilled water and allowed to dry. The sections were permanently mounted with Depex (Sigma) and glass coverslips before viewing with a Nikon Optiphot-2 nomanski with Lucia image capturing software or a Zeiss Stemi SV6 binocular.

3.3 RESULTS

3.3.1 General *sks* Mutant Morphology

The *sks* mutant was originally isolated on the basis of its seedling phenotype from an En-element mutagenised population (Marchant and Bennett, unpublished results). The phenotype of the *sks* mutant becomes increasingly severe as seedling development progresses (figure 3.3.1 B-J). Whilst wild type seedlings develop new leaves, roots elongate and lateral root primordial emerge (figure 3.3.1 A-I), the *sks* mutant progressively exhibits an increasingly callus-like appearance where the new expanding leaves curl round over the older leaves, root elongation is retarded and anchor roots develop (figure 3.3.1 B-J).

To pinpoint the first stage that the *sks* phenotype was apparent, confocal analysis of mature *sks* and WT embryos was undertaken (figure 3.3.2). The vasculature of *sks* embryos (figure 3.3.2 D) appears normal, but the epidermal cells of *sks* seedlings (figure 3.3.2 A) appear squarer and less sinuous than WT (figure 3.3.2 B). The roots of *sks* embryos can appear to be altered (figure 3.3.2 G) but the underlying root morphology appears largely normal (figure 3.3.2 F & G). Hence, major phenotypic differences between wild type and *sks* seedlings were first apparent following germination.

The *sks* mutant is a recessive mutation, segregating in a monogenic fashion with a ratio of 1:3 ($p=0.05$), with 2176 WT seedlings and 629 *sks* seedlings out of 2805 seedlings that were counted in an F2 generation backcross of *sks* to Columbia. The *sks* mutant exhibits a seedling lethal phenotype and does not normally survive being planted out on soil. However, the *sks* mutant exhibits variable penetrence resulting a large degree of phenotypical differences with 36% of seedlings displaying a "wild type" phenotype in a population of homozygous *sks* seedlings (figure 3.3.1 F, H, J & I).

These "wild type" *sks* seedlings survive when planted out on soil but display an altered phenotype when compared to wild type plants (figure 3.3.3). Six-week-old "wild type" *sks* plants have a dwarf phenotype compared to Columbia and possess small crinkled leaves, have reduced lateral branching and may have shorter siliques containing fewer seeds (Figure 3.3.3).

The *quasimodo* (*qua*) mutant encodes a family 8 glycosyltransferase and displays an extraordinarily similar phenotype to *sks* including the variable phenotype which range

from almost normal physiology to strongly perturbed development (Bouton *et al*, 2002). In *qua* it was suggested that the highly variable phenotype associated with the T-DNA insertion was due to incomplete penetrence of the allele as a result of variable translational efficiency of the transcript (Bouton *et al*, 2002).

In the case of *sks*, the mutation is not tagged and the *SKS* locus is likely to contain an En-induced "footprint" that may cause variable penetrence by forming a mutant protein with limited activity. Sequence analysis of En-revertant *superroot2* (*sur2*) alleles reported the insertion of AT-rich footprints, between 2 and 4 bases in length (Barlier *et al*, 2000).

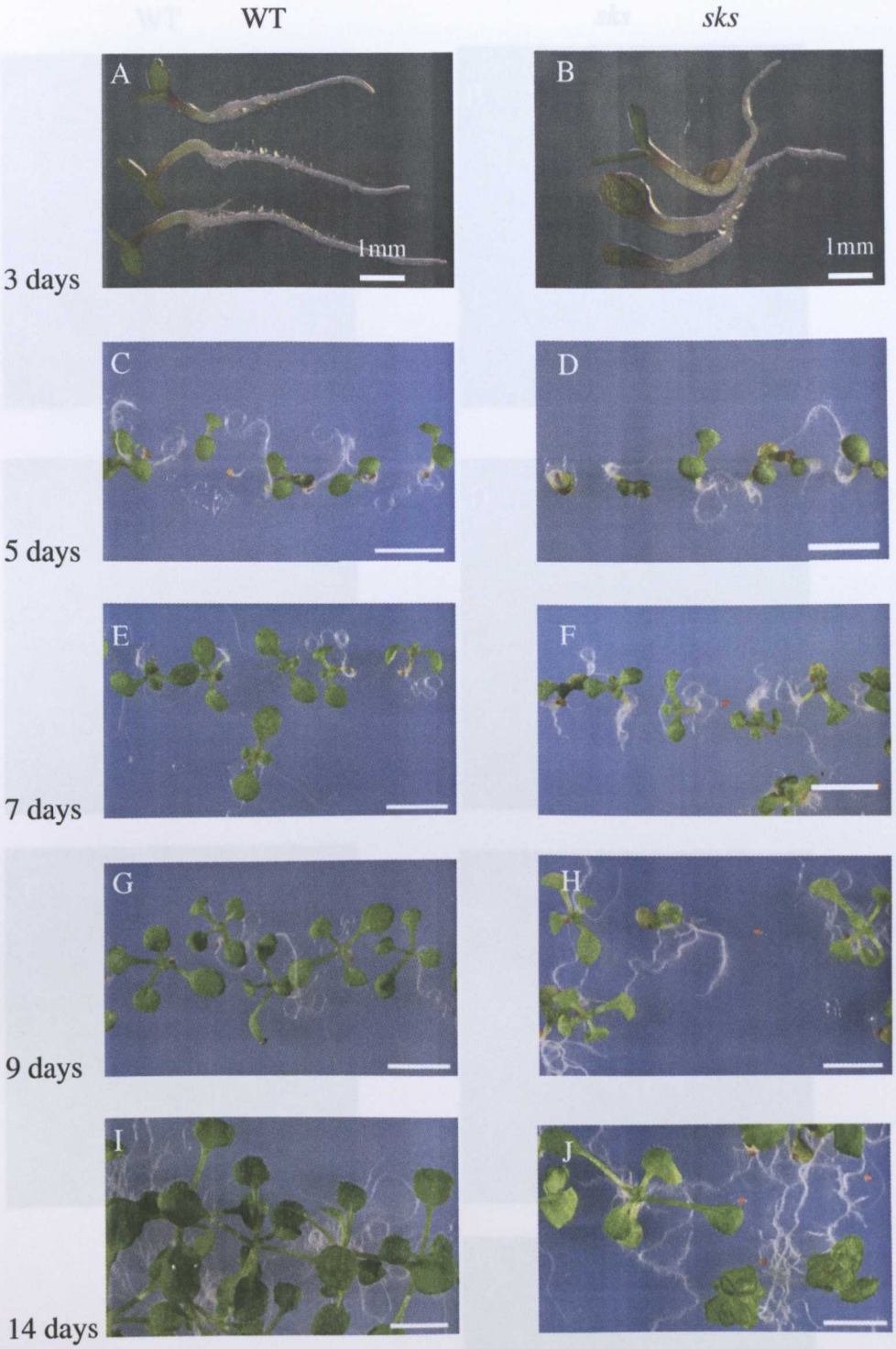

FIGURE 3.3.1: Growth developmental series of WT and *sks* seedlings from 3 to 14 days of age when grown horizontally on agar plates in the light. The sks seedlings shown (B, C, E, F, H & I) show a range of phenotypes from "normal" to severe callus-like as development proceeds. At 3 days *sks* seedlings (B) are darker green than WT seedlings (A). At 5 days of age *sks* (D) and WT (C) cotyledons are expanding and in sks (D) the cotyledon and hypocotyl epidermis are beginning to show cell-to-cell separation. At 7 days the first leaves have emerged in WT seedlings (E) and *sks* seedlings (F), in *sks* the phenotypic variation is discernable, epidermal cell-to-cell separation increases on cotyledons, new leaves and hypocotyl. At 9 days primary leaf expansion has commenced in WT (G) and *sks* seedlings (F), in *sks* epidermal cell-to-cell linkages worsen, anchor roots have emerged at the base of the hypocotyl and the cotyledons and new leaves are beginning to curl around one another. By 14 days of age the second set of primary leaves are emerging in WT seedlings (I) and *sks* seedlings (J) however, in *sks* growth does not progress much beyond this stage due to worsening epidermal cell-cell adhesion. Scale bars: 5mm.

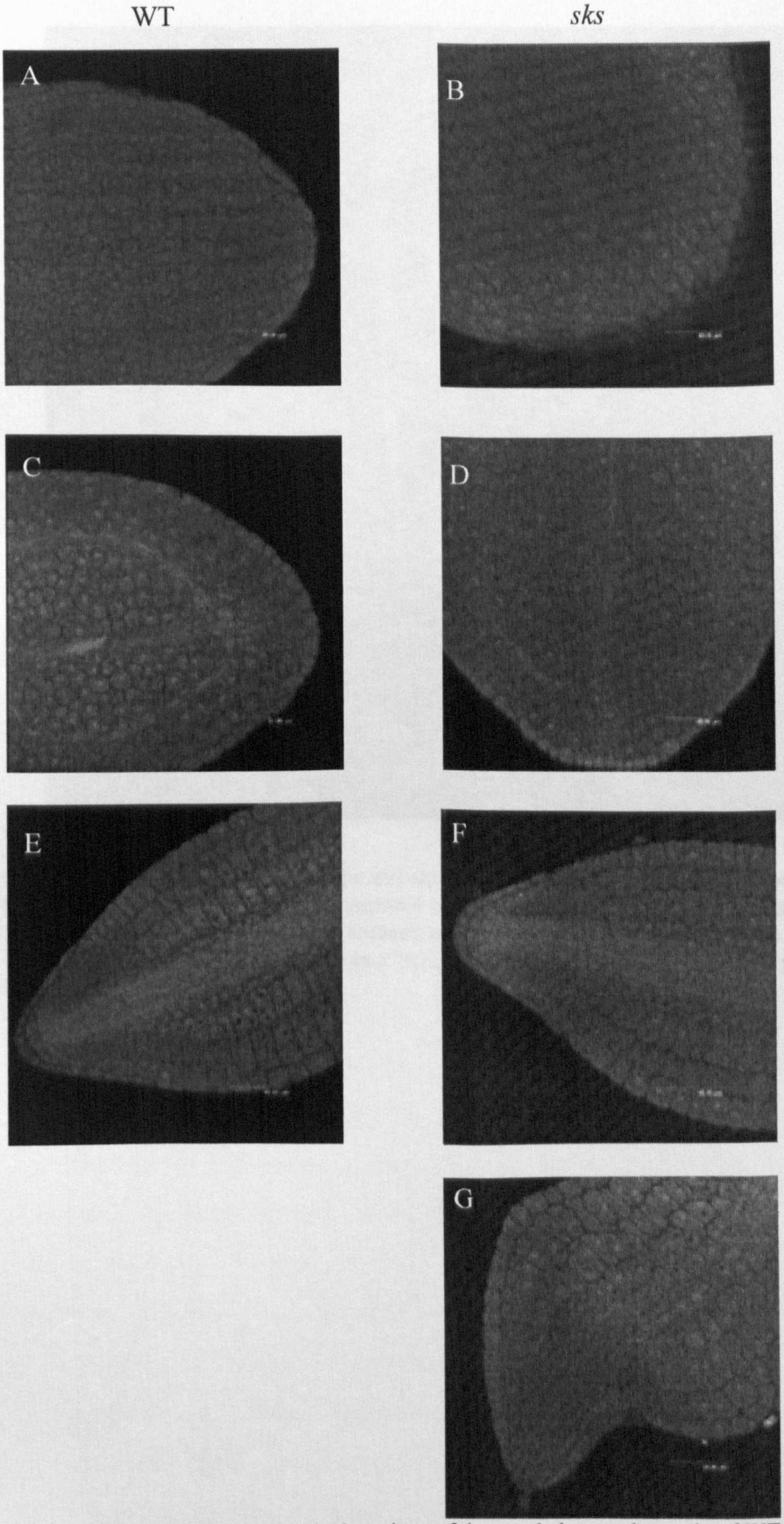

FIGURE 3.3.2: Longitudinal optical sections of the cotyledons and root tip of WT and *sks* mature embryos. No differences were detected between the epidermis and vasculature of WT (A & C) and *sks* (B & D) cotyledons. The root tips of *sks* seedlings appear to have normal structure (F), however *sks* root tips can appear altered but they retain normal root morphology (G). Scale bars: 10μM.

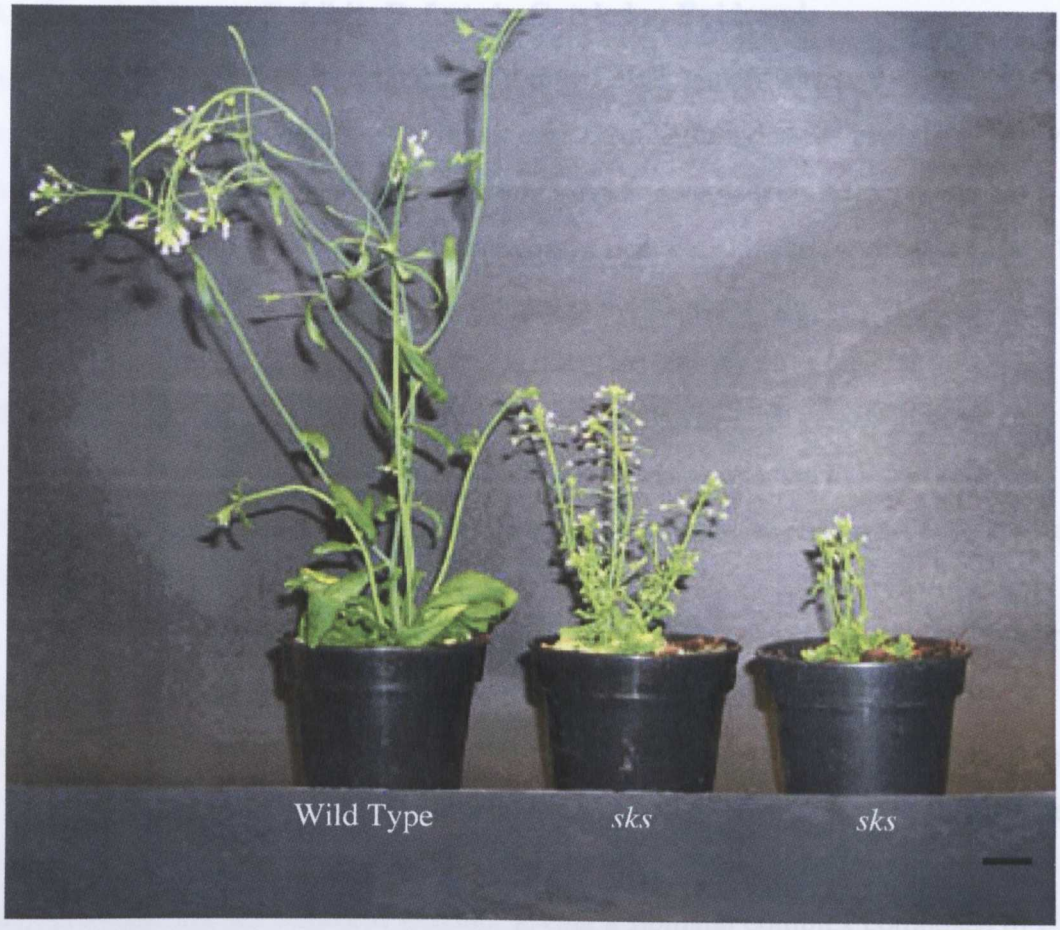

FIGURE 3.3.3: Six-week-old wild type and *sks* plants. The wild type displays a normal growth habit with large basal leaves, long floral inflorescences with lateral branching and long siliques. The *sks* plants are dwarfed with small crinkled leaves, reduced apical dominance and appear to have shorter siliques with reduced seed set. Even between the two "wild type" *sks* plants shown, a range in phenotypic severity can be seen. Scale bar: 1cm.

3.3.2 The *sks* Mutant Exhibits Defects in Cotyledon Epidermis

Cryo-SEM was used to gain further insight into the *sks* mutant phenotype. In WT plants the pavement epidermal cells on the upper surface of the cotyledon develops a highly convoluted-jigsaw shaped morphology from 3 days onwards (figures 3.3.4 and 3.3.5 A, C and E). In contrast, equivalent epidermal pavement cells of *sks* cotyledons appear to be larger than wild type cells and form a more cuboid shape (figure 3.3.4 and 3.3.5 B, D and E). Figures 3.3.4 and 3.3.5 B, D and E illustrate that the intra-cellular bonds between the individual epidermal cells are breaking down. This results in large gaps in the epidermal pavement cells through which the underlying mesophyll cells can be observed (data not shown). Similarly, cell-to-cell linkages between guard cells appear to be breaking down (figure 3.3.5 F).

The stomatal complexes are interspersed at fairly regular intervals throughout WT epidermal pavement cells (figures figure 3.3.4 and 3.3.5 A, C and E). Wild type stomatal complexes are composed of a pair of stomatal guard cells and are surrounded by 3-5 pavement epidermal cells, neighbouring stomata are found to have at least one epidermal pavement cell separating them (figure 3.3.5 C and E). In *sks* many of the stomatal complexes are clustered together giving a stomatal complex composed of 2 to 3 pairs of guard cells (figure 3.3.5 D and F).

The *AtPME15*::GUS marker was utilised to investigate the patterns of stomatal division and differentiation in the *sks* cotyledon epidermis. The *AtPME15*::GUS reporter highlights the location of stomatal complexes within the epidermis of developing cotyledons (figure 3.3.6). *AtPME15* stained stomatal complexes are usually found to have at least one epidermal cell between them in WT cotyledons (figure 3.3.6 A). However, in the *sks* background (figure 3.3.6 B) there are an increased number of stomatal complexes and many of them appear to be in direct contact with one another.

The stomatal index and stomatal density were calculated for the upper cotyledon epidermis of 3-day-old *sks* and WT seedlings. Epidermal integrity is still fairly normal in *sks* seedlings of this developmental stage and so stomatal density and stomatal index can readily be determined. The stomatal density is number of stomata per mm^2 and the stomatal index equals the number of stomata / (number of epidermal cells + number of stomata) X 100 and is a measure of stomatal density on a cell number basis (Berger and Altmann, 2000). In WT seedlings the stomatal density and stomatal index are 0.12 and 14.52 respectively. In *sks* seedlings the stomatal density only increased slightly to 0.19

however, the stomatal index increased almost 2 fold to 24.91 respectively. It appears that there are twice as many stomatal complexes associated with the epidermal cells of *sks* seedlings indicating that more divisions are occurring in the epidermis of *sks*.

The *Cyclin B1*::GUS marker (Ferreira *et al*, 1994) was used to probe the relative mitotic activity of *sks* cotyledon epidermal cells(figure 3.3.7). The apical meristem, cotyledons and root tip of *Cyclin B1*::GUS seedlings in the WT background (figure 3.3.7 A, C, E) show high levels of cell division. Cell division is expected in these tissues due to the high level of cell differentiation and expansion that is required during leaf development and plant growth.

However, the *Cyclin B1*::GUS reporter in the *sks* background (figure 3.3.7 B, D, F) illustrates that cell division is highly up-regulated in the apical meristem, cotyledons, root tip and in the apical part of the hypocotyl from 1 day after germination. The *AtML1*::GUS and *AtPME15*::GUS markers indicate that increased epidermal divisions are occurring in the cotyledons of *sks* seedlings leading to abnormally distributed stomatal complexes. The increase in *Cyclin B1*::GUS expression in the *sks* background (figure 3.3.7 B, D, F, G) is not only coupled to increased stomatal division but to an overall increase in epidermal and underlying mesophyll cell division. The observation that hypocotyl cells appear to undergo post-embryonic division in the *sks* background (figure 3.3.7 B, D) merits further investigation.

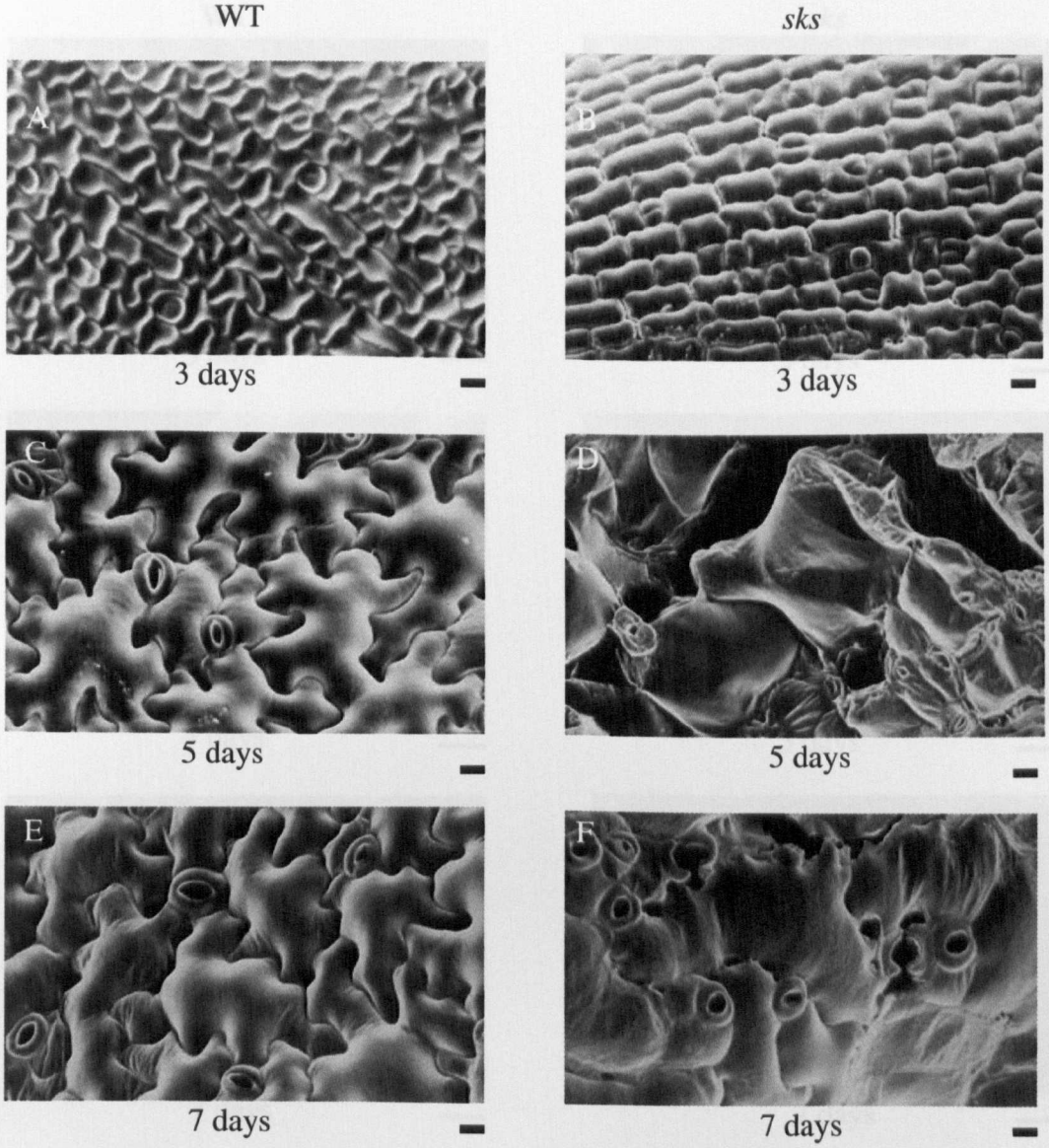

FIGURE 3.3.4: Scanning electron micrographs of the upper epidermis of 3 day, 5 day and 7 day old wild type and *sks* cotyledons. The epidermal cells of both *sks* and wild type increase in size as the seedlings increase in age. However, the epidermal cells of the wild type seedlings become more jigsaw shaped and those of the *sks* become more cubical over time. It can also be noted that the epidermal cells of *sks* become increasingly separated and alterations in stomatal distribution and structure occur. Scale bars: 10μM

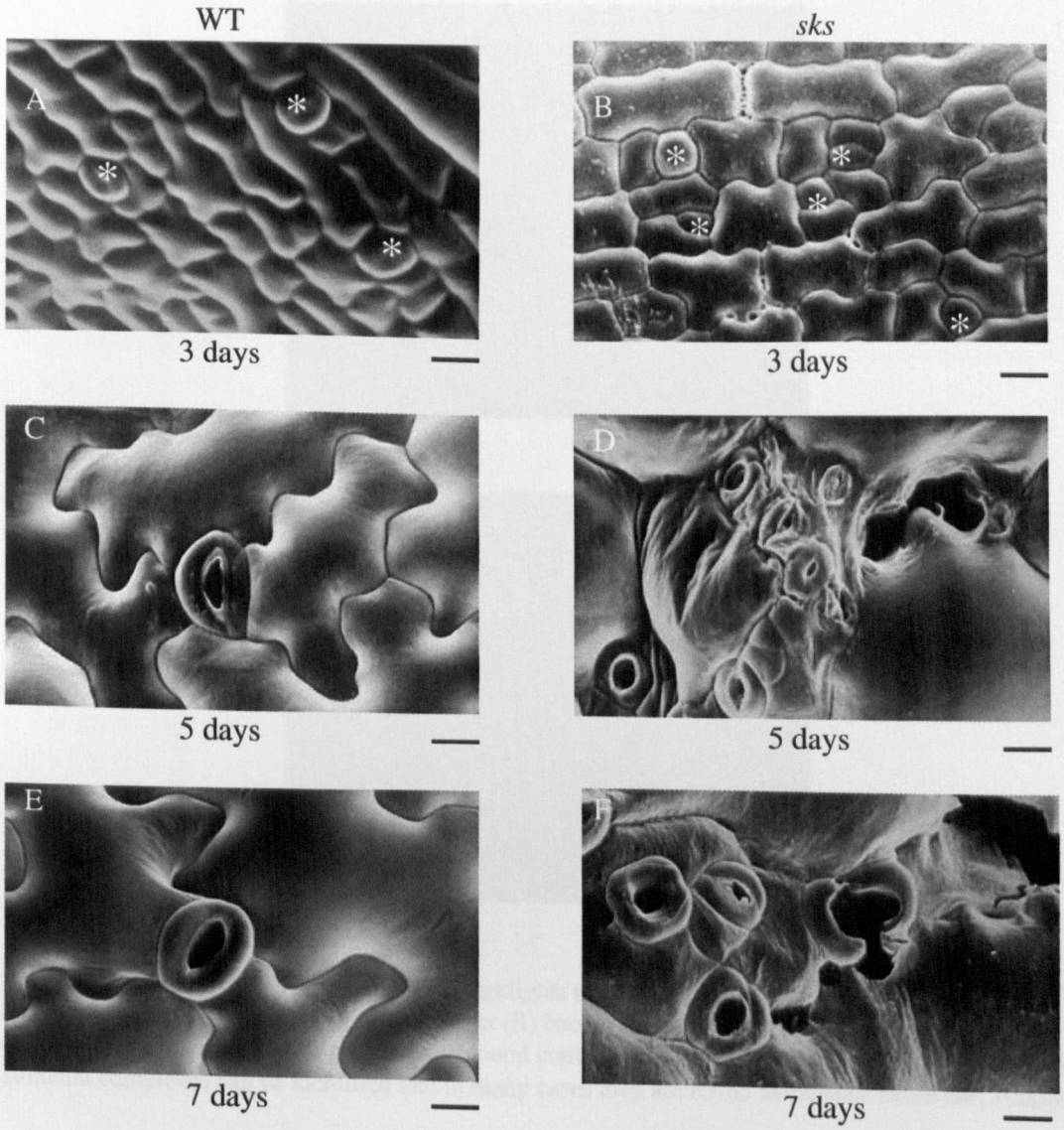

FIGURE 3.3.5: Higher power scanning electron micrographs of the upper cotyledon epidermis in 3, 5 and 7 day old wild type and *sks* seedlings. These micrographs show the increasingly aberrant stomatal distribution and structure in *sks* (D, F) when compared to wild type stomata (C, D). In the epidermis of *sks* seedlings (B) at 3 days there appears to be more stomatal initials,as indicated by the asterisks, interspersed within the cubical epidermal cells compared to WT (A). Scale bars: 10μM.

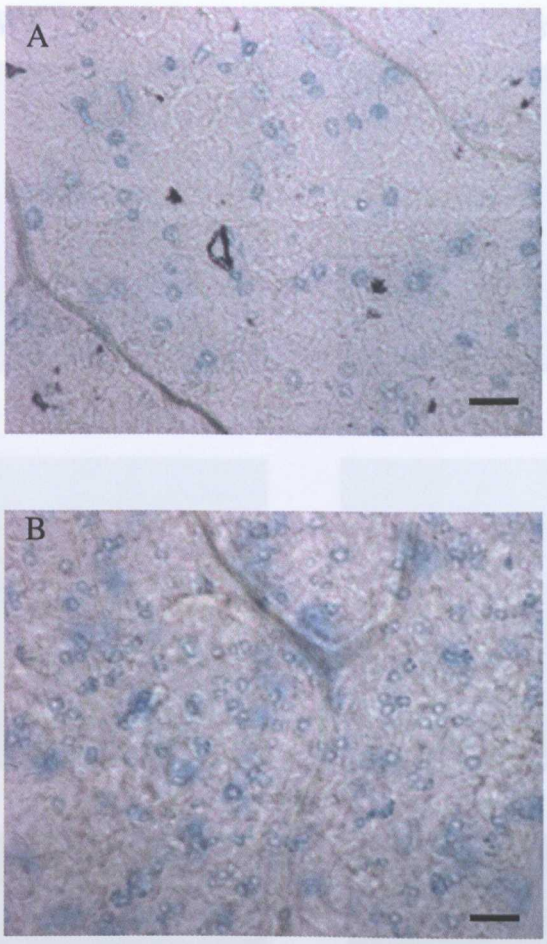

FIGURE 3.3.6: The *AtPME15*::GUS marker highlights the distribution of stomata within the upper epidermis of cotyledons in the WT (A) and *sks* (B) background at 7 days old. In WT (A) stomatal complexes are widely spaced and are rarely found contacting one another. In *sks* (B) a greater number of stomatal complexes can be identified and in many cases they are found in clusters. Scale bar: 100μM

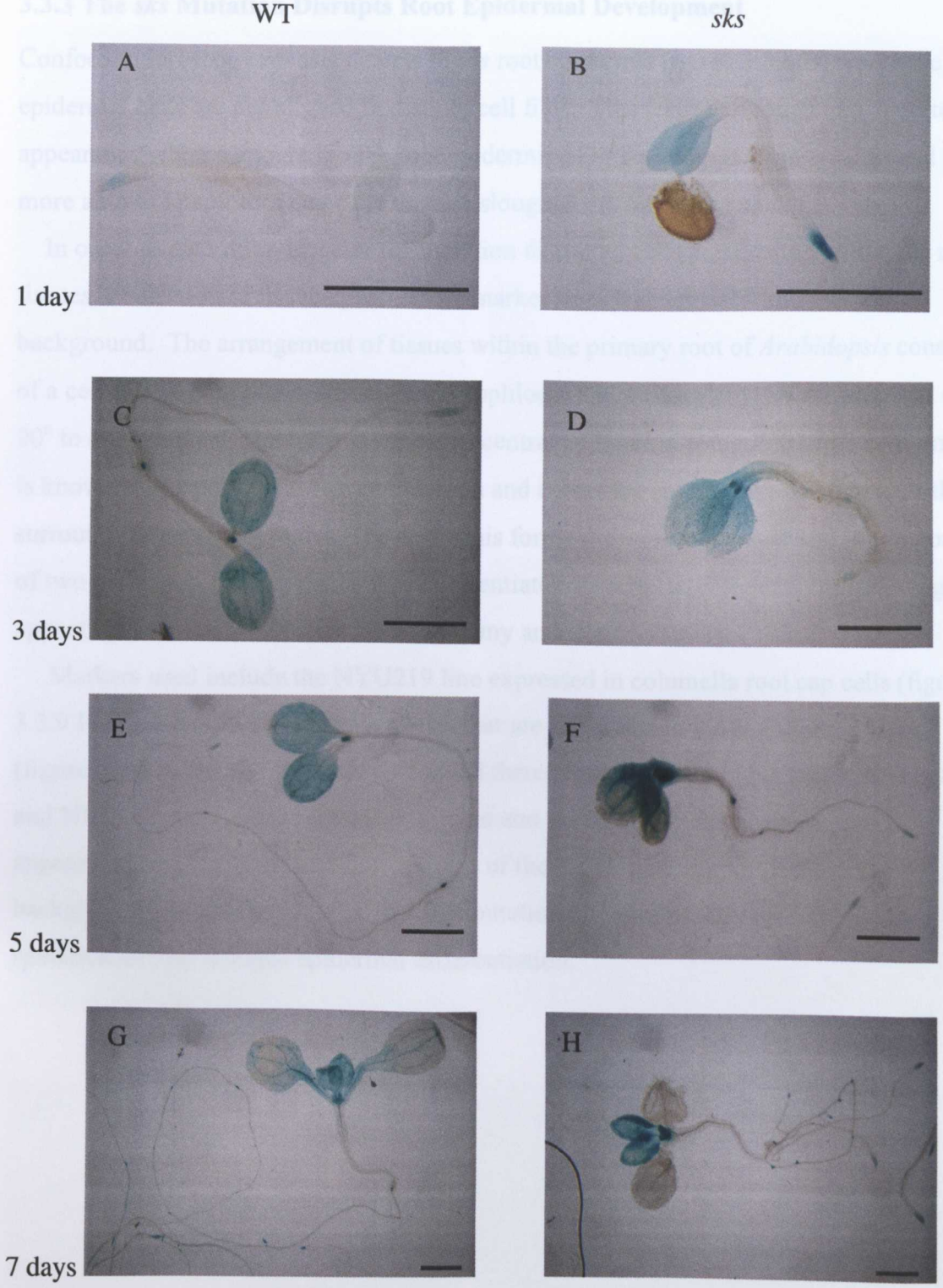

FIGURE 3.3.7: Expression of the *Cyclin B1*::GUS marker in *Arabidopsis* seedlings from 1 to 7 days after germination. In the WT background *CyclinB1*:: GUS expression increases in the cotyledons, root meristem and the apical meristem from 1 day after germination (A, C & E). At 7 days after germination (G) staining is lost from the cotyledons as they have reached maturity and instead is focused on the shoot apical meristem, developing leaves, root meristem and lateral root primordia. In the *sks* background GUS expression shows altered staining in the root meristem, cotyledons and apical meristem from 1 to 5 days after germination (B, D & F), by 7 days (H) staining is confined to developing new leaves and lateral root primordia. From 1 to 3 days after germination (B, D), *CyclinB1*::GUS in the *sks* background is also expressed in the apical part of the hypocotyl. Scale bars: 1mm.

3.3.3 The *sks* Mutation Disrupts Root Epidermal Development

Confocal microscopy reveals defects in *sks* root epidermis (figure 3.3.8 B) where the epidermal cells are not aligned in distinct cell files. This leads to a rough and distorted appearance when compared to the root epidermis of WT seedlings (figure 3.3.8) and is more akin to lateral root cap calls that are sloughed off at the root apex.

In order to determine whether the mutation disrupted cell specification within the root tissues, a selection of tissue-specific root marker lines were crossed into the *sks* background. The arrangement of tissues within the primary root of *Arabidopsis* consists of a central cylinder that contains the protophloem and protoxylem that are arranged at 90° to one another. The outer layer of the central cylinder is composed of 12 cells and is known as the pericycle. The endodermis and cortex are single rings of eight cells that surround the central cylinder. The epidermis forms the outermost layer and is composed of two cell types, root hair cells that differentiate into tubular, elongated, tip-growing appendages and non-root- hair cells (Malamy and Benfey, 1997).

Markers used include the NYU219 line expressed in columella root cap cells (figure 3.3.9 I & J) and NYU lines 195 and 199 that are expressed in the endodermal layer (figure 3.3.9 A-H). GUS staining revealed there was no change in NYU219, NYU195 and NYU199 expression between wild type and *sks* lines. In the absence of any apparent change in the expression patterns of the NYU marker lines in the *sks* background, it can be concluded that the mutation does not modify epidermal tissue specification but disrupts epidermal differentiation.

WT

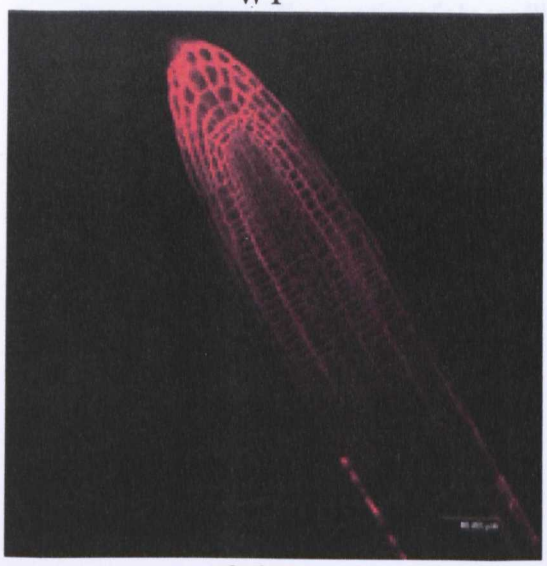

3 days

sks

3 days

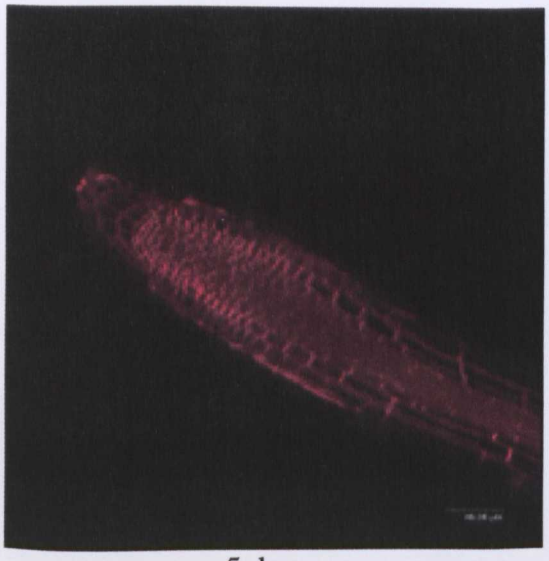

5 days

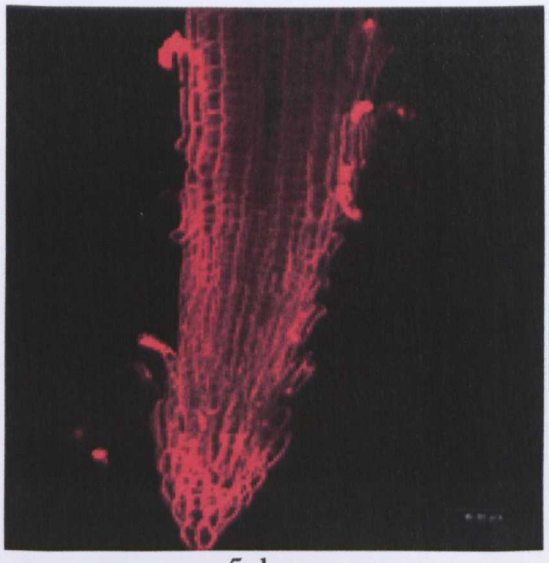

5 days

7 days

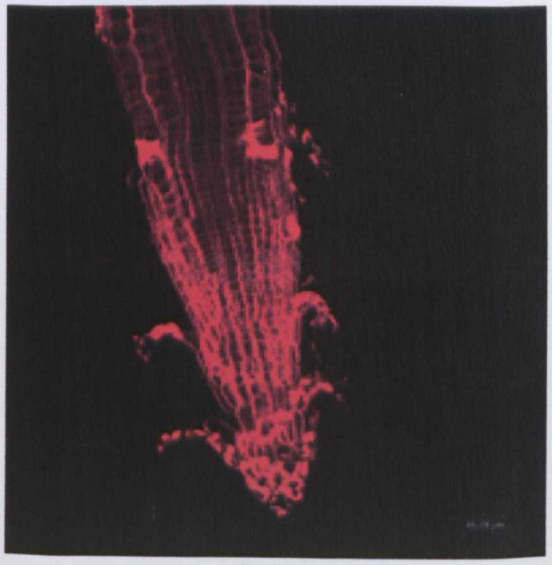

7 days

FIGURE 3.3.8: Confocal images of WT (A, C & E) and *sks* (B, D & F) root tips epidermis of at 3, 7 and 9 days after germination. The root tips of *sks* seedlings (B) show no obvious morphological differences compared to WT seedlings (A). In maximum projections of WT and *sks* roots, the epidermis of *sks* roots show abnormal morphology. The epidermal layer of *sks* appears rough and distorted due to disruption of the epidermal cell files and epidermal cells can be seen to be peeling away from the root surface. Scale bar: 100μM.

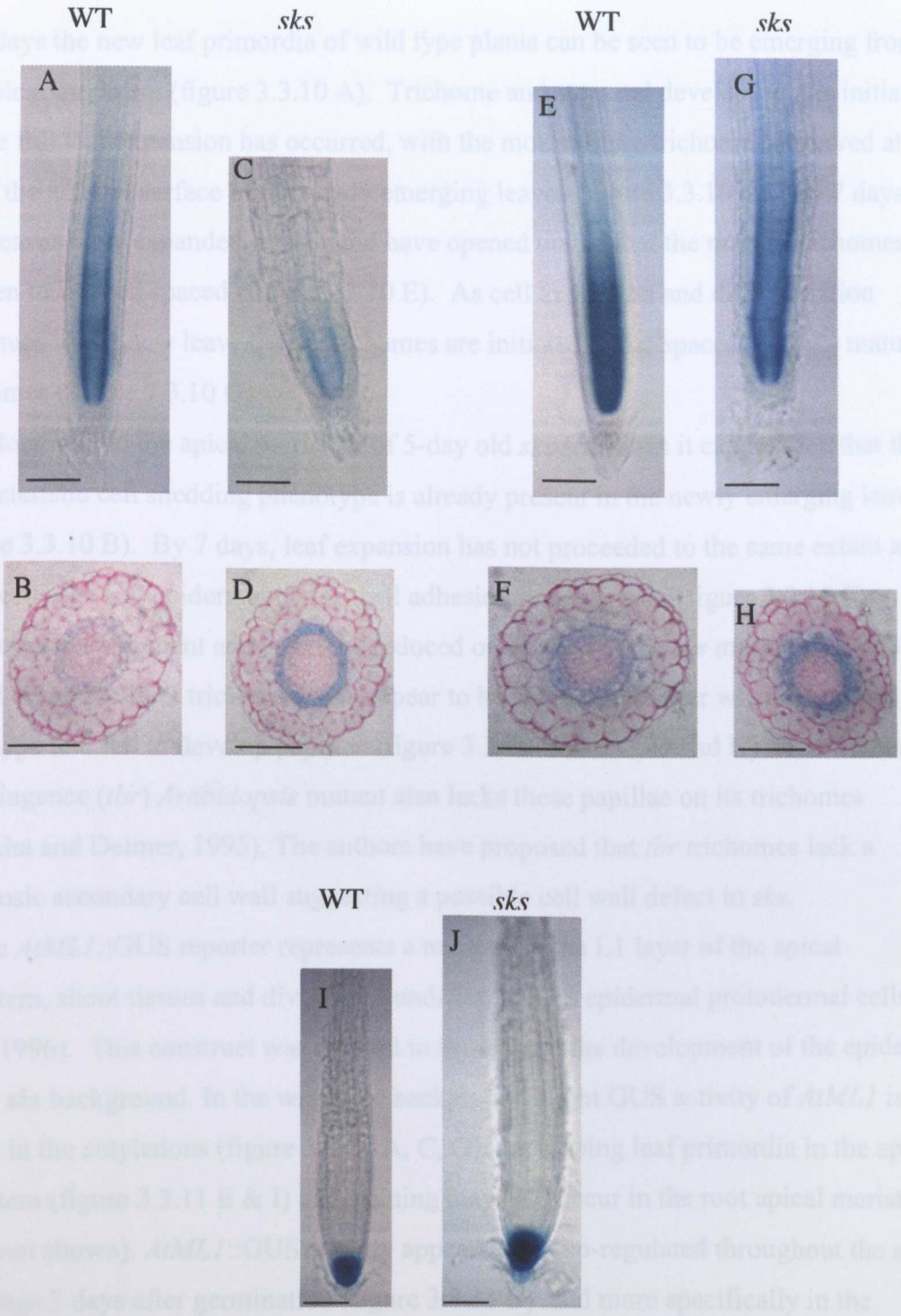

FIGURE 3.3.9 Nomarski whole mount and transverse sections of the NYU lines GUS expression in 7-day-old wild type and *sks* root tips. Images A, C, E and G are whole mounts and images B, D, F and H are transverse sections. In wild type (A) and *sks* (C) seedlings expressing NYU195::*uid*A the GUS expression is specific to the endodermal layer as shown by the transverse sections of wild type (B) and *sks* roots (D). NYU199::*uidA* is also an endodermis specific root marker as shown by the GUS expression patterns and transverse sections of wild type (E, F) and *sks* seedlings (G,H). The NYU line 219 shows GUS specific columella root cap staining in wild type (I) and *sks* seedlings (J). Scale bars, 50μM

3.3.4 The *sks* Mutant Exhibits Defects in Newly Formed Leaf Primordium

At 5 days the new leaf primordia of wild type plants can be seen to be emerging from the apical meristem (figure 3.3.10 A). Trichome and stomatal development is initiated before full leaf expansion has occurred, with the most mature trichomes observed at the tip of the adaxial surface of the newly emerging leaves (figure 3.3.10 C). By 7 days, the new leaves have expanded further and have opened out so that the mature trichomes can be seen to be well spaced (figure 3.3.10 E). As cell expansion and differentiation continues in the new leaves, new trichomes are initiated in the spaces between mature trichomes (figure 3.3.10 G)

However, in the apical meristem of 5-day old *sks* seedlings it can be seen that the characteristic cell shedding phenotype is already present in the newly emerging leaves (figure 3.3.10 B). By 7 days, leaf expansion has not proceeded to the same extent as WT seedlings and epidermal cell-to-cell adhesion remains poor (figure 3.3.10 F). Trichome development appears to be reduced or delayed in the *sks* mutant (figure 3.3.10 D and H) and mutant trichomes also appear to be shorter and fatter when compared to wild type and fail to develop papillae (figure 3.3.10 C and G, D and H). The trichome birefringence (*tbr*) *Arabidopsis* mutant also lacks these papillae on its trichomes (Potikha and Delmer, 1995). The authors have proposed that *tbr* trichomes lack a cellulosic secondary cell wall suggesting a possible cell wall defect in *sks*.

The *AtML1*::GUS reporter represents a marker for the L1 layer of the apical meristem, shoot tissues and division in undifferentiated epidermal protodermal cells (Lu *et al*, 1996). This construct was utilised to investigate the development of the epidermis in the *sks* background. In the wild type background slight GUS activity of *AtML1* is found in the cotyledons (figure 3.3.11 A, C, G), developing leaf primordia in the apical meristem (figure 3.3.11 E & I) and staining may also occur in the root apical meristem (data not shown). *AtML1*::GUS activity appears to be up-regulated throughout the *sks* seedlings 3 days after germination (figure 3.3.11 B) and more specifically in the emerging new leaves and developing leaf primordia (3.3.11 B, F & J), possibly indicating that increased protodermal cell division and epidermal cell differentiation is occurring within the cotyledons and new leaves of *sks* seedlings.

Increased mitotic cell division and protodermal cell division, indicated by the *CyclinB1*::GUS marker (figure 3.3.7) and *AtML1*::GUS marker (figure 3.3.11), are found to occur in the same tissues of *sks* seedlings. An increase in mitotic and protodermal cell division could account for the increased number of stomata seen in

Cryo SEM micrographs and with the AtPME15::GUS marker of *sks* cotyledons (figures 3.3.4, 3.3.5 and 3.3.6). Increased cell division of epidermal cells may also occur in *sks* seedlings to try and compensate for the loss of epidermal cells through the breakage of cell-to-cell linkages. The ability of adjacent cells to "sense" and compensate for the reduced growth of slow-growing sectors has been observed in maize leaves (Qui *et al*, 2002).

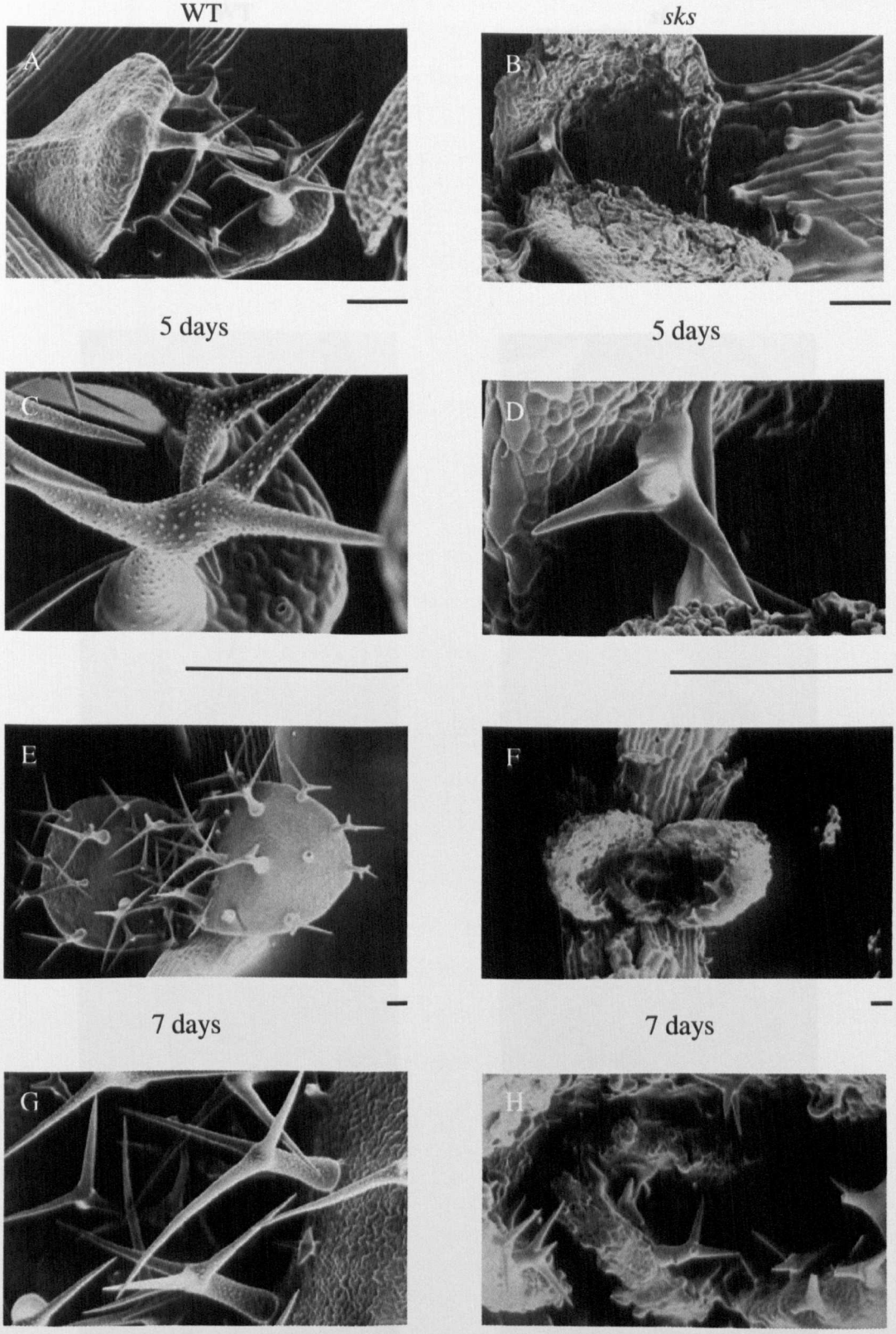

FIGURE 3.3.10: Apical meristems of *sks* (B, D, F, H) and WT (A , C, E, G) 5 and 7 day old seedlings showing the emerging new leaves and trichomes. Figures A and E show the new leaves emerging from the apical meristem of WT seedlings at 5 and 7 days and figures B and F of *sks* with the petioles of the cotyledons in the background. From figures B and F it can be seen that even the new leaves and petioles show the characteristic *sks* phenotype with the cell-to-cell linkages breaking down. Figure C and G show WT trichome morphology with a stalk, three branches and papillae at 5 and 7 days. *sks* trichomes (D &H) appear stunted and lack the characteristic papillae of WT trichomes. Scale Bars: 100μM

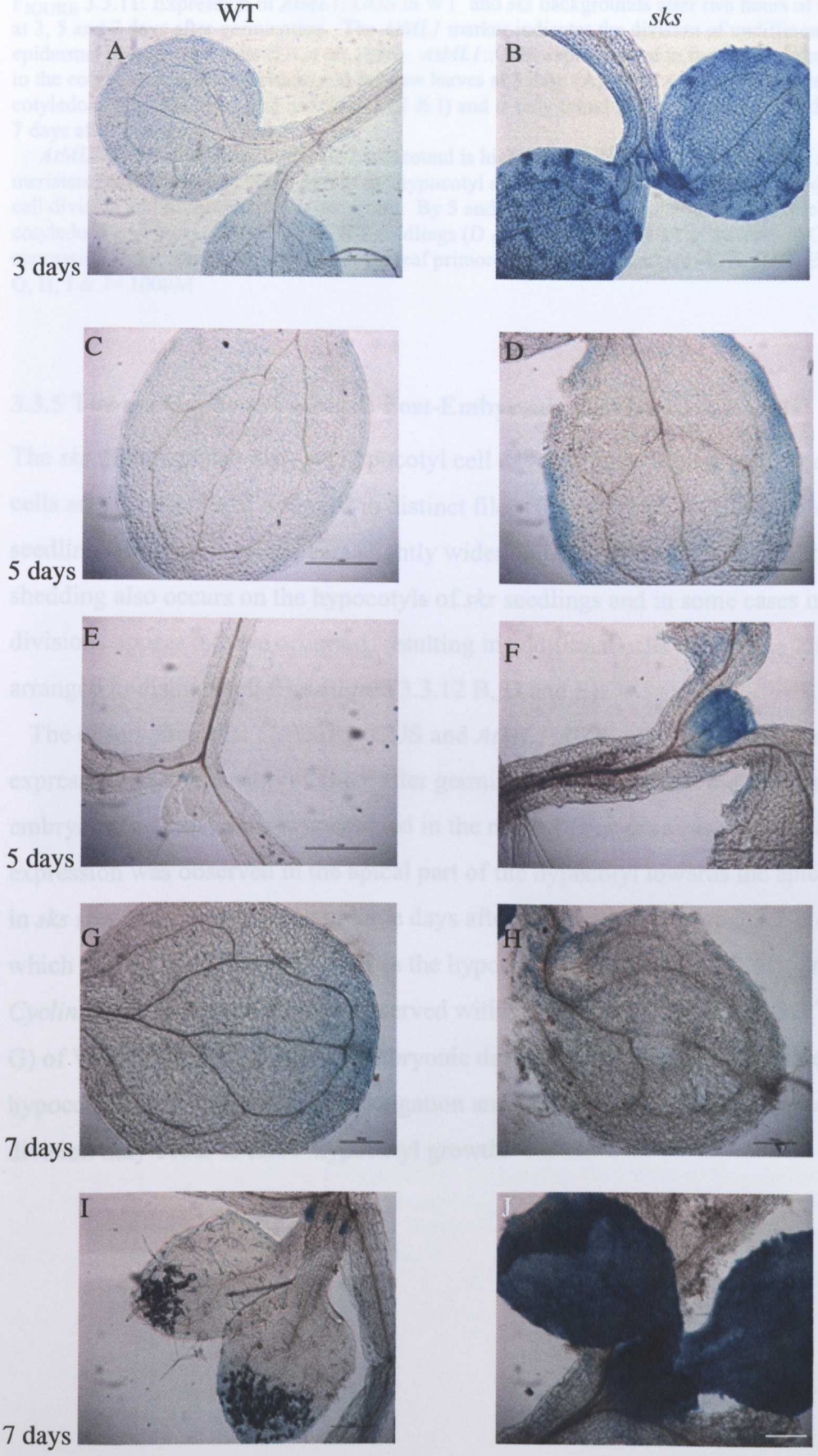
WT
sks
A
B
3 days
C
D
5 days
E
F
5 days
G
H
7 days
I
J
7 days

FIGURE 3.3.11: Expression of *AtML1*::GUS in WT and *sks* backgrounds after two hours of GUS staining at 3, 5 and 7 days after germination. The *AtML1* marker indicates the division of undifferentiated epidermal protodermal cells (Lu *et al*, 1996). *AtML1*::GUS expression of in the WT background is found in the cotyledons, apical meristem and the new leaves at 3 days (A), GUS expression then reduces in the cotyledons (C & G), emerging new leaves (E & I) and is only found in the new leaf primordia from 5 and 7 days after germination (E & I).

AtML1::GUS expression in the *sks* background is highly up-regulated in the cotyledons, apical meristem, new leaves and upper part of the hypocotyl at 3 days (B) indicating that increased epidermal cell division and differentiation is occurring. By 5 and 7 days after germination GUS expression in the cotyledons is at level comparable to WT seedlings (D & H) but there is a large increase in GUS expression in the emerging new leaves and leaf primordia (F & J). Scale bars: A, B, C, D, E & F 1mm. G, H, I & J= 100μM

3.3.5 The *sks* Hypocotyl exhibits Post-Embryonic Cell Division Events

The *sks* mutation also disrupts hypocotyl cell development. Whilst wild type hypocotyl cells are elongated and arranged in distinct files (figure 3.3.12 A and C), in *sks* seedlings the hypocotyl appears slightly wider and the hypocotyl cells are shorter. Cell shedding also occurs on the hypocotyls of *sks* seedlings and in some cases irregular divisions appear to have occurred, resulting in additional cells that are no longer arranged in distinct cell files (figure 3.3.12 B, D and E).

The observation that *CyclinB1*::GUS and *AtML1*::GUS markers are transiently expressed in *sks* hypocotyl tissues after germination confirm that the repression of post-embryonic cell divisions is uncoupled in the mutant. For example, the *CyclinB1*::GUS expression was observed in the apical part of the hypocotyl towards the apical meristem in *sks* seedlings between one to three days after germination (figure 3.3.7 B & D), after which cell division does not occur in the hypocotyl (figure 3.3.7 (F & H). In contrast no *CyclinB1*::GUS expression was observed within hypocotyl cells (figure 3.3.7 A, C, E & G) of WT seedlings during post-embryonic development. This may indicate that *sks* hypocotyls have a defect in cell elongation and to compensate for this, increased cell division may occur to allow hypocotyl growth.

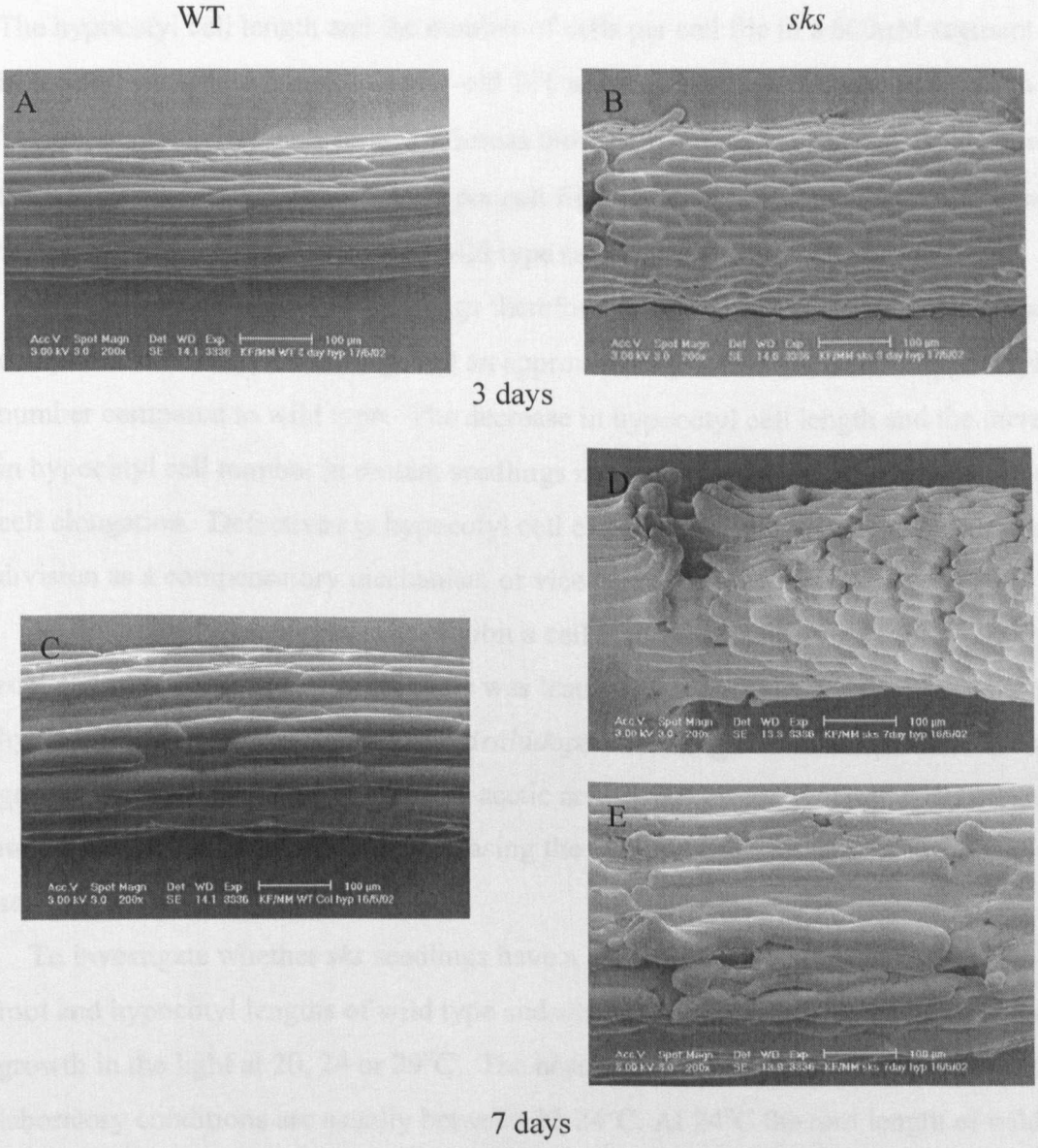

FIGURE 3.3.12: 3 (A &B) and 7 day old (C, D & E)wild type (A, C) and *sks* (B, D, E) hypocotyl cells. The hypocotyl cells of *sks* at 3 days old (B) appear to be significantly shorter than those of wild type (A) at this stage and epidermal cell-to-cell adhesion is still apparent. By 7 days, *sks* hypocotyl cells seem to be dividing irregularly (B, D, E) which leads to distorted cell files when compared to wild type cells (A, B) and epidermal cell-to-cell adhesion is poor. Figures D and E illustrate the phenotypic variation that can be found within *sks* seedlings Scale bars: 100μM

3.3.6 Mutant Hypocotyl Tissues Exhibit a Finite Capacity for Elongation

The hypocotyl cell length and the number of cells per cell file in a 600μM segment of hypocotyl were determined in 7-day-old WT and *sks* seedlings. The average length of WT hypocotyl cells was ~220μM whereas those of *sks* were 150μM. In *sks* seedlings there were ~3.5 to 4 hypocotyl cells per cell file in a 600μM length of hypocotyl and ~2 to 3 hypocotyl cells per cell file in wild type seedlings.

The hypocotyl cells of *sks* seedlings therefore show a 2-fold decrease in length when compared to wild type seedlings and an approximately 2-fold increase in hypocotyl cell number compared to wild type. The decrease in hypocotyl cell length and the increase in hypocotyl cell number in mutant seedlings may indicate that there is a defect in *sks* cell elongation. Defective *sks* hypocotyl cell elongation could lead in an increase in cell division as a compensatory mechanism or vice versa.

To determine whether *sks* cells exhibit a cell elongation defect, the capacity of mutant root and hypocotyl tissues to elongate was tested. High temperature promotes dramatic hypocotyl elongation in light-grown *Arabidopsis* seedlings. This temperature induced growth response depends on indole-3-acetic acid (IAA) or auxin. High temperature may promote cell elongation by increasing the free and conjugated IAA present within a seedling. (Gray *et al*, 1998)

To investigate whether *sks* seedlings have a defect in cell elongation or division the root and hypocotyl lengths of wild type and *sks* seedlings were measured after 7 days of growth in the light at 20, 24 or 29°C. The normal temperatures for plant growth under laboratory conditions are usually between 22-24°C. At 24°C the root length of wild type seedlings is twice the length of *sks* seedlings (figure 3.3.13) and the hypocotyl length of both *sks* and wild type seedlings were approximately the same (figure 3.3.14).

An increase in temperature from 20°C to 29°C leads to a dramatic decrease in the root length of wild type seedlings, which is coupled with a dramatic increase in hypocotyl length (figures 3.3.13 and 3.3.14). However, at all growth temperatures the root length of *sks* is approximately half that of wild type seedlings (figure 3.3.13). The hypocotyl length of *sks* grown in the light at 24°C does not differ significantly from wild type and both WT and *sks* hypocotyls are two fold shorter than those grown at 20°C, but at 29°C the hypocotyl length of *sks* is a four fold shorter than that of wild type seedlings (figure 3.3.14). The failure of *sks* hypocotyls to elongate at high temperatures

may indicate that *sks* seedlings have a finite capacity for cell elongation and/or altered auxin levels or distribution as all hypocotyl growth occurs primarily by cell elongation under the control of auxin.

Seedlings grown in the dark exhibit dramatically increased hypocotyl cell elongation compared to hypocotyls grown in the light (Gray *et al*, 1998). To investigate whether *sks* has defects in elongation in the dark, WT and *sks* seedlings were grown in the dark for 7 days at 20, 24 or 29°C and the root and hypocotyl lengths were then measured.

The growth temperature does not affect the root and hypocotyl elongation of seedlings that are grown in the dark to the same extent as seedlings that are grown in the light. Root lengths of 12-15mm are obtained at all growth temperatures when wild type seedlings are grown in the dark (figure 3.3.15). The root length of *sks* seedlings follows a similar growth pattern to that of wild type seedlings when grown in the dark, however at 29°C the root length of *sks* is half that of wild type (figure 3.3.15).

The hypocotyls of wild type seedlings grown in the dark elongate 10 fold compared to those grown in the light at 24°C, four fold when grown at 20°C and elongate to twice the length of those grown in the light at 29°C (figures 3.3.14 and 3.3.16). The hypocotyls of *sks* grown in the dark for 7 days are approximately the same length at 20°C and show a two to three fold decrease in elongation compared to wild type seedlings grown in the dark at 24 and 29°C (figure 3.3.16). However, dark grown *sks* seedlings show a four fold increase in hypocotyl elongation compared to *sks* seedlings grown in the light at 24 and 29°C (figures 3.3.14 and 3.3.16).

In summary, the *sks* mutant is impaired in both dark and light hypocotyl and root elongation. The roots of *sks* seedlings grown in the dark show a fairly wild type response but only as a result of the inhibition of wild type root elongation in the dark. The hypocotyls of dark grown *sks* seedlings show increased elongation compared to those grown in the light, but their elongation is still reduced compared to wild type seedlings.

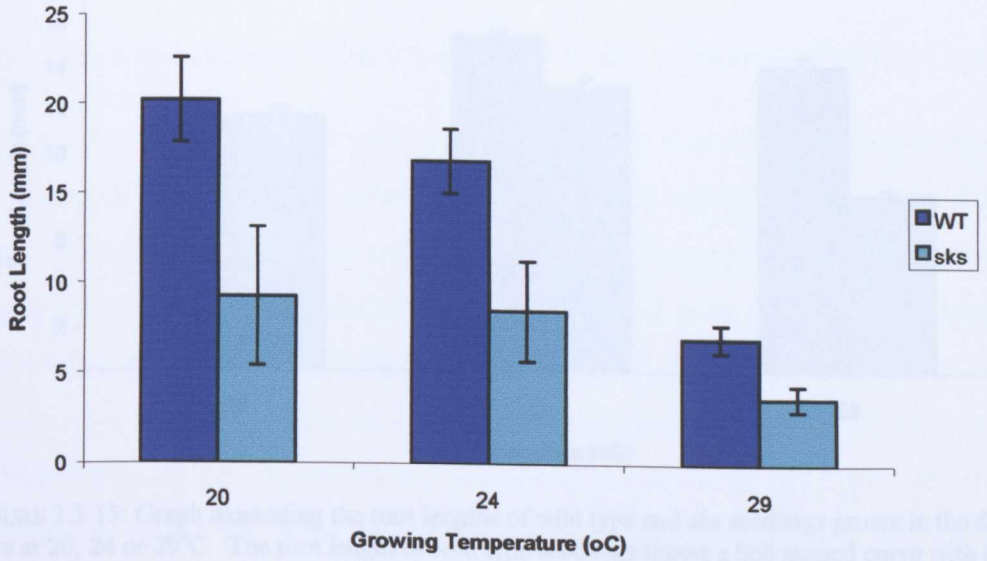

FIGURE 3.3.13: Graph of the length of wild type and *sks* roots when grown in the light at 20, 24 and 29°C for 7 days. Wild type root length decreases as the temperature increases, with root length at 29°C being half the length of roots at 20°C. The root length of *sks* follows this general trend but, their initial root length at 20°C is half that of wild type roots.

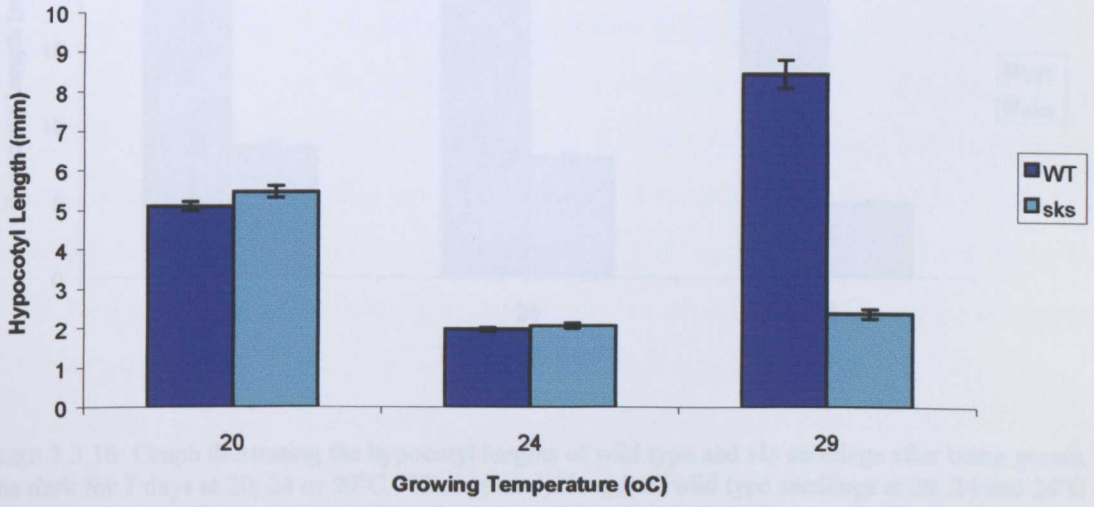

FIGURE 3.3.14: Graph illustrating the hypocotyl length of wild type and *sks* seedlings grown in the light for 7 days at 20, 24 or 29°C. In wild type seedlings the hypocotyl lengths are shortest at 24°C, increases 2 fold at 20°C and at 29°C the hypocotyl length increases by 4 fold. In *sks* seedlings the hypocotyl length remains at approximately the same length at 24 and 29°C but increases in length 2 fold at 20°C.

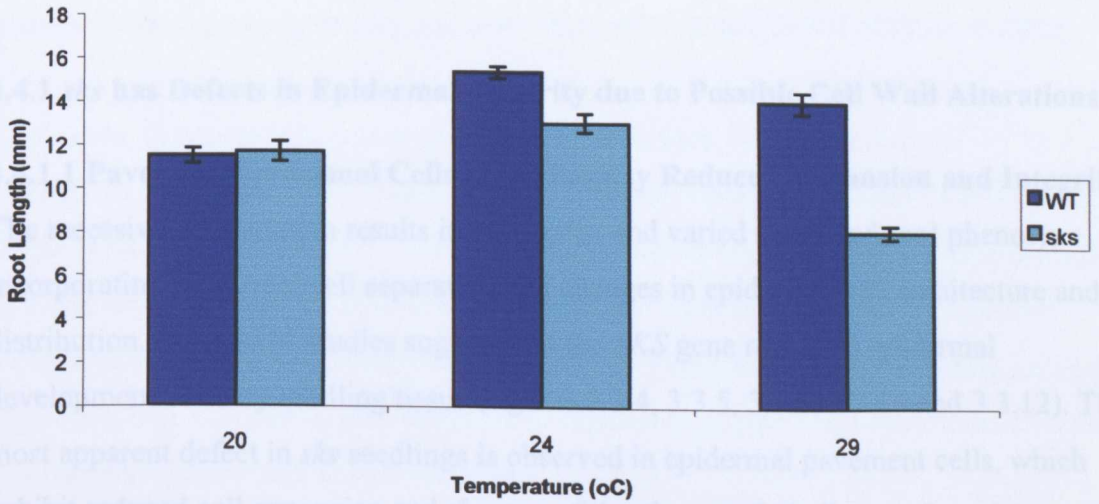

FIGURE 3.3.15: Graph illustrating the root lengths of wild type and *sks* seedlings grown in the dark for 7 days at 20, 24 or 29°C. The root length of wild type seedlings shows a bell shaped curve with the maximum root length at 24°C. The root lengths of *sks* seedlings also show a similar response but the root lengths at 24 and 29°C are slightly shorter.

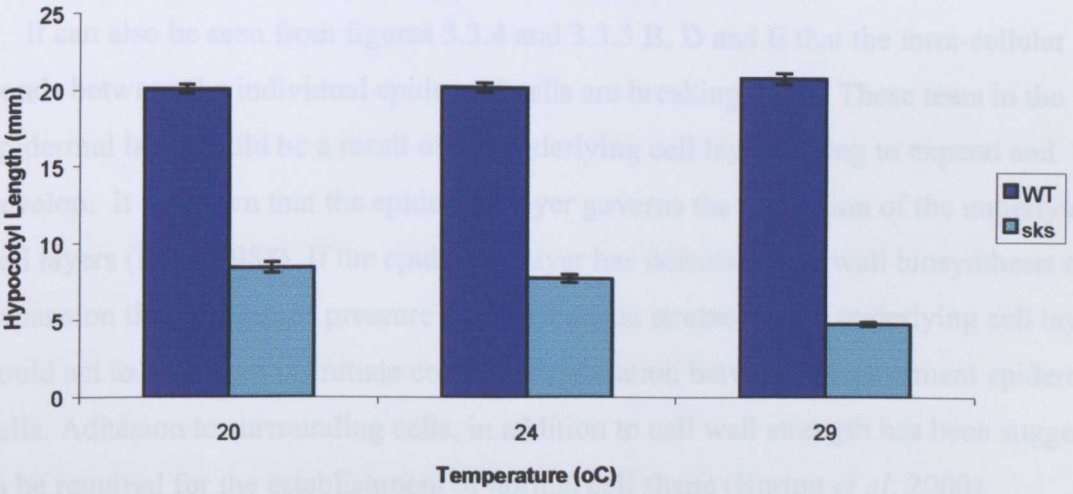

FIGURE 3.3.16: Graph illustrating the hypocotyl lengths of wild type and *sks* seedlings after being grown in the dark for 7 days at 20, 24 or 29°C. The hypocotyl length of wild type seedlings at 20, 24 and 29°C remains the same at all temperatures. The *sks* hypocotyl length is half the length of wild type hypocotyls at 20°C and decreases as the growth temperature increases further.

3.4 DISCUSSION

3.4.1 *sks* has Defects in Epidermal Integrity due to Possible Cell Wall Alterations

3.4.1.1 Pavement Epidermal Cells of *sks* Display Reduced Expansion and Integrity

The recessive *sks* mutation results in a complex and varied shoot and root phenotype incorporating epidermal cell separation and changes in epidermal cell architecture and distribution. Cryo-SEM studies suggest that the *SKS* gene regulates epidermal development of every seedling tissue (figures 3.3.4, 3.3.5, 3.3.8, 3.3.10 and 3.3.12). The most apparent defect in *sks* seedlings is observed in epidermal pavement cells, which exhibit reduced cell expansion and absence of the characteristic jigsaw shaped epidermal cell lobes. It has been suggested that the jigsaw shape of epidermal cells represents a reserve of wall substance that is used up as the leaf expands (Dale, 1988). If this is the case then it is possible that the epidermal cells of *sks* seedlings (figure 3.3.4 and 3.3.5 B, D and E) have expanded to their maximum and cannot replace or expand their cell walls further and so adopt a cuboid shape.

It can also be seen from figures 3.3.4 and 3.3.5 B, D and E that the intra-cellular bonds between the individual epidermal cells are breaking down. These tears in the epidermal layer could be a result of the underlying cell layers trying to expand and develop. It is known that the epidermal layer governs the expansion of the underlying cell layers (Dale, 1988). If the epidermal layer has defects in cell wall biosynthesis or expansion then the turgor pressure and mechanical stresses in the underlying cell layers could act to pull apart or initiate cell wall degradation between the pavement epidermal cells. Adhesion to surrounding cells, in addition to cell wall strength has been suggested to be required for the establishment of normal cell shape (Burton *et al*, 2000).

The *spike1-1* (*spk1-1*) mutant also displays defects in epidermal cell-cell adhesion and epidermal cell expansion similar to that of the *sks* mutant (Qiu *et al*, 2002). Analysis of the cell wall composition and ultrastructure of *spk1-1* revealed no differences to that of WT. To account for the epidermal cell defects it was suggested that the reduction in interdigitation of unlobed cells and subtle cell wall defects led to the failure of epidermal cells to withstand the forces of organ expansion (Qui *et al*, 2002). Increased numbers of epidermal cells were also found in the cotyledons of *spk1*, it was proposed that this was a secondary response to defective cell expansion or

adhesion. The ability of adjacent cells to "sense" and compensate for the reduced growth of slow-growing sectors has been observed in maize leaves (Qui *et al*, 2002).

3.4.1.2 *sks* Trichome Morphology Infers a Secondary Cell Wall Defect

Cryo-SEM studies of *sks* trichomes revealed that they lack papillae and have a smooth surface (figure 3.3.10 C and G, D and H). The smooth *sks* trichomes could be a result of a cell wall defect that is similar to that of the *tbr* trichomes that lack a cellulosic secondary cell wall (Potikha and Delmer, 1995). If the basis for *sks* trichomes lacking papillae is cell wall based, then the reduced expansion of pavement epidermal cells due to a cell wall defect may be corroborated.

A variety of mutants have been isolated in *Arabidopsis* that display similar epidermal cell phenotypes to *sks* in one or more of their organs, these mutants have been characterised and are often cell elongation, cell division or cell wall mutants. The *kor* mutant is cellulose deficient resulting in reduced cell elongation and irregular epidermal cell shape (His *et al*, 2001) and the *keule* mutant is cytokinesis defective and results in bloated epidermal cells similar to that of *sks* (Assad *et al*, 2001).

3.4.2 The *sks* Mutation Results in Reduced Cell Expansion and Increased Division

3.4.2.1 Increased Stomatal Division in *sks* Compensates for Reduced Cell Expansion

The defects in *sks* epidermal pavement cell architecture results in altered stomatal morphology and distribution. Many stomatal complexes in the epidermis of *sks* seedlings are found to be located next to one another (figure 3.3.5 D and F); this may be due to the disruption of cell-cell signalling processes that govern stomatal patterning. However, divisions in a stomatal complex lineage are important for producing not only stomatal complexes but also the majority of cells in the foliar epidermis (Geisler *et al*, 2000).

Expression of the *AtPME15*::GUS marker in *sks* seedlings has indicated an increase in stomatal complexes present in the cotyledon epidermis (figure 3.3.6) that leads to an increase in stomatal density and stomatal index. It is known that each asymmetric division in the development of a stomatal complex results in a larger sister cell that rejoins the pool of epidermal pavement cells (Geisler *et al*, 2000). If this is the case,

then increasing the number of stomatal complexes in the epidermis of *sks* could be a compensatory mechanism for limited expansion of *sks* epidermal cells resulting in a concurrent increase in pavement epidermal cells.

The *ATML1* gene encodes a transcription factor of the homeodomain-*GLABRA2* class that is expressed specifically in the L1 layer (Lu et al, 1996). The *Arabidopsis PROTODERMAL FACTOR1* (*PDF1*) gene has high homology to *ATML1* and is also expressed specifically in the L1 layer (Abe *et al*, 2003). Both *ATML1* and *PDF2* contain a cis-regulatory element known as the L1 box that is required for L1-specific gene expression (Abe et al, 2003). When an *atml1 pdf1* double mutant was created the resulting homozygous seedlings were found to lack an epidermal layer indicating that both *PDF2* and *ATML1* are required to activate L1-specific genes through interaction of the L1 box and therefore trigger epidermal cell differentiation (Abe *et al*, 2003).

Both the *AtML1*::GUS (figure 3.3.11) and *CyclinB1*::GUS markers (figure 3.3.7) have been found to be highly up-regulated in the apical meristems, new leaves and in the cotyledon epidermis of *sks* seedlings indicating that there is increased expression of L1 specific genes in conjunction with an increase in mitotic division. This results in an increase in epidermal differentiation and cell recruitment in the L1 layer resulting in an increased number of stomatal complexes and pavement epidermal cells. Recruitment of protodermal cells to various epidermal cell fates is competitive and an increase in one cell type, such as stomata leads to a decrease in other cell types, such as trichomes (Glover *et al*, 2000). Although trichome numbers have not been determined for *sks* leaves, fewer trichomes have been seen to be initiated in the new leaves emerging from the apical meristem (figure 3.3.10 B and F)

3.4.2.1 Increased *sks* Hypocotyl Cell Division Compensates for Limited Expansion

In *Arabidopsis*, hypocotyl growth during normal development occurs primarily by cell expansion without cell division (Gendreau *et al*, 1997). Although the length of the *sks* hypocotyl is equal to that of WT at 24°C (figure 3.3.6.2), the hypocotyl cells of *sks* seedlings show a 2-fold decrease in length and a 2-fold increase in hypocotyl cell number compared to WT. This was shown by cryo-SEM studies where irregular cell divisions were seen in *sks* hypocotyl cells and the cells were no longer arranged in distinct cell files, hypocotyl cells were also seen to have lost cell-to-cell adhesion resulting in gaps in the hypocotyl epidermis (figure 3.3.12 B, D and E). Both the *CyclinB1*::GUS marker (figure 3.3.7 B & D) and the *AtML1*::GUS marker (figure 3.3.11)

indicated that increased epidermal cell division is occurring in the *sks* hypocotyl where it meets the shoot. This is indicative that *sks* hypocotyl epidermal cells have a defect in cell elongation that results in increase in cell division as a compensation mechanism to achieve limited hypocotyl growth.

However when *sks* seedlings are grown under conditions of stress like high temperature or limited light availability hypocotyl elongation is limited. Under growth conditions of high temperatures of 29°C *sks* hypocotyls failed to elongate indicating that *sks* hypocotyls have a limited capacity for elongation (figure 3.3.14). This temperature induced growth response depends on auxin and primarily occurs by cell elongation and not cell division. When grown in the dark the hypocotyls of *sks* seedlings show increased elongation compared to when grown in the light, but their elongation is still greatly reduced compared to WT seedlings (figure 3.3.16).

Many mutants involved in hypocotyl elongation have been identified but the *procuste1* (*prc1*) mutant is particularly interesting. The *prc1* mutant hypocotyl when grown in the dark has epidermal cells that are a very irregular shape, some being swollen and others compressed, giving the hypocotyl a highly irregular surface (Desnos *et al*, 1996). The roots of *prc1* seedlings are slightly shorter and many epidermal cells are swollen. This phenotype has been found to be completely reversible in the light indicating that this mutation is a developmentally regulated process (Desnos *et al*, 1996). The *mur1* mutant is deficient in L-fucose and has a short deformed hypocotyl phenotype in dark grown conditions also similar to *prc1*, indicating that cell wall structure and biosynthesis are important in elongation processes (Desnos *et al*, 1996).

3.4.3 Conclusions

It can be concluded that that *sks* seedlings have severe altered epidermal cell architecture and distribution changes that may have basis in a cell wall defect. *snakeskin* seedlings also display cell elongation and division defects in their hypocotyls, roots and pavement epidermal cells. Growth processes i.e. elongation and division are co-ordinated within an organism by growth substance signalling. This creates an interaction between cellular and whole-organ behaviour and can allow cells to compensate for impaired cell expansion by increasing cell division (Beemster *et al*, 2003).

4.0 The *sks* Mutant Exhibits Altered Cell Wall Composition

4.1 INTRODUCTION

The importance of the plant cell wall in plant cell morphology, cell expansion and cell-to-cell communication cannot be over emphasised. Phenotypic characterisation of *sks* indicates that the mutant displays reduced epidermal cell-to-cell adhesion that may be due to a defect in cell expansion. A change in the ability of a cell to expand may be attributed to a defect in the cell wall surrounding it. This chapter describes the characterisation of the cell wall of *sks* and reveals that this mutant has alterations in its pectin and cellulose-xyloglucan components.

4.1.1 Structure of the Primary Cell Wall

The primary cell wall comprises of a cellulose-xyloglucan framework which comprises about 50% of the wall mass that is embedded within a matrix of pectic polysaccharides (about 30% of the total mass). The components of each of these domains can change independently depending on the developmental state or in response to stress. Cellulose is regarded as being the major load-bearing polymer in the wall (Zablackis *et al*, 1995). Cellulose microfibrils are several dozen linear chains of (1-4)-β-linked D-glucose that are condensed to form long crystals that wrap around each cell (Cosgrove, 1997). In dividing cells the microfibrils are wound round each cell randomly and this pattern is continued during isodiametric expansion. When cell elongation commences, the microfibrils are wound transversely in a shallow helix around the longitudinal axis of the cell (Carpita and Gibeaut, 1993).

Xyloglucan (XG) has a carbohydrate backbone structurally similar to cellulose with linear chains of (1-4) linked β-D-glucan residues with mono- di- and tri-saccharide side chains containing xylose units linked to the O-6 position of the glucosyl units (Fry, 1989). The basic repeating unit of XG is of α-D-xylosyl attached to the O-6 position on three adjoining glucosyl units interspersed by a single unbranched glucosyl residue (Fry, 1989).

β-D-galactose and occasionally α-L-arabinose residues are added to the O-2 of some xylose units and any of the galactose residues have an α-L-fucose to the O-2 position to give a trisaccharide sidechain (Fry, 1989). A few of the trisaccharide sidechains are

substituted further with another α-L-fucosyl-(1-2)-β-D-galactosyl unit to form an undecasaccharide (Carpita and Gibeaut, 1993). The monosaccharide side chains maintain the solubility of XG, the disacaccharide sidechains containing xylose and galactose prevent the self association of XG and the fucosylated sidechain has been implicated in cellulose binding (Levy *et al*, 1997).

As the structure of cellulose and xyloglucan are very similar it leads to strong hydrogen-bond interactions between the two polymers and the creation of a strong 3-D network. Only one surface of the linear XG backbone is able to bind tightly to the surface of the cellulose microfibril as the xylosyl units prevent the stacking of the glucan chains (Levy *et al*, 1991). As the primary cell wall contains approximately equal amounts of XG and cellulose, not all of the XG can bind to the cellulose microfibrils. Xyloglucan binds tightly to the exposed faces of glucan chains in the cellulose microfibrils through the folding of the fucosylated trisaccharide side chain and also interlocks with other XGs to space and lock the cellulose microfibrils into place (Levy *et al*, 1997).

The cementing of cells to one another depends not only on the interaction between pectin molecules but also on the interactions between pectin and other cell wall components. Complexes of pectin, xylan and xyloglucan have been reported in the cell walls of cauliflower (Feminia *et al*, 1999). The covalent bonds that hold XG in the cell wall include glycosidic linkages to the side chains of pectin, ester bonds to the carboxyl groups of pectin and benzyl-sugar ether bonds to polysaccharide bound dimers of ferulic acid and related phenolics (Fry, 1989).

The pectins are a group of three polysaccharides known as polygalacturonic acid or homogalacturonan, rhamnogalacturonan I (RG-I) and RG-II. Pectic polysaccharides are the most abundant matrix components of the primary cell walls of flowering plants (Jarvis, 1984) and appear to have roles in the control of cell wall ionic status and porosity, cell-to-cell adhesion, cell expansion and signalling (Willats *et al*, 2000).

Homogalacturonan consists of helical chains of 100-200 (1-4)linked-α-D-galactopyranosyluronic acid (Gal*p*A) residues in which some of the carboxyl groups are methyl-esterified (Ridley *et al*, 2001). Rhamnogalcturonan I (RG-I) is a heteropolymer of 100 repeating (1-2)α-L-rhamnosyl-(1-4)α-D-Gal*p*A disaccharide units. The rhamnosyl units can be substituted at C-4 with α-L-arabinofuranosyl and/or β-D-galactopyranosyl residues (Ridley *et al*, 2001). The backbone of RG-II is composed of

1,4-linked α-D-Gal*p*A residues with nonasaccharide and octasaccharide sidechains attached to C-2 of some backbone residues and disaccharides attached to C-2 of other backbone residues (Ridley *et al*, 2001).

Homogalacturonan is believed to be synthesised in a highly esterified form but is subsequently de-esterified by the action of pectin methylesterases which can remove methyl groups in a blockwise or random fashion (Willats *et al*, 2000). Homogalacturonan rich pectin is commonly found in the middle lamella region of the wall where two adjacent cells abut (Atkinson *et al*, 2002). The helical chains of unbranched, de-esterified PGAs can condense by non-covalent Ca^{2+} crosslinking to form junction zones and strengthen the middle lamella (Jarvis, 1984). The helical chains of PGA are not twisted together but are held alongside one another where they can run parallel or anti-parallel to one another (Jarvis, 1984).

Homogalacturonan could be crosslinked to other components by uronyl esters and up to ~2% of the galacturonic acid residues could be cross-linked in this way. It has recently been suggested that pectin methylesterases could catalyse a transesterification reaction using methylesterified HGA as a donor substrate and other HGA molecules as an acceptor substrate (Gelineo-Albersheim *et al*, 2001). Homogalacturonan and RG-II are likely to be covalently linked to one another through association of their 1-4-linked a-D-GalpA backbone but it is not known how RG-I is associated with other pectins (Ridley *et al*, 2001).

The inter-junction pectin segments are usually RG-I pectins and carry ester-groups that prevent calcium binding or possess side chains that prevent aggregation (Jarvis, 1984). The neutral oligosaccharide or polysaccharide chains such as arabinans, galactans and aribinogalactans (Knox *et al*, 1990) are attached to the O-4 of many of the rhamnosyl residues on RG-I (Carpita and Gibeaut, 1993). The arabinose-rich side chains of RG-I and are thought to be involved in intercellular attachment and may be associated with cellulose-hemicellulose complexes through covalent crosslinks (Iwai *et al*, 2001). Methyl esterified primary cell wall pectins like those of RG-I form a network that is co-extensive with, but independent of the cellulose/hemicellulose network (McCann *et al*, 1992).

Rhamnogalacturonan II (RG-II) consists of a relatively short galacturonan backbone with side chains and has an extremely complex composition of glycosyl linkages and sugars (Willats *et al*, 2000). There are four structurally different oligosaccharide chains formed from galacturonic acid, rhamnose, apiose, glucuronic acid, 2-*O*-Me-xylose, 2-*O*-

Me-fucose, galactose, arabinose, aceric acid, 3-deoxy-D-*manno*-2-octulosonic acid, 3-deoxy-D-*lyxo*-2-heptulosaric acid and fucose (Iwai *et al*, 2002). RG-II forms dimers by di, di-ester crosslinks in association with boron between two apiosyl residues in the 2-*O*-Me-xylosyl-containing side chains with Ca^{2+} to promote and stabilise this complex (Kobayashi *et al*, 1999 and Iwai *et al*, 2002). RG-II is thought to be an integral part of HGA and borate-diol esters can crosslink two HGA chains leading to an important role in intercellular attachment and secondary wall structure or assembly (Iwai *et al*, 2002 and Ryden *et al*, 2003).

Pectins may also be linked to one another by various covalent bonds including ester linkages through phenolic dimers such as diferulic acid (Fry, 1983). Cell wall phenols readily undergo oxidative coupling reactions and may play an important structural role by crosslinking the polymers to which the phenols are bound (Fry, 1983). Crosslinking of phenolic groups in the wall such as HRGPs, ferulate residues attached to pectin and lignin precursors is believed to be mediated by a wall-bound peroxidase in the outer epidermal wall and plays a major role in wall stiffening and maturation (Schopfer, 1996). The feruloyl sugars involved in phenolic crosslinking are found in the L-arabinose and D-galactose side chains of XG, rhamnogalacturonan I (RG-I) and RG-II pectin (Fry, 1983). It has been suggested that peroxidase-catalysed coupling of pectin bound phenols would increase the tendancy of pectins to bind tightly in the cell wall, restrict cell expansion and they may also have a role in intracellular attachment (Fry, 1983).

In addition to polysaccharides plant cell walls contain many proteins, glycoproteins and proteoglycans. Some of these apoplastic proteins are involved in modification of the cell wall during growth processes, fruit ripening or abscission. Others play structural roles and are classified as glycine rich proteins (GRPs) and hydroxyproline rich glycoproteins (HRGPs). The HRGPs are a superfamily encompassing arabinogalactan-proteins, extensins and repititive proline-rich proteins. The arabinogalactan proteins are not tightly associated with the cell wall and are therefore considered apoplastic polymers rather than true cell wall components (Reiter, 1998) and extensins form a network that may have a role once growth has ceased (McQueen-Mason, 1995).

Although the structures of the various pectin constituents are largely known it is unclear how these structural elements are combined into a macromolecular structure (Vincken *et al*, 2003). However, a new model of pectin structure has recently been

proposed where the HGA is depicted as a side chain of RG-I found in various conformations perpendicular to the backbone (Vincken *et al*, 2003). The types and distributions of RG-I sidechains have not been determined and the side chains may consist of only one type, random distributions, cluster-like distributions of the same type or cluster-like distributions of different types (Vincken et al, 2003).

This model is in contrast to a model where pectins are branched blocks where the main HGA chain is interrupted and bent by RG-I and RG-II pectins carrying rhamnose units, many of which carry side chains, and unbranched blocks where rhamnose units are absent or spaced about 25 units apart (Jarvis, 1984). In the branched blocks both arabinan and galactan chains are attached to rhamnose and further arabinan chains may be present on the galactan chains (Jarvis, 1984).

4.1.2 Cell Wall Maturation and Secondary Cell Wall Formation

Growth cessation during cell maturation is generally irreversible and is accompanied by a reduction in wall extensibility. These physical changes in the wall may come about by a reduction in the wall loosening process, an increase in wall cross-linking or an alteration in the composition of the wall, making it more rigid or less susceptible to wall loosening (Cosgrove, 1997). The primary strategy available for a cell wall to modulate its mechanical strength is for it to control the levels of cellulose (Whitney *et al*, 1999). It has been suggested that the orientation of the cellulose microfibrils establishes the final cell shape, whereas the dynamic interaction of cellulose and the polysaccharide matrix governs the rate of cell expansion and the extent that the microfibrils are pulled apart (Carpita and Gibeaut, 1993).

Extensive crosslinking of cellulose by XG leads to decreased stiffness and increased extensibility when compared to cellulose alone (Whitney *et al*, 1999). This implies that the crosslinking XGs are the principal tension bearing molecules in the longitudinal axis of an elongating cell. Hydolysis or dissociation of the XGs from cellulose microfibrils allows the helically arranged microfibrils to be pulled apart in the long axis and is considered to be the rate limiting step for growth (Carpita and Gibeaut, 1993). The pectin network has also been implied to have a role in the strength of the cell wall (Whitney *et al*, 1999) and a reliable model of the organisation of pectins with the cellulose- xyloglucan framework is needed to understand how dissociation of XG from cellulose is controlled (Carpita and Gibeaut, 1993).

Pectin may act as physical barriers between XG and xyloglucanase. A drop in the pH or a change in the charged environment could alter localised pore size and could then allow access of the hydrolase to the substrate (Carpita and Gibeaut, 1993). Expansins have been implicated in the acid growth response of plant cell walls and they may cause wall creep by loosening non-covalent bonds between wall polysaccharides. It has been suggested than expansins act at the interface between cellulose and one or more hemicelluloses. 1-4 β-glucanases have also been implicated in the cell wall loosening process, especially during auxin-induced cell elongation. It is possible that endogenous wall hydrolases or transglycosolases might enhance wall expansion by making the wall more sensitive to expansin-induced creep.

Once elongation is complete the primary cell wall is locked into shape. One component of the locking mechanism may be the hydroxyproline-rich glycoprotein extensin (McQueen-Mason, 1995). Formation of an extensin-cellulose framework may prepare the cell to stop growing and is associated with an increase in the tensile strength of the cell wall (McQueen-Mason, 1995). Other proteins may be necessary to lock the extensins together; one candidate is the repetitive proline-rich protein (PRP). These proteins are more highly expressed later in cell development and have been found in the same vascular cells as extensin (Carpita and Gibeaut, 1993).

Several modifications of the maturing cell wall may contribute to wall rigidification. Newley secreted matrix polysaccharides may be altered in structure so that they form tighter complexes with cellulose or other wall polymers or they may be resistant to wall-loosening activities. (1-4)-β-D-xylosyl residues lose their arabinose sidechains and becomes less branched during coleoptile maturation resulting in tighter hydrogen bonding between XG and cellulose (Carpita, 1984). During growth cessation in dicotyledons pectin becomes de-esterified leading to a more rigid pectin gel (McCann *et al*, 1994).

Formation of a secondary cell wall occurs in a fully expanded cell between the primary cell wall and the plasma membrane (Cano-Delgado *et al*, 2000) and may differ from primary walls in both composition and architecture (McCann *et al*, 1990). Secondary wall formation is restricted to specialised cells and provides additional mechanical strength and rigidity to support aerial structures and hydrophobicity for transport functions. Actin may be involved in secondary wall deposition; as wall thickening commences, the alignment of the actin filaments changes to become parallel to the thickening (Gardiner *et al*, 2003). Sucrose synthase is thought to supply UDP-

glucose as a substrate to cellulose synthase and has been found to localise to regions of cell wall thickening and binds to actin (Gardiner *et al*, 2003).

The process of secondary cell wall formation can also involve the deposition of lignin by the polymerisation of monolignol precursors after polysaccharide deposition (Ilyama *et al*, 1994). Lignin deposition is initiated at the cell corners, moves to the middle lamella and then proceeds throughout the primary cell wall into the secondary wall. The hydrophobic lignin replaces the water in the wall and encrusts the cellulosic, non-cellulosic polysaccharides and the protein components allowing covalent crosslinking and cell wall strengthening (Ilyama *et al*, 1994).

4.1.5 Generation of Intracellular Spaces

Cells within plants are normally polyhedral with flat faces and distinct angles due to their need to remain attached to one another during plant development. The more the shape of a cell deviates from spherical, the stronger the tendency of turgor pressure to return it towards a spherical shape to minimise its surface to volume ratio. This can only occur by separating the cell from its two neighbours at a tricellular junction (Jarvis, 1998). The formation of an intracellular space occurs at the central point of contact between the daughter cells and the parent cell at a tricellular junction that then spreads along the middle lamella and terminates at electron dense intrawall structures (Knox, 1992).

The middle lamella between cells has been found to be more strongly attached to the edges of cell faces than to the faces themselves by calcium crosslinking of localised, weakly esterified pectins (Parker *et al*, 2001). Where a tricellular junction has opened to make way for an intracellular space, reinforcing zones with pectic polysaccharides structurally similar to those at the original tricellular junction are present along the three cell-cell-space junctions where the walls of adjacent cells diverge (Jarvis, 1998). These electron dense intra-wall structures are located in the corners of the pre-determined intercellular spaces and if intercellular space formation continued it would result in cell separation (Knox, 1992).

4.2 METHODS

4.2.1 Fourier Transform Infrared Spectroscopy

14 day-old *sks* and wild type leaves were freeze dried by immersing individual leaves in 90% (v/v) ethanol and clearing them by changing the ethanol as required. Once the leaves are cleared, the ethanol was poured off and the leaf rinsed in water. Enough water was then added so that the leaf stayed flat and the leaf was then frozen in liquid nitrogen. The samples were freeze-dried overnight and stored in sealed eppendorf tubes.

The freeze-dried leaves were flattened and were placed on a 2-mm-thick × 13-mm-diameter barium fluoride window. The windows were supported on the stage of a UMA500 microscope accessory of an FTS175c Fourier transform infrared (FTIR) spectrometer (Bio-Rad, Hemel Hempstead, UK) equipped with a liquid nitrogen-cooled mercury cadmium telluride detector. Mapping software allowed the collection of 30 FTIR spectrums from an area of 150 × 150 μm from 30 wild type and *sks* leaves. To reveal the major spectral differences between *sks* and wild type leaves, a principal component analysis (PCA) was applied to all spectra.

4.2.2 TEM and Immunogold Labelling

The preparation of the 7 day old *sks* and wild type cotyledons and hypocotyls for immunogold labelling and transmission electron microscopy was undertaken by Brian Wells (Department of Cell Biology, John Innes Institute, Colney Lane, Norwich, NR4 7UH). The protocol for embedding tissue at low temperatures is described in full by Wells, 1985.

The tissue was fixed in 2.5 % (v/v) gluteradehyde in 0.05 % (w/v) sodium cacodylate pH7.2 for 16 hours at room temperature. If the tissue floated, the trapped air was removed with a slight vacuum and the fixative was replaced. The tissue was then dehydrated in an increasing ethanol series at increasingly lower temperatures. 30 % (v/v) ethanol for one hour on ice, 50 % (v/v) ethanol for one hour at –20°C, 70 % (v/v) ethanol for one hour at –35°C, 90 % (v/v) ethanol for one hour at –35°C and 100 % ethanol for one hour at –35°C.

The tissue was then gradually infiltrated with resin over 20 hours at –20°C; the resin was LR white, medium grade with 0.5 % (v/v) benzoin methyl ester. 1:1 resin:ethanol

for one hour at –20°C, 2:1 resin:ethanol for one hour at –20°C, 3:1 resin:ethanol for one hour at –20°C, 100% resin for one hour at –20°C, 100% overnight at 20°C and 100% resin:ethanol for eight hours at –20°C.

The samples were then transferred to pre-cooled resin filled Beem capsules (TAAB), at –20°C. The resin was then polymerised with indirect UV radiation for 24 hours at –20°C and then with indirect UV radiation for 16 hours at room temperature. Thin sections (100nm) were cut on an ultramicrotome (Leica, Milton Keyes, UK) and picked up on carbon-coated and plastic-filmed gold grids.

The sections were then immunogold labelled using the antibodies JIM5 and JIM7 that are specific to pectins as outlined below. The blocking solution consists of 1% (v/v) acetylated bovine serum albumin (Aurion, Wageningen, The Netherlands) in phosphate-buffered saline pH7.4 plus 0.1 % (v/v) Tween 20, and the incubation solution for washes was 0.1% (v/v) acetylated bovine serum albumin in phosphate-buffered saline plus 0.01% (v/v) Tween 20.

The blocking solution was added to the sections for 1 hour before being removed. The first antibody was then diluted 1:5 in 0.1% (v/v) bovine serum albumin C with 0.01% (v/v) Tween 20, added to sections and left to incubate overnight at 4°C. The slides were then washed three times in phosphate buffered saline for 10 minutes. The second antibody was then diluted 1:30 in 0.1% bovine serum albumin C with 0.01% (v/v) Tween 20, added to sections and left to incubate for 3 hours at room temperature. The slides were then washed for 10 minutes with phosphate buffered saline. The slides were then fixed with 1%(v/v) gluteradehyde in 0.1M PO_4 for five minutes before being washed with water for one hour. The slides were then contrast stained with uranyl acetate for one hour, then with lead citrate for 30 seconds before being viewed with a transmission electron microscope.

4.2.3 Cell Wall Neutral Sugar Analysis

4, 7, 9 and 14-day-old *sks* and wild type seedlings were grown on square plates as described in section 3.2.2 for cell wall sugar analysis by Gillian West (Nutritional Biochemistry, University of Nottingham, Sutton Bonington Campus, Leicestershire, LE12 5RD).

4.2.3.1 Preparation of Acetone Insoluble Solids

The tissue was homogenised in 4 volumes of 100% acetone at 20°C before being filtered on miracloth. The filter was then washed with 10 volumes of 80 % (v/v) acetone at 4°C and then further washed with 10 volumes of 100% acetone at 4°C. The residue was then dried under vacuum and weighed before hydrolysation.

4.2.3.2 Acid Hydrolysis of Polysaccharides

2ml of 12M sulphuric acid was added to the dried residue and dispersed by vortexing. The residue was then left at 35°C for one hour, vortexing occasionally to disperse the cellulose. 22ml of water was then added to the residue and vortexed. Place in boiling water for 2 hours, stirring continuously and then cool to room temperature.

4.2.3.3 Gas Chromatography Determination of Neutral Sugars

To determine the quantities of the constituent sugars released by acid hydrolysis the Englyst method (Englyst *et al*, 1982) was used. 0.5ml of the internal standard (1mg allose/ml in 50 % (v/v) saturated benzoic acid) was added to 3ml of cooled hydrolysate (of a total 24ml). 1.2ml of 12M ammonium hydroxide was added, vortexed, the pH was then tested and if it was not alkaline more ammonium hydroxide was added. 0.4ml fresh 3M ammonium hydroxide containing 50mg/ml of sodium borohydrate was added, vortexed, and left for 1 hour at 40°C. 0.5ml of glacial acetic acid was then added and vortexed

0.5ml of 1-methylimidazole and 5ml of acetic anhydride was added to 0.5ml of the acidified solution, vortexed, and left for 10 minutes. 0.8ml ethanol was added, vortexed, and left for 5 minutes. 5ml of water was added, vortexed, and left for 5 minutes before the addition of 0.5ml of 0.04 % (v/v) bromophenol blue.

The solution was then placed in cold water to aid the dispersal of heat before 5ml of 7.5M potassium hydroxide was added and left for 2 minutes. A further 5ml of 7.5M potassium hydroxide was added, vortexed and then left until the solution had separated completely into two phases. The clear upper phase was transferred to a small vial for analysis by GLC, making sure that none of the lower blue phase remained. The prepared alditol acetates are stable for one week at 5°C, but for increased stability a small amount of sodium sulphate was added to the storage vials.

The GC used was a Perkin Elmer PE8500 with a Flame Ionisation Detector with a 0.32mm diameter and a 30m long BPX column made by SGE Ltd and a Perkin Elmer

LCI-100 computing integrator. The helium carrier gas was set at 10 ml/min and the temperature programme was 190°C to 230°C at 3/min followed by 5 min at 230°C.

The neutral sugars were quantified by the flowing equation:

$$\text{Total mg} = \frac{\text{Area of sugar}}{\text{Area of allose}} \times \text{response factor (0.5)}$$

4.2.3.4 Determination of Uronic Acids

0.3ml of the hydrolysate was diluted to 0.10mg uronic acids/ml with 0.3ml of a salt/boric acid solution in a 50ml tube. The salt/boric acid solution consisted of 2g NaCl and 3g of boric acid in 100mls of water.

5ml of concentrated sulphuric acid was added to the diluted hydolysate, heated at 70°C for 40 minutes and cooled to room temperature in water. 0.2ml of dimethylphenol solution was then added to the solution and vortexed. The dimethylphenol solution consisted of 0.1g of dimethylphenol in 100ml of glacial acetic acid.

After 10-15 minutes the absorbance at 400nm and 450nm were read against a water reference and the reading at 400nm subtracted from that at 450nm. The difference in absorbance obtained for glucuronic acid standards over the range of 0.025 to 0.125 mg/ml was plotted and the sample readings can then be calculated or read from the graph.

4.2.3.5 Determination of Starch

50mg of soluble starch (100mg wheat) was added to 2ml of 0.1M MES buffer, pH6.5 and 10ul of Termamyl and heated at 100oC for 1 hour, a further 10ul of Termamyl was added and heated at 90oC for a further hour.

The pH was adjusted to 4.6 using 3-5 ml of 0.1M acetate buffer pH 4.1 and 0.1ml of amyloglucosidase (Novo) was added. The acetate buffer consisted of 0.1M sodium acetate, 2M hydrogen acetate (HAc) and 1.5mM Calcium oxide (CaO_2). The solution was diluted to 100ml (250ml for soluble starch) and the glucose content was determined using the glucose oxidase method (Nicol, 1998).

4.3 RESULTS

4.3.1 FT-IR Analysis of *sks*

To investigate whether *sks* has a cell wall defect, the mutant was initially analysed by Fourier transform infrared microscopy (FT-IR). FT-IR has a wide potential for use in cell wall research as a crude but rapid chemical assay system for walls and polymers. FT-IR can detect conformational changes in wall components and detect which putative cross links may be present in the wall. The energy of molecular vibration corresponds to the infrared (IR) region of the electromagnetic region of the spectrum.

For IR radiation to be absorbed by a molecule there must be an interaction of the radiation with an oscillating dipole movement associated with a vibrating bond. The vibration must cause a change in dipole movement for the absorption to occur and so strong absorption occurs only for asymmetric bonds. Different functional groups absorb in different parts of the spectrum and so IR spectra are used for structural elucidation and frequency-structure correlation charts are common. Coupling of vibrations can lead to complicated spectra, although an important result of coupling is to produce "fingerprint" patterns in the region 1200 to 900cm^{-1}, so that even complex polymers can usually be distinguished. (McCann *et al*, 1992)

The carboxylic ester group representing partially methylated pectin absorbs at approximately 1735-1750 cm^{-1}, amide stretching bands of protein occur at 1650 and 1550cm^{-1}, carboxylic acid groups on pectins absorb at 1605-1620cm^{-1}, phenolics absorb at 1600 and 1500cm^{-1} (McCann *et al*, 1992), and crystalline cellulose absorb between 1200 and 900cm^{-1}, with peaks at 991, 1035, 1057, 1111 and 1162cm^{-1} (Schindelman *et al*, 2001 and Wilson *et al*, 2000). Bands observed at 1626 and 1420cm^{-1} are polygalacturonic acid (Manrique and Lajolo, 2002). Unfortunately peaks cannot be assigned to particular vibrational characteristics below 1500cm^{-1} as many sugar absorbances overlap in this region (Carpita and Gibeaut, 1993).

PCA is a mathematical operation that allows samples to be characterised by their scores on a small number of new variables (PC axes) instead of large numbers of original measurements (absorbancies). PCA allows you to summarise the information while highlighting the differences. The variability in each individual spectrum relative to the mean of the population can then be represented as a smaller set of values (axes) termed principal components (PCs). The effect of this process is to concentrate the sources of variability in the data into the first few PCs. Plots of the PC scores

(projected onto PC axes) against one another can reveal clustering or structure in the data set (Chen *et al*, 1998).

The IR spectra produced from wild type and *sks* leaves were analysed by PCA as shown in figure 4.3.1. The scatter plot of *sks* v wild type indicates that *sks* is different from wild type seedlings in terms of cell wall composition as wild type spectra and *sks* spectra form two distinct groups. In PCA 1 the peaks above the *x*-axis are cell wall components that have been increased in *sks* and those below the axis have been decreased. However, in PCA 3 the situation is reversed with the peaks above the *x*-axis indicating a decrease of cell wall components in *sks* and the peaks below the axis indicating an increase.

In PCA 1 peaks 1531 and 1626 relate to proteins that appear to be decreased in *sks*, however in PCA 3 peaks 1547 and 1647 indicate that other protein species have increased. It also appears that there has been alteration in the distribution of cellulose and pectin within the cell walls of *sks* seedlings. Peaks 936 and 1036 in PCA1 indicate an increase in cellulose whereas peaks 1115 and 1167 in PCA3 indicate a decrease although a positive peak associated with cellulose at 1040 can also be seen (figure 4.3.1). The peaks 1075, 1149 and 897 in PCA 1 relate to an increase in arabinan a side chain commonly attached to RG-I pectin. Peak 936 in PCA1 indicates an increase in HGA which in conjunction with the peaks 1370, 1422 and 1596 in PCA 3 indicates an increase in the carboxylate ions on PGA pectin and may be indicative of an increase in de-esterified pectin (figure 4.3.1).

To summarise, an overall increase in cellulose can also be inferred although the contradictory results may also be related to changes in cell elongation or maturation affecting the orientation of the microfibrils. Cellulose is the major load bearing polysaccharide in plant cell walls and the easiest way for a plant to modulate the strength of its cell walls is to alter its cellulose content (Whitney *et al*, 1999). It can also be deduced that there is an increase in arabinan side chains on RG-I and an increase in de-esterified homogalacturonan. Both arabinan side chains and de-esterified pectins are associated with intercellular attachment (Jarvis, 1984 and Iwai *et al*, 2002).

A.

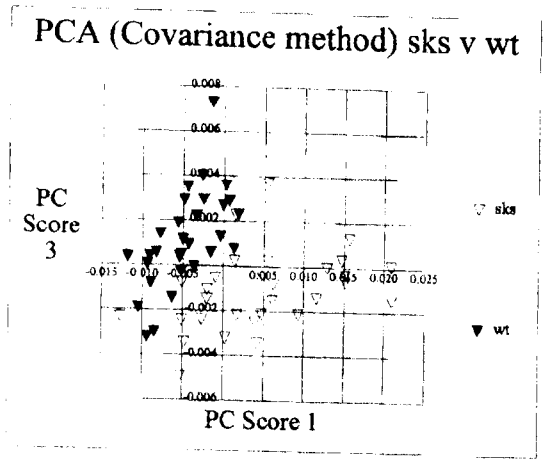

B.

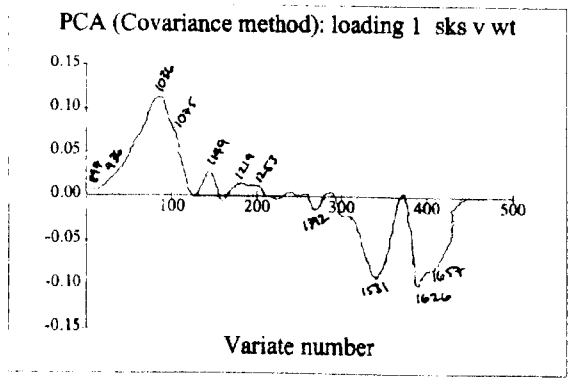

C.

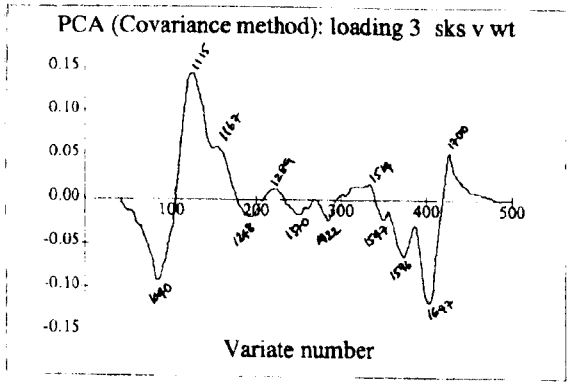

FIGURE 4.3.1: Principal component analysis of *sks* versus wild type 14-day-old leaves. 14 day-old leaves were used as many *sks* seedlings cannot survive beyond this stage and so it theoretically represents the maximum difference in cell wall composition between *sks* and WT. The PCA *sks* V WT scatter chart (A) indicates that the cell wall composition of *sks* is different from WT seedlings, as two distinct clusters of data have been formed. The PCA 1 (B) and PCA 3 (C) line graphs indicate which particular cell wall components have been altered in *sks* seedlings with the numbered peaks and troughs relating to specific increases or decreases in a specific cell wall component.

4.3.2 Immunogold Labelling of *sks* and Wild Type Cell Walls

The monoclonal antibodies JIM5 and JIM7 were used to probe pectin esterification in mutant cell walls. JIM5 reacts with pectin with a low degree of esterification (0-50%) and JIM7 reacts with pectin with a high degree of esterification (35-90%). For both JIM5 and JIM7 the degree rather than the pattern of methyl esterification appears to be the more important factor influencing binding (Knox *et al*, 1990).

TEM scans revealed no difference in immunogold labelling with JIM7 antibodies between wild type and *sks*. Gold particles labelled by JIM7 were distributed evenly throughout the cell wall of both mesophyll (figure 4.3.4) and hypocotyl epidermal cells (figure 4.3.5) of WT and *sks* seedlings. In wild type mesophyll and hypocotyl sections (figure 4.3.2 A and figure 4.3.3 A), gold particles labelled by JIM5 were located to the cell wall close to the plasma membrane, the middle lamella and to the cell corners exposed at the intercellular spaces (Knox *et al*, 1990). However, in *sks* hypocotyl sections (figure 4.3.4.B) JIM5 is localised throughout the primary wall and is not limited to the cell wall close to the plasma membrane, the middle lamella and to the cell corners.

The immunogold labelling of *sks* with the JIM7 antibody indicates that the distribution of methylesterified pectins that are intercalated with the hemicellulose/cellulose network are unaffected. However labelling of *sks* hypocotyl sections with the JIM5 antibody indicates that de-esterified pectins that are involved in calcium crosslinking and strengthening of the cell wall are not just at the intercellular junctions and middle lamella but localised throughout the cell wall. This suggests that the *sks* mutation may have defects in cell wall adhesion or strength.

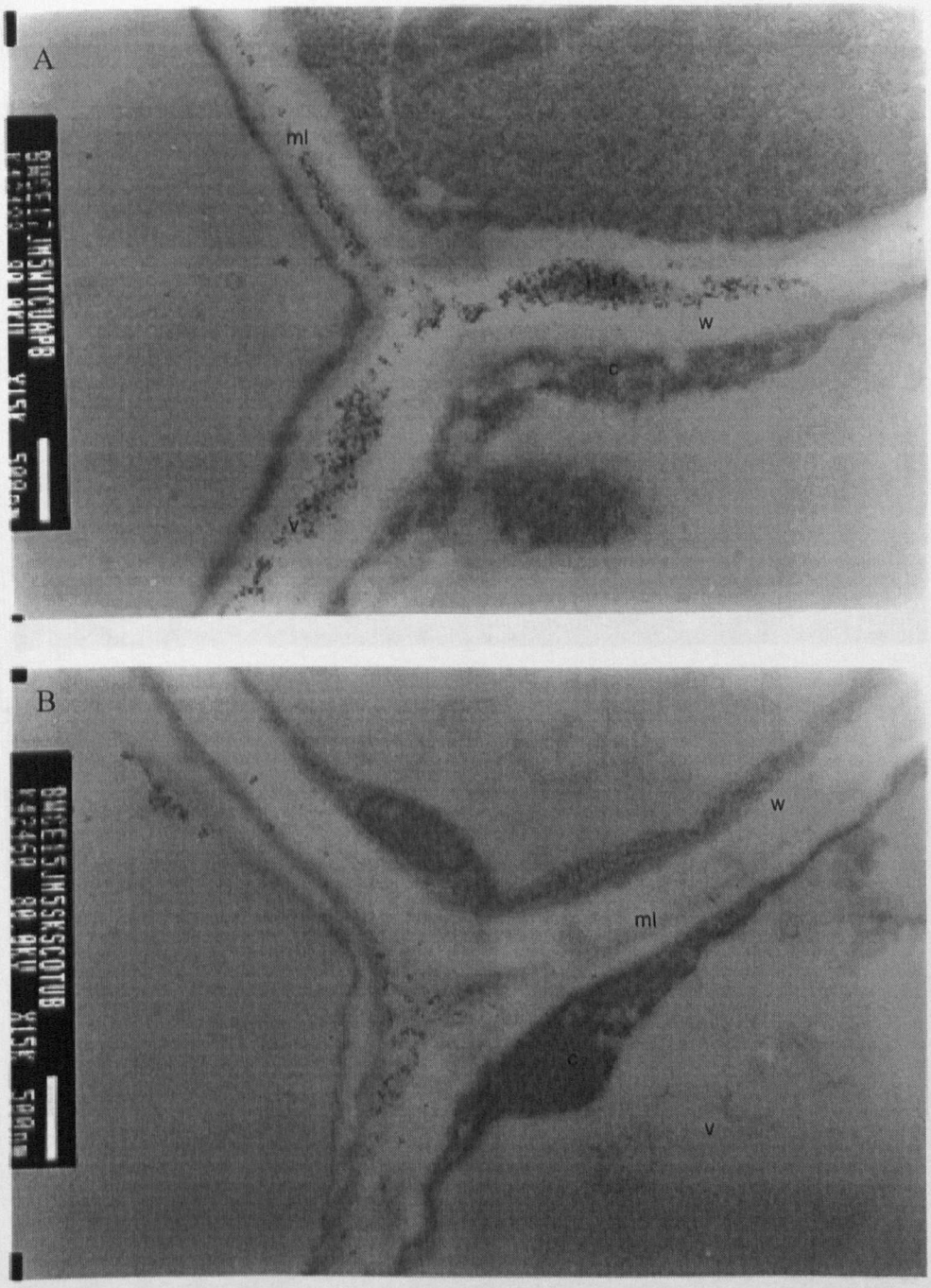

FIGURE 4.3.2: TEMs of 7-day-old wild type (A) and *sks* (B) cotyledon showing the junction between two epidermal cells and an underlying mesophyll cell. The cell walls have been immuno-labelled with JIM5 antibody that is specific to de-esterified pectin. Labelling extends slightly further into the cell wall of WT cotyledons (A) than can be seen in *sks* cotyledons, but no real labelling differences can be seen. c, cytoplasm; v, vaculole; ml, middle lamella; w, cell wall; is, intercellular space.

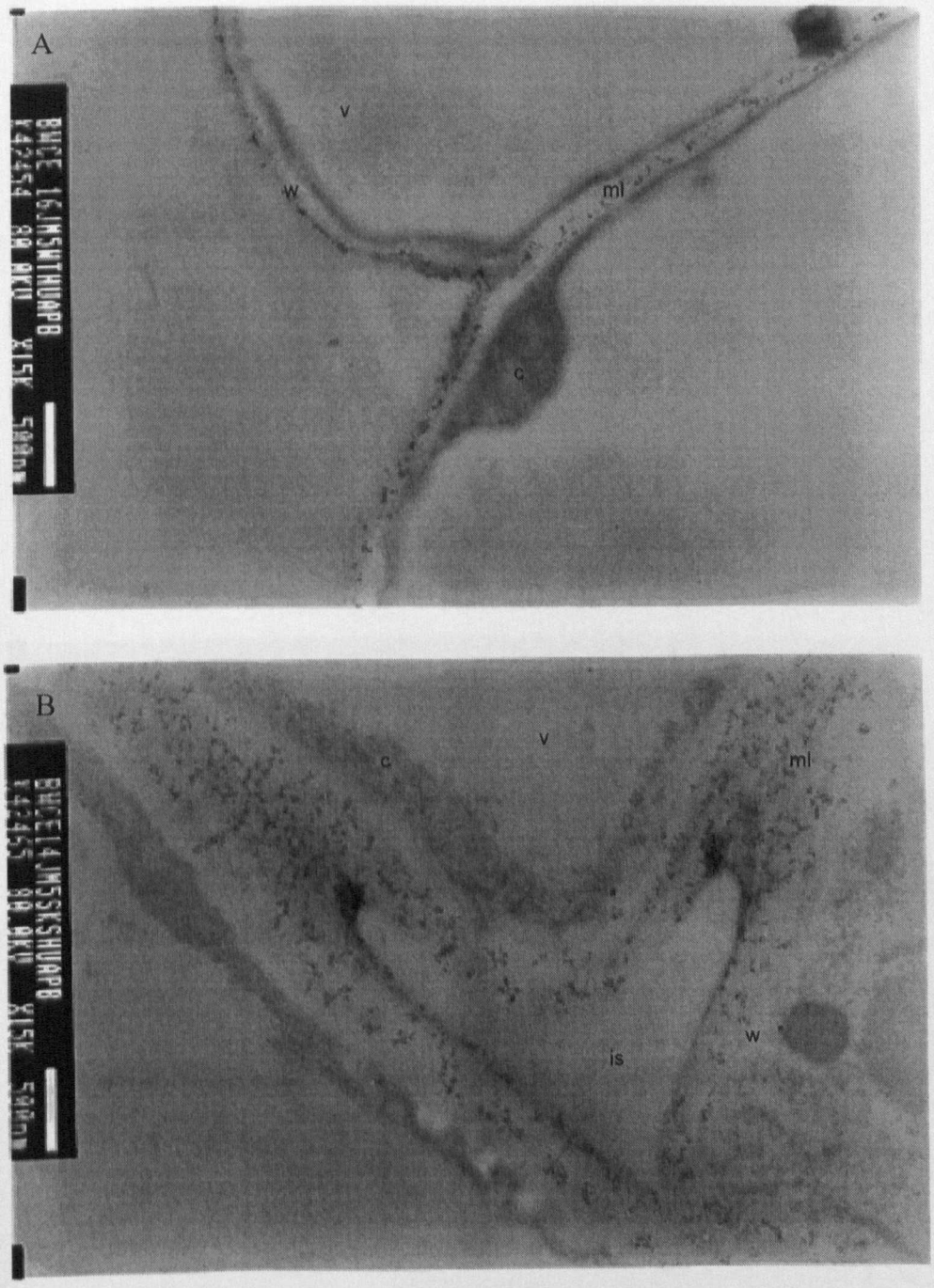

FIGURE 4.3.3: TEMs of 7-day-old wild type (A) and *sks* (B) hypocotyls showing the junction between two epidermal cells and an underlying cortical cell. The cell walls have been labelled with the JIM5 antibody that is specific to de-esterified pectin. In WT hypocotyl cells (A) the JIM5 labelling is confined to the middle lamella and the cell corners where it is involved in calcium crosslinking and cell wall strengthening. However, in *sks* hypocotyls (B) JIM 5 labelling extends throughout the cell wall, not just in the middle lamella or the cell corners; this indicates that there may be an increase in cell wall strengthening. c, cytoplasm; v, vacuole; ml, middle lamella w, cell wall; is, intercellular space.

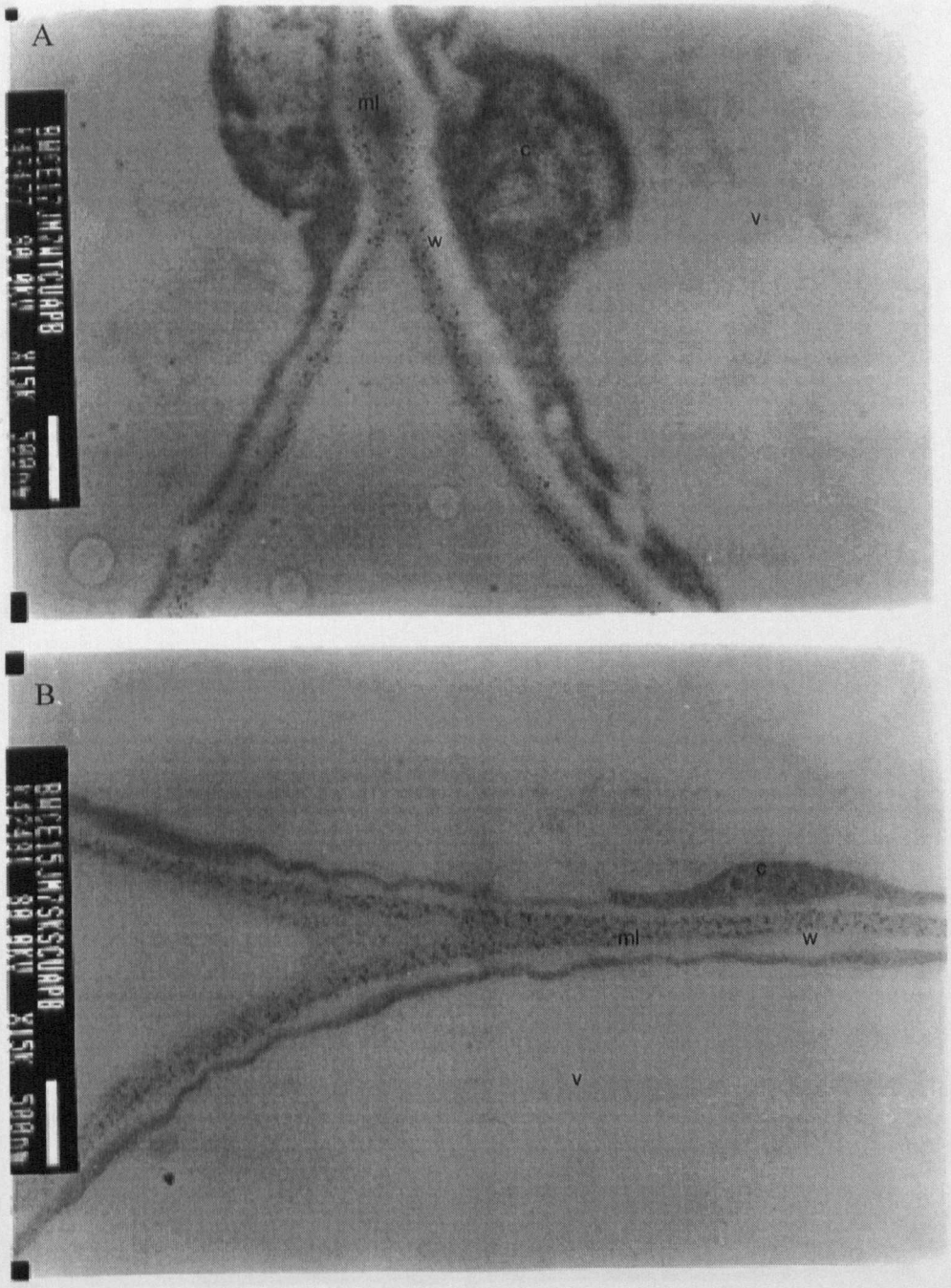

FIGURE 4.3.4: TEMs of 7-day-old wild type (A) and *sks* (B) cotyledons showing the junction between two epidermal cells and an underlying mesophyll cell. The cell walls have been labelled with JIM7 antibody that is specific for methyl-esterified pectin, this label is found throughout the cell wall of both WT (A) and sks (B) coyledons. c, cytoplasm; v, vacuole;ml, middle lamella; w, cell wall; is, intercellular space.

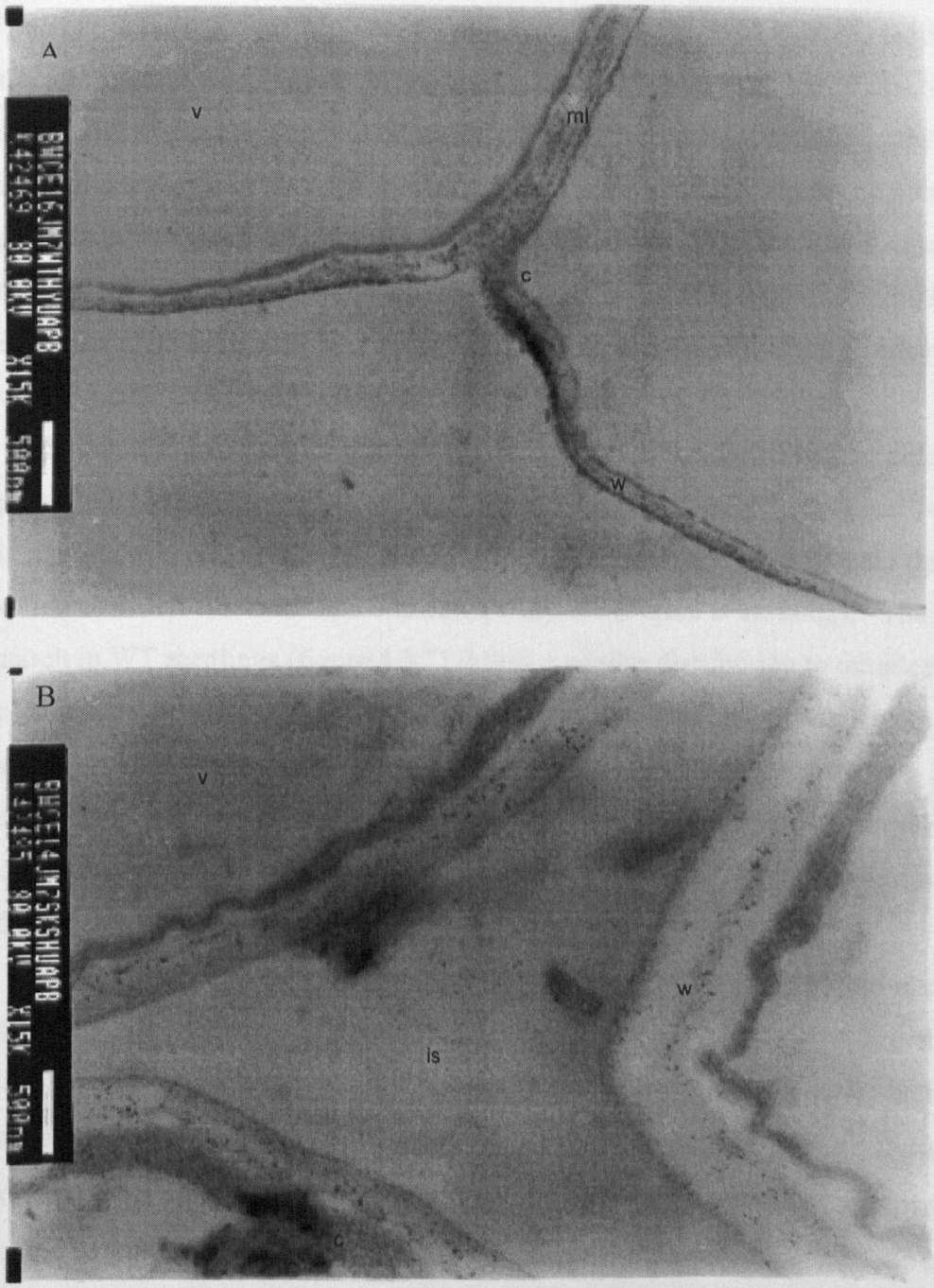

FIGURE 4.3.5: TEMs of 7-day-old wild type (A) and *sks* (B) hypocotyls showing the junction between two epidermal cells and an underlying cortical cell. The cell walls have been labelled with JIM7 antibody that is specific for methyl-esterified pectin, this label is found throughout the cell wall of both WT (A) and sks (B) hypocotyls. c, cytoplasm; v, vacuole;ml, middle lamella; w, cell wall; is, intercellular space.

4.3.3 Neutral Sugar Analysis of *sks*

Sucrose is the main product of photosynthesis and is exported from the leaves to supply the rest of plant with the carbon and energy required for growth and production of storage reserves (Lunn and MacRae, 2003). Sucrose synthesis occurs in the cytosol and utilises sucrose-phosphate synthase which catalyses the synthesis of sucrose-6^{F}-phosphate from UDP-glucose and fructose-6-phosphate. The sucrose-6^{F}-phosphate is then hydrolysed to sucrose by sucrose phosphatase (Lunn and MacRae, 2003). The synthesis of sucrose, starch, cell wall components and glycolysis are all interlinked with UDP-glucose as the centre point as indicated by figure 4.3.6.

Starch synthesis occurs in the plastid and involves the conversion of glucose-6-phosphate to glucose-1-phosphate by a phosphoglucomutase. The glucose-1-phosphate is phosphorylated to ADP-glucose and the polymerisation reactions occur through the action of starch synthases and branching enzymes (Fernie *et al*, 2002). The levels of starch in WT seedlings (figure 4.3.7) follow a similar distribution to other cell wall components including glucuronic acids, arabinose, xylose and galactose. In *sks* seedlings starch levels (figure 4.3.7) decrease from a maximum of 160mg/g AIS at 4 days, compared to a WT level of 60mg/g AIS, to 40mg/g AIS at 14 days. The alteration in starch distribution in *sks* seedlings may reflect delayed starch utilisation in the developing seedling or an increase in starch as storage product.

It is known that there are about equal amounts of cellulose and xyloglucan (XG) in the cell wall (Carpita and Gibeaut, 1993) and the glucose level relates directly to the level of cellulose and xyloglucan present within the plant cell wall as both comprise of linear chains of (1-4)β-linked D-glucose (Carpita and Gibeaut, 1993). Xyloglucan has xylosyl units on 75% of glucosyl units and β-D-galactose and α-L-arabinose can be added to some of these xylose units to give disaccharide sidechains, α-L-fucose units can then be added to the galactosyl units to produce a trisaccharide side chain (Carpita and Gibeaut, 1993).

In *sks* seedlings (figure 4.3.7) glucose levels are increased by 25% at 4 days, 50% at 7 days and by 31% at 14 days compared to corresponding WT levels (figure 4.3.7). This would indicate that there was a 15 to 25% increase of both cellulose and xyloglucan within the *sks* cell wall and this may lead to an increase in cell wall strength and rigidity. In WT seedlings there is 75% more galactose than xylose and arabinose but they display the same pattern of accumulation (figure 4.3.7). In *sks* there is gradual

accumulation of galactose above that of WT from 75mg/g AIS at 4 days to a maximum of 85mg/g AIS at 14 days (figure 4.3.7). Galactosyl residues are important for XG to become a load bearing element in the cell wall (Ryden *et al*, 2003) and also form part of the sidechains on RG-I and RG-II pectin that are involved in intercellular attachment (Kikuchi *et al*, 1996) through ester linkages by phenolic dimers (Fry, 1983).

The xylose and arabinose levels in WT seedlings at 4, 7 and 14 days are identical and display a 1:1 ratio where each xylose could potentially be associated with an arabinose unit (figure 4.3.7). However, in *sks* both xylose and arabinose levels increase above that of WT and they lose their 1:1 ratio with the arabinose levels increasing above that of xylose (figure 4.3.7). Arabinose levels in *sks* (figure 4.3.7) are approximately 1.5 to 2-fold higher than in WT seedlings, and while they can be associated with XG they can also be associated with side chains on RG-I and RG-II domains (Iwai *et al*, 2002). The sidechains of arabinan and arabinogalactan in the RG-I domains of pectin are thought to be involved in intercellular attachment via covalent crosslinks to xyloglucan (Iwai *et al*, 2001).

Pectin consists of PGA, RG-I and RG-II domains and is associated with cell wall polymers through covalent and non-covalent bonds via these domains (Iwai et al, 2002). The glucuronic acid residue is one of glycosyl residues in RG-II and is usually located on one of 2-*O*-Me-xylosyl containing sidechains of RG-II that is involved in borate ester crosslinking (Iwai *et al*, 2002). In *sks* the level of uronic acids, of which comprise glucuronic acids and therefore RG-II pectin domains, (figure 4.3.3.1) is comparable to WT at four days and 14 days. The largest difference in uronic acid levels is at 7 days where *sks* contains 1.5-fold less uronic acid than WT. So at 7 days there may be fewer borate linkages occurring between RG-II pectin in *sks* and this could lead to reduced intercellular attachment between epidermal cells.

To summarise, in *sks* there appears to be an increase in cellulose and in xyloglucan leading to stiffening of the cell wall. There appears to be a more specific increase in galactose residues on XG, RG-I and RG-II indicating that general strengthening and interlinking of the cell wall components has occurred through ester-linkages from the association of phenolic dimers. The distribution of arabinan side chains on RG-I appears to have increased leading to an increase in covalent crosslinks to xyloglucan and the promotion of intercellular attachment. However, this may be coupled to a decrease in glucuronic acid residues on RG-II and so intercellular attachments via borate-diol ester crosslinks may therefore be reduced.

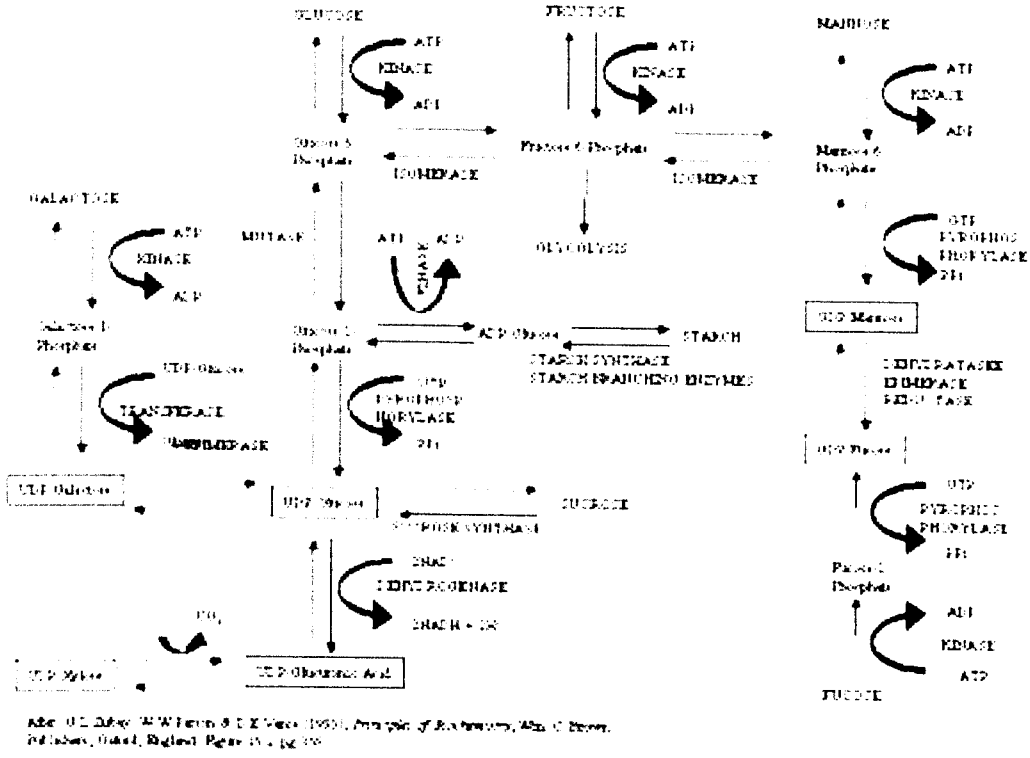

FIGURE 4.3.6: The monosaccharide interconversion pathway showing the fate of glucose in the plant. Glucose or its derivatives are involved in sucrose, starch, cell wall synthesise and in glycolysis. Glucose forms the backbone of glucuronic acid, xylose, galactose, mannose and fucose all of which are major neutral sugars in the plant cell wall and form essential parts of major cell wall components including pectin, cellulose and hemicellulose.

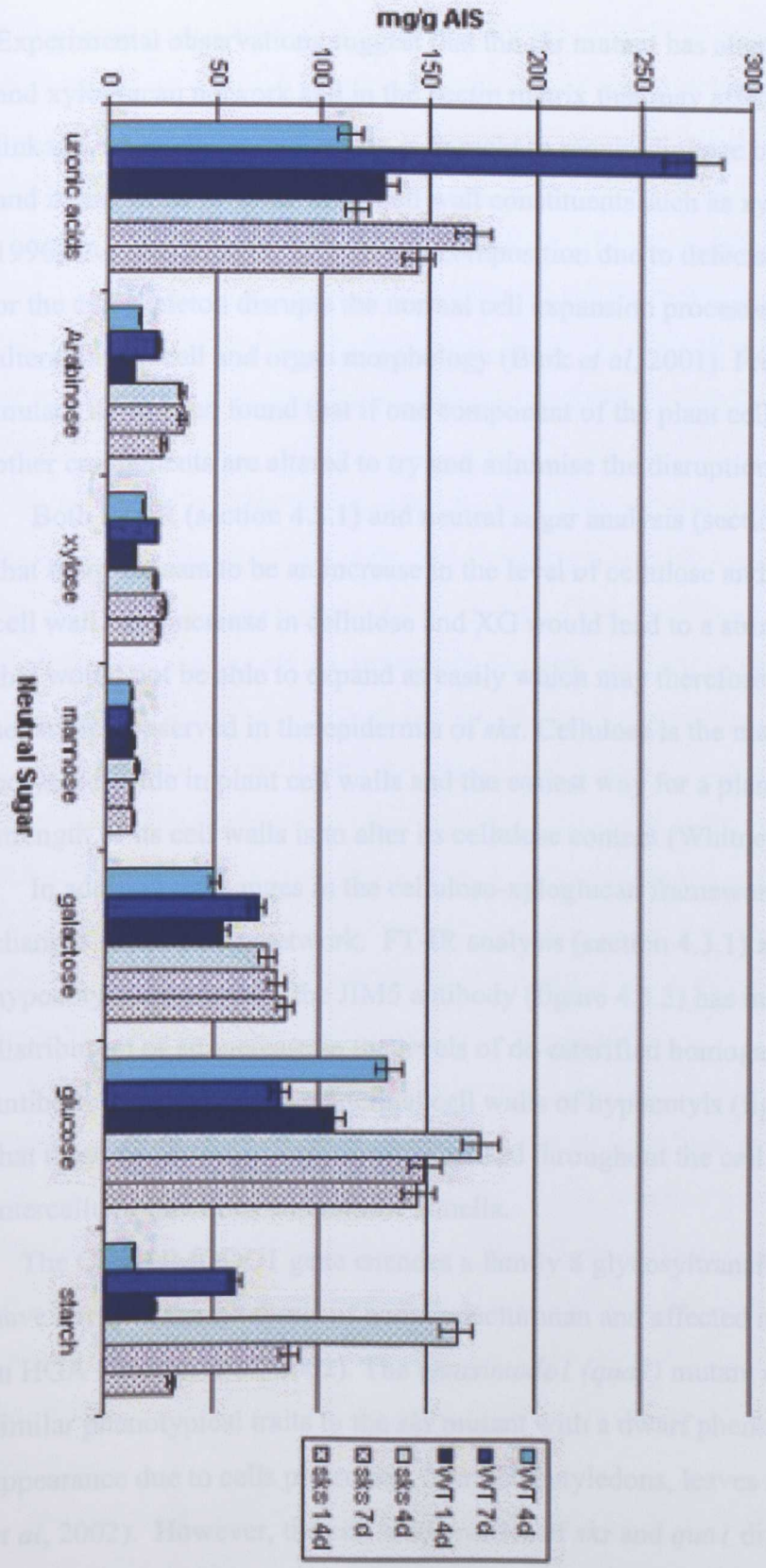

FIGURE 4.3.7: This graph indicates the distribution of the major neutral sugars (mg/g AIS) found in the cell walls of whole seedlings of WT and *sks* at 4 days, 7 days and 14 days after germination. IN WT seedlings most neutral sugars reach a maximum at 7 days and then decrease by 14 days, the only exception is glucose. In *sks* seedlings glucuroninc acids, arabinose, galactose, glucose and starch levels are altered compared to WT.

4.4 DISCUSSION

Experimental observations suggest that the *sks* mutant has alterations in the cellulose and xyloglucan network and in the pectin matrix that may affect epidermal cell-cell linkage. Intercellular attachment is thought to require linkage between pectin molecules and interactions between other cell wall constituents such as xyloglucan (Kikuchi *et al*, 1996). An alteration in the cell wall composition due to defects in cell wall biosynthesis or the cytoskeleton disrupts the normal cell expansion processes that can lead to alterations in cell and organ morphology (Burk *et al*, 2001). From studies of the *kor* mutant it has been found that if one component of the plant cell wall is altered then other components are altered to try and minimise the disruption (His *et al*, 2001).

Both FT-IR (section 4.3.1) and neutral sugar analysis (section 4.3.3) have indicated that there appears to be an increase in the level of cellulose and XG contained in the *sks* cell wall. An increase in cellulose and XG would lead to a stronger and stiffer cell wall that would not be able to expand as easily which may therefore lead to the cell-cell separation observed in the epidermis of *sks*. Cellulose is the major load bearing polysaccharide in plant cell walls and the easiest way for a plant to modulate the strength of its cell walls is to alter its cellulose content (Whitney *et al*, 1999).

In addition to changes in the cellulose-xyloglucan framework there may also be changes in the pectin network. FT-IR analysis (section 4.3.1) and labelling of *sks* hypocotyl sections with the JIM5 antibody (figure 4.3.3) has indicated a change in the distribution or an increase in the levels of de-esterified homogalacturonan. JIM5 antibody labelling of the epidermal cell walls of hypocotyls (figure4.3.2.2) indicates that these de-esterified pectins are localised throughout the cell wall and not just at the intercellular junctions and middle lamella.

The QUASIMODO1 gene encodes a family 8 glycosyltransferase that is thought to have a role in the synthesis of homogalacturonan and affected mutants have a reduction in HGA (Bouton *et al*, 2002). The *Quasimodo1 (qua1)* mutant displays remarkably similar phenotypical traits to the *sks* mutant with a dwarf phenotype and a rough appearance due to cells protruding from the cotyledons, leaves and hypocotyls (Bouton *et al*, 2002). However, the cell wall profiles of *sks* and *qua1* differ significantly with *sks* exhibiting alterations in the cellulose-xyloglucan network and *qua1* showing differences in HGA content.

The *Colourless non-ripening* (*Cnr*) of tomato is characterised by fruit that do not soften and have reduced cell adhesion between pericarp cells (Orfila *et al*, 2002). It has been found that the primary cell walls of *Cnr* fruit possesses de-esterified homogalacturonan that has an altered de-esterified block structure throughout the cell wall, not only at the middle lamella. This may contribute to the increased hardness of the *cnr* cell wall and promote cell separation (Orfila *et al*, 2002). A similar situation may exist in *sks*, where there is an increase in cellulose and XG leading to a more rigid cell wall and de-esterifed HGA is found throughout the cell wall but could potentially have an altered block-structure leading to a decrease in intercellular attachment within the cell walls of *sks*.

However, virus induced silencing of a cellulose synthase gene (CesA) in *Nicotiana benthamiana* (Burton *et al*, 2000) and the disruption of an endo-1,4-β-D-glucanase in the *Arabidopsis* mutant *korrigan* (Nicol *et al*, 1998 and His *et al*, 2001) resulted in a decrease in cellulose and an increase in de-esterified HGA. These plants seem to have compensated for reduced deposition of cellulose by increasing deposition of pectin polysaccharides. By increasing the regions containing de-esterified pectin they allow the formation of more extensive Ca^{2+} bridged junction zones that strengthen the pectin network in walls weakened by the loss of cellulose (Burton *et al*, 2000). An increase in cellulose and XG leads to increased cell wall rigidity and decrease in intercellular attachment but there is an increase in de-esterified HGA with normal block structure to hold the epidermal cells together via Ca^{2+} crosslinks.

The distribution of methylesterified pectin (assayed using the JIM7 antibody), appear normal. Methylesterified pectin is intercalated with the hemicellulose-cellulose network and holds both parts of the cell wall pectin matrix together through transesterification reactions (Gelineo-Albersheim *et al*, 2001). FT-IR analysis has suggested that there is an increase in arabinan sidechains on RG-I. Arabinan sidechains are involved covalent crosslinking to xyloglucan (Iwai *et al*, 2001) and this in association with a normal distribution of methyl-esterified HGA leads to the promotion of intercellular attachment.

Neutral sugar analysis (figure 4.3.7) may indicate an increase in galactose residues on XG, RG-I and RG-II indicating that general strengthening and interlinking of the cell wall components has occurred through ester-linkages from the association of phenolic dimers. However, this may be coupled to a decrease in uronic acid and therefore glucuronic acid residues that are present in xylosyl containing sidechains on RG-II. The

2-O-Me-xylosyl-containing side chain of RG-II pectin associates to form a dimer that is crosslinked by a 1:2 borate-diol ester to generate complex pectin networks and intercellular attachment (Iwai *et al*, 2002). Therefore a reduction in xylosyl containing sidechains on RG-II leads to reduced intercellular attachment via borate-diol ester crosslinks.

Iwai and co-workers, (2002) isolated a glycosyltransferase gene known as *NpGUT1* in mutant haploid *Nicotiana plumbaginifolia* non-organogenic callus with loosely attached cells (*nolac-H18*) that had reduced ability to form intercellular attachments similar to that of *sks*. The *nolac-H18* mutant contained no glucuronic acid residues and half the amount of galactose found in normal callus and so it was postulated that 2-O-Me-xylosyl-containing side chain of the RG-II pectin domain lacked its terminal galactose as the glucuronic acid could not be transferred and so borate RG-II side chain dimers were reduced (Iwai *et al*, 2002).

4.4.1 Conclusions

The *sks* mutant displays defects in epidermal cell expansion and in epidermal cell-to-cell adhesion. Both of these defects appear to correlate with from alterations in the cellulose, xyloglucan and pectin components of the plant cell wall. There also appears to be an increase in cellulose and xyloglucan that may result in an increasingly rigid cell wall. This could lead to limited cell wall expansion and therefore reduced cell-to-cell adhesion due to the pressure of underlying cell layers. It appears that the cross-linking mechanisms between pectin and xyloglucan may also be disrupted resulting in reduced intercellular attachment.

There appears to be an increase and change in the distribution on de-esterified pectin within the cell wall of *sks*. If the de-esterified block structure is normal this could lead to strengthening of the cell wall. Unfortunately, this has not been determined and it could equally lead to reduced cell-to-cell adhesion. There may also be a reduction in the xylosyl containing sidechains on RG-II leading to reduced intercellular attachment via borate-diol ester crosslinks. However, the distribution of methyl-esterified pectin appears unaltered indicating that linkages between HGA and RG-I pectin may be normal and that the arabinan sidechains on RG-I may be increased leading to strengthening of the crosslinks of RG-I to XG fibrils.

5.0 Map-Based Cloning of the *sks* Mutation

5.1 INTRODUCTION

To gain greater insight into the molecular function of the *SKS* gene, map based cloning was undertaken employing a combination of simple sequence length polymorphisms (SSLPs), insertion-deletion differences (InDels) and single nucleotide polymorphisms (SNPs). Two marker types SSLPs and InDels were used to map the *sks* mutation to the bottom arm of chromosome 1. Fine mapping revealed that the *SKS* gene lies on BAC clones T11I11 at approximately 29, 460, 000bp on chromosome 1. To pinpoint the *sks* mutation to a specific gene, SALK insert lines have been utilised in a candidate gene approach.

5.1.1 Forward Genetics and Map Based Cloning

Two distinct approaches are currently employed by researchers to link the sequence and function of a specific gene: forward and reverse genetics. In the case of reverse genetic approaches the underlying functions are determined by selecting for mutations that disrupt the sequence of interest and therefore its gene function. When the mutation causing the phenotype is the result of a T-DNA or transposon insertion, rapid identification of the gene of interest is theoretically possible by locating the sequence tag and analysing the neighbouring sequences (Peters *et al*, 2003).

Forward genetic approaches aim to identify the sequence change that underlies a specific mutant phenotype that already exists (Peters *et al*, 2003). However, identification of a gene affected by chemical, radiation- induced mutation requires a map-based or positional cloning where the process of identifying the genetic basis of a mutant phenotype is by looking for linkage to markers whose physical location in the genome is known (Jander *et al*, 2002).

Positional cloning of genes in *Arabidopsis* has been greatly improved by the sequencing of Columbia-0 (Col-0) and Landsberg *erecta* (*Ler*) genomes. The Col-0 accession was sequenced in a clone-by-clone approach by a large international sequencing project (The *Arabidopsis* Genome Initiative, 2000), whilst the Monsanto Company (formerly Cereon Genomics) completed the Landsberg *erecta* genome by low coverage shotgun sequencing (Jander *et al*, 2002). The sequencing of the Columbia and

Landsberg *erecta* accessions was undertaken as they represent two of the most commonly employed accessions by *Arabidopsis* researchers. Many markers have been analysed in these lines and the genetic maps produced from this work have become the standard against which other *Arabidopsis* genetic maps are aligned (Jander *et al*, 2002).

The availability of a wide range of genetic markers is no longer the limiting factor for fine-scale genetic mapping needed for map-based cloning. Instead the process is now limited by our ability to generate recombination events at a high enough density and to rapidly and inexpensively genotype plants using these markers (Jander *et al*, 2002). Using a combination of markers and methods to map a mutation it has been estimated that it is possible to find a gene in approximately one year and new advances in mapping technologies will hopefully improve and speed this process up considerably.

Gene mapping in *Arabidopsis* is initially undertaken on genomic DNA samples obtained from the F2 progeny of an outcross between the mutant and an opposite accession. DNA from at least twenty F2 individuals that display the mutant phenotype are initially used to determine genetic linkage to one or more of 25 markers spaced every 30cM throughout the genome (Ponce *et al*, 1999). Additional markers are used with further F2 mutants to narrow down the region of interest using the two markers closest to the mutation on either side. The ultimate goal of fine mapping is to narrow down the region containing the gene of interest to 40Kb or less, then the whole region can be sequenced to pinpoint the mutation (Jander *et al*, 2002).

Insertion-deletion events (InDels) and simple sequence length polymorphisms (SSLPs) can be detected by PCR amplification and gel electrophoresis separation and this is one of the quickest and easiest ways to assign a mutation a rough position on a chromosome. SSLPs are based on the presence of stretches of a short nucleotide sequence that can be repeated many times in tandem and are present throughout the genome of *Arabidopsis* (Casacuberta *et al*, 2000). PCR primers are designed to flank these regions, and as these regions can differ in length between two accessions, PCR products of different sizes are produced (Lukowitz *et al*, 2000).

The Monsanto Company created a database of DNA polymorphisms between the Col-0 and Landsberg *erecta* sequences that can be used as genetic markers. Differences between the accessions were classified into two types: single nucleotide polymorphisms (SNPs) where a single nucleotide present at a specific position in the genome is altered and insertion-deletion (InDel) differences where one accession has an insertion of a number of nucleotides relative to the other. To design an InDel marker, pairs of PCR

primers are designed to amplify a segment of DNA spanning the InDel and the size differences in the amplified products are detected using high percentage agarose gels (Jander *et al*, 2002).

InDels and SSLPs are scored as co-dominant markers with one band seen on the gel for either homozygous class or two bands are seen for heterozygous individuals. This collection of polymorphisms will be useful for mapping QTLs or mutations in most other *Arabidopsis* accessions and are available through registration via the *Arabidopsis* Information Resource Web site http://www.arabidopsis.org/cereon/index.jsp. However, it must be noted that one-half of all attempted InDel markers will fail due to the less stringent selection criteria during sequence alignment compared to SNP markers (Jander *et al*, 2002).

Single nucleotide polymorphism (SNP) changes comprise the largest set of sequence variants in most organisms (Drenkard *et al*, 2000) and therefore are the most useful as molecular markers, especially for the fine mapping of a mutation. It is thought that there is on average one SNP every 3.3Kb, or ~ 40,000 SNPS between the Columbia and Landberg *erecta* accessions (Drenkard *et al*, 2000).

Matrix-assisted laser desorption ionisation time-of-flight mass spectrometry (MALDI-TOF MS) represents a versatile tool for high throughput detection of SNPs (Ross *et al*, 1998). A segment of DNA containing the polymorphism is amplified by PCR and then an oligonucleotide primer is annealed directly upstream of a known point mutation. The primer is then extended by a single di-deoxynucleotide in a thermal cycled reaction and the products analysed by the MALDI-TOF MS (Ross *et al*, 1998). Each of the homozygous parent lines will show individual mass peaks whilst the heterozygous lines will show both mass peaks.

5.1.2 Reverse Genetics and Insertional Mutants of *Arabidopsis*

An essential tool for the functional analysis of a completely sequenced genome such as *Arabidopsis* is the ability to create loss-of-function mutations for all of the encoded genes. Currently the most effective strategy is random large-scale insertional mutagenesis and the high gene density in the *Arabidopsis* genome means that every second insertion will disrupt a gene sequence. The insertion of a large T-DNA or transposon constructs most often leads to the inactivation of a gene that would create a

null allele, and this is generally the most direct way to understand gene function (Parinov and Sundaresan, 2000).

Plant transformation by *Agrobacterium* results in the integration into the nuclear genome of a sequence called T-DNA, which is carried on a bacterial plasmid. Although the precise mechanism of T-DNA integration into the host genome is not fully understood, a variety of host proteins appear to play important roles in T-DNA transport and integration processes (Tzfira and Citovsky, 2002). One advantage of using T-DNA as an insertional mutagen is that it directly generates stable insertions into genomic DNA. However, chromosomal rearrangements, concatameric T-DNA insertion and transfer of vector sequences can lead to difficulties in the genetic analysis of the insertion which can lead to mutant phenotypes not associated with a T-DNA insertion (Parinov and Sundarasen, 2000).

Agrobacterium T-DNA has been used to establish large collections of sequence indexed *Arabidopsis* insertion mutants: these include the SAIL lines (Sessions *et al*, 2002), the SALK collection (Alonso *et al*, 2003), the GABI-Kat collection (Li *et al*, 2003) and the INRA-Versailles collection http://flagdb-genoplante-info.infobiogen.fr/projects/fst/DocsIntro/Page_accueil.html (Balzergue *et al*, 2000).

To screen for a mutant in a gene of interest a search is carried out for the corresponding sequenced insertion site. Primers complementary to the end of the insertion and the gene of interest are used for PCR screening of plants carrying an insertion within the gene of interest (Parinov and Sundarasen, 2000). Sequenced insertion site T-DNA populations such as the SALK collection represent useful tools to test gene function. These collections are particularly useful following fine mapping of a mutant to a handful of genes.

5.2 METHODS

5.2.1 Generation of a Mapping Population

Homozygous *sks* and L*er* seedlings were grown up on plates as described in section 3.2.2 and then transferred to soil at approximately 14 days old. Once the plants had bolted, crosses were performed using *sks* as the maternal recipient and L*er* as the pollen donor plant (section 3.2.3). The F1 seeds were collected, planted out on soil and allowed to self-pollinate. Only one F2 line was used for further analysis and was labelled F2-1.

Seed from this F2-1 *sks* x L*er* line was plated out and grown for 14 days on MS agar. Approximately 1000 seedlings that displayed the *sks* phenotype were then collected in racked 8 strip cluster tubes and DNA isolations were then undertaken immediately or the rack was stored at -80°C.

5.2.2 DNA Extraction

DNA was extracted from seedlings for the sequencing of potential candidate genes using a variation of the Dellaporta DNA Isolation Protocol (Dellaporta *et al*, 1983) or using a Qiagen DNeasy kit. The tissue was placed in an eppendorf and frozen in liquid nitrogen. The tissue was then ground to a fine powder and 600ul of extraction buffer and 80ul of 10 % (v/v) SDS was added. The extraction buffer consists of; 0.1M Tris pH7.4, 0.05M EDTA, 0.5M NaCl, 1% (w/v) polyvinyl pyrolidone and 0.01 % (v/v) β-mercaptoethanol. The tissue was then ground further and vortexed vigorously for 30 seconds. 200ul of 5M potassium acetate was added and then the tissue was vortexed again for 30 seconds. The tissue was then placed on ice for 20 minutes.

The eppendorfs were then spun at 10 000g for 15 minutes at 4°C (Hettich Universal 16R Centrifuge). The supernatant was then transferred to fresh eppendorf tubes and 0.7 volumes of isopropanol was added. The eppendorf tubes were then mixed thoroughly and left at –20°C for at least 30 minutes. After being spun at 4°C for 20 minutes at 10 000g (Hettich Universal 16R Centrifuge) the aqueous phase was discarded and the pellet was allowed to air dry.

The pellet was then resuspended in 100ul of TE buffer, 1ul of Rnase (2mg/ml) was then added and the eppendorf tubes were incubated at 37°C for 30 minutes. The TE buffer consists of 0.05M Tris pH 8 and 0.01M EDTA. To precipitate the DNA 0.7

volumes of isopropanol and 0.1 volume of 3M Sodium Acetate, pH 8 was added to the eppendorf tubes. The tubes were mixed well and then placed on ice for 20 minutes.

The eppendorf tubes were then spun at 4°C for 20 minutes at 10 000g (Hettich Universal 16R Centrifuge). The supernatant was removed and the pellets were then washed with 70 % (v/v) ethanol before being allowed to air dry. The DNA was then resuspended in 30ul of TNE buffer. The TNE buffer consists of 20mM Tris pH8, 20mM NaCl and 1mM EDTA.

5.2.3 DNA Extraction for 96-samples

DNA was extracted from *sks* x Ler F2 seedlings displaying the *sks* mutation using a variation of the Dellaporta DNA Isolation Protocol that has been adapted for undertaking 96-DNA isolations simultaneously (Dellaporta *et al*, 1983). 14 day old seedlings were placed in racked 8-strip cluster tubes (Costar) and 600ul of extraction buffer and 80ul of 10 % (v/v) SDS was added to each cluster tube with a steel ball bearing. The extraction buffer consists of 0.1M Tris pH7.4, 0.05M EDTA, 0.5M NaCl, 1% (w/v) polyvinyl pyrolidone and 0.01 % (v/v) β-mercaptoethanol. The cluster tube rack was then clamped into a paint mixer-mix and the tissue was homogenised for 15 minutes.

The ground tissue was transferred to a 2.2ml storage plate (ABgene) by removing the lids from each row of cluster tubes and pouring the supernatant directly into each row of the storage plate. 200ul of 5M potassium acetate was added to each well and then Thermowell Sealing Tape for 96 well plates (Costar) was used to seal the storage plate. The storage plate was inverted to mix the solutions and then placed on ice for 20 minutes.

The storage plate was spun at 6000g for 20 minutes at 4°C (Beckman Coulter Allegra 25R Centrifuge). The supernatant was then transferred to a fresh 2.2ml storage plate and 0.7 volumes of isopropanol was added. Thermowell Sealing Tape for 96 well plates (Costar) was used to seal the storage plate and was then inverted to mix the solutions and placed at -20°C for at least 30 minutes.

The storage plate was then spun at 6000g for 25 minutes at 4°C (Beckman Coulter Allegra 25R Centrifuge). The aqueous phase was discarded by inverting the storage plate over a sink and then the plate was allowed to drain on tissue. The pellets were dried in dessicator under vacuum for 10 minutes.

The pellets were resuspended in 100ul of TE buffer and then transferred to a standard 96 well microplate (ABgene). The TE buffer consists of 0.05M Tris pH 8 and 0.01M EDTA. To precipitate the DNA 0.7 volumes of isopropanol and 0.1 volume of 3M Sodium Acetate, pH 8 was added to the microplate. The microplate was sealed with Thermowell Sealing Tape for 96 well plates (Costar), inverted and then placed on ice for 20 minutes.

The microplate was then spun at 6000g for 25 minutes at 4°C (Beckman Coulter Allegra 25R Centrifuge). The supernatant was removed by inverting the storage plate over a sink and then the plate was allowed to drain on tissue. The pellets were then dried in dessicator under vacuum for 10 minutes. The DNA was then resuspended in 30ul of TNE buffer. The TNE buffer consists of 20mM Tris pH8, 20mM NaCl and 1mM EDTA.

5.2.4 Mapping using SSLP and INDEL Markers

20 SSLP primers pairs were initially chosen to test for linkage, two for each arm of the 5 *Arabidopsis* chromosomes and were spaced ~30cM apart. Figure 5.3.1 illustrates the distribution of the SSLPs used to initially localise the *sks* mutation and a full list of SSLP and InDel primers used to map the *sks* mutation can be found in section 5.2.6.3. Once the *sks* mutation was localised to a chromosome further SSLP and Insertion Deletion (InDel) markers were used to map closer to the mutation as illustrated by figure 5.3.3. InDels of 10 to 30bp were selected in the region of interest and pairs of PCR primers are designed to amplify a segment of DNA 200-300bp in length spanning the InDel.

Both SSLP and InDel markers are PCR based: 10ul PCR reactions were set up by hand and consisted of 1ul of 10x reaction buffer (ABgene), 0.8ul of 25mM $MgCl^{2+}$, 0.02ul of each 100mM dNTP (Promega) and 0.2ul of each 10pM primer (MWG), 7.12ul of SDW, 0.1ul RedHot Taq polymerase (ABgene) and 0.5ul of template genomic DNA. These reactions were carried out on a GeneAmp PCR system 9700, Applied Biosystems thermocycler. The PCR conditions were 1min at 94°C followed by 35 cycles of 30s at 94°C, 30s at 50-60 °C, 1min 30s at 72°C followed by 10mins at 72°C. The size differences in the amplified products were detected using 2% (w/v) agarose gel and ran at 100V for 1.5 hours. SSLP and InDel markers are co-dominant markers with one

band seen on the gel for either homozygous class or two bands are seen for heterozygous individuals.

5.2.5 Localisation of the *sks* Mutation using SNPs

All SNP primers were designed and SNP reactions carried out by John Wright, (Genome Laboratory, Plant Sciences, Sutton Bonington Campus, Leicestershire, LE12 5RD). 10µl PCR reactions were set up containing: 1x HotStarTaq PCR Buffer, 0.05mM each dNTP, 0.5 units HotStarTaq Polymerase (Qiagen), 0.5µl Forward PCR primer pool, 0.5µl Reverse PCR primer pool and 0.5µl genomic DNA. All primers in the pool should be at a 10µM concentration and the concentration of each primer should be further adjusted using MALDI-TOF to give even peak intensities. 1µl of Betaine (Q-solution) may be added to the reaction volume to improve the PCR. The PCR thermocycle conditions are as follows: 95°C for 15min, 30secs at 72°C and then 40 cycles of 30secs at 94°C, 30secs at 54°C and 1min at 72°C, this is followed by 10 minutes at 72°C.

To polish the PCR product before the SNP primer extension reactions, 0.5 units of Shrimp Alkaline Phosphatase (USB) and 7.5 units of Exonuclease I (NEB) (5 units for a single primer reaction) was added to 5µl of the PCR product. The PCR products were then thermocycled for 20mins at 37°C, 20mins at 80°C and then held at 4°C.

The SNP primer extension reactions consist of 5µl polished multiplex PCR product, 1x Therminator reaction buffer without Triton X-100, 0.025µM of each ddNTP, 0.5µl SNP extension primer pool and 1unit of Therminator DNA polymerase (NEB). The Buffer supplied with Therminator contains Triton X-100 that interferes with purification of extension reactions. It is necessary to make up 10x buffer without Triton X-100 containing: 100mM KCl, 100mM $(NH_4)_2SO_4$, 200mM Tris-HCl, pH8.8 and 20mM $MgSO_4$. The PCR thermocycle conditions for the extension of the SNP primers were 35 cycles of 10secs, 1min at 37°C and 1min at 72°C.

The SNP primer extension products were purified by adding 20µl vortexed POROS 50 R1 media (Applied Biosystems) in 20% (w/v)Acetonitrile to a well on a 96 well Extra fine FilterPlate (Robbins) resting on a 2.2ml 96 Deep Well Plate (ABgene). The plate was then centrifuged at 1500rpm for 1min (Beckman Coulter Allegra 25R Centrifuge) and the filtrate was discarded. 20µl of 100mM Triethylammonium acetate,

pH6.5 (TEAA) was added to wash media before being centrifuged at 1500rpm for 1min and the filtrate was discarded.

10µl 100mM TEAA, pH6.5 was added to each extension reaction (1:1) and mixed by pipetting. Add the mixture to a marked well containing the washed POROS before centrifuging at 1500rpm for 1min and discarding the filtrate. 20µl of 100mM TEAA pH6.5 was added to each to the well to wash the sample, centrifuged at 1500rpm for 1min and the filtrate discarded. This step was then repeated before placing a 96 well Thermofast PCR plate (ABgene) under the FilterPlate. 10µl of 20% (w/v) Acetonitrile was added to each sample and centrifuged at 1500rpm for 1min to elute.

To spot the samples, 1µl of eluted sample was mixed with 1µl of matrix and 1µl of this mixture was spotted onto a well on a clean MALDI plate and allowed to dry. The matrix is made up from a 2:1:1 mix of 0.2M 2,4,6 Trihydroxyacetophenone (THAP) in 50% (w/v) acetonitrile; 0.2M 2,3,4 THAP in 50% (w/v) acetonitrile and 0.3M diammonium hydrogen citrate in water.

The MALDI plate containing spotted, dried samples was loaded into *Perseptive Biosystems Voyager DE* MALDI-TOF Mass Spectrometer and the spectra acquired using the following criteria: Min laser intensity – 2900, Max laser intensity – 3200, Step size – 50, Minimum signal intensity – 400, Acquire 5 spectra that pass acceptance criteria, Criteria evaluation mass range – 3000 - 6000Da, Search pattern – Centre bias, Stop after 6 consecutive failed acquisitions, Matrix – 3-Hydroxypicolinic acid.

The spectra are processed and analysed using the Mass Genotyping software, the guide processing conditions are as follows: Baseline Correction – Advanced, Peak Deconvolution – Off, Peaks for internal calibration – Primers Only, Relative Peak Intensity – 10%, Mass Tolerance – 10Da, Max Outlier Error – 2Da, Allele Tolerance 4Da, Heterozygote Threshold – 15%. Acquisition and processing conditions may need adjusting for a given sample set to give better results, but these represent a good set of guidelines. Spectra should also be checked by eye, to ensure base calls are accurate.

5.2.6 Primers Used in Mapping and Cloning the *sks* Mutation

5.2.6.1 *Quasimodo* Sequencing Oligos

Primer Name	Sequence
QuasF1	TTCCGTCTTGCCGTAGAG
QuasF2	TATAATCGGTCTTGTTCC
QuasF3	TCGCTTCAGATTCTAACG
QuasF4	TCAAGTGATTGCTGAAGC
QuasF5	ATCTTGGAGCTATGCAGG
Quas-F5a	ATGTGCCTGTGTTGAAGC
QuasF6	TGATCTTGATGCTTGGAG
QuasF7	TGTTACTTCAGCTCTACG
QuasR1	GGAGTGTCTCACTAATCG
QuasR2	TGACCGATGATCATCAGC
QuasR3	GCAGAGTTCACAACCACC
QuasR4	GAGCGTACCGATGAAACG
QuasR5	GCGTTGCGGATCTCATCC
QuasR6	TCTCTTTCTTCATGTGGC

5.2.6.2 At1g77130 Sequencing Primers

Primer Name	Sequence	Primer Name	Sequence
At1g77130-F1	cgttttattcttcctcttcgcg	At1g77130-R1	caaacttaacattgaccc
At1g77130-F2	gcaaagcttcatcttcctg	At1g77130-R2	gcaatgtggttgagtatgtgc
At1g77130-F3	CAAGTTGCGCCTTCTGTTTCG	At1g77130-R3	ctcactgtcagcatatagc
At1g77130-F4	CCAGAGTTGAAGAGCGTAGC	At1g77130-R4	cgtcaaggaaacatatggctg
At1g77130-F5	cagcttaggaggggagaac	At1g77130-R5	cagaaacccgaaagctgaagc
At1g77130-F6	CAACTTCATCAATCCATTCCG	At1g77130-R6	ggtatgcttcagagactacg
At1g77130-F7	CCTCCTACTTGTCTTCTCA	At1g77130-R7	ccgtactactgtgtgtg
At1g77130-F8	gattttggaccaaggcac	At1g77130-R8	gtagcttcacacacatggttg
At1g77130-F9	CGATCCCACTCAAGTTGCGC	At1g77130-R9	gcgagtatcaaggaattggtc
Atg177130-F10	GGAGTTGAAGAGCGTACCGTCG	At1g77130-R10	Gtcaagaacttgttgcccgtc
At1g77130-F11	cagcttaggaggagagaatag	At1g77130-R11	ccaaatgcctacaacgaatgg
At1g77130-F12	GGAACTTGAATCCAAGGAAG	At1g77130-R12	Ggttatgcttcagagactatg
At1g77130-F13	CAGACTAGAGAAGTTGACAC	At1g77130-R13	ctctgcctttcgccaacc
A1g77130-F14	Gaagctggatgcatcgag		

5.2.6.3 SSLP and InDel Mapping Oligos

SSLP Marker	*Primer Sequence*	Map Position	Size Col	Size Ler	Tm (°C)
Chromosome 1 (3020614bp) (132.79cM)					
F21M12	1U-F GGCTTTCTCGAAATCTGTCC	9.37cM 3212193bp	200bp	160bp	58°C
	1U-R TTACTTTTTGCCTCTTGTCATTG				
nga392	nga392-F TTGAATAATTTGTAGCCATG	39.52cM 9831900bp	143bp	129bp	50°C
	nga392-R GGTGTTAAATGCGGTGTTC				
ciw1	1L-F ACATTTTCTCAATCCTTACTC	72cM 17951444bp	159bp	135bp	52°C
	1L-R GAGAGCTTCTTTATTTGTGAT				
nga128	Nga128-F ATCTTGAAACCTTTAGGGAGGG	83.32cM 20217128bp	180bp	190bp	61°C
	Nga128-R GGTCTGTTGATGTCGTAAGTCG				
F5114	F5114-F CTGCCTGAAATTGTCGAAAC	24079041bp	196bp	310bp	56°C
	F5114-R GGCATCACAGTTCTGATTCC				
MSAT1.13	MSAT1.13-F CAACCACCAGGCTC	25532481bp	221bp	210bp	48°C
	MSAT1.13-R GTCAAACCAGTTCAATCA				
nga111	nga111-F CTCCAGTTGGAAGCTAAAGGG	115cM 27005122bp	128bp	162bp	58°C
	nga111-R TGTTTTTTAGGACAAATGGCG				
T23E18	T23E18-F gcctaaacacaaagatgacc	283678807bp	215bp	241bp	56°C
	T23E18-R gactgttaggcaagagatgg				
F22K20	F22K20-F gctctgtttctcctagc	28989387bp	175bp	192bp	54°C
	F22K20-R cttcactccaaggacacagc				
T14N5	T14N5-F gagcagatggaatataccg	29040139bp	234bp	244bp	55°C
	T14N5-R caacatccccattgttgc				
F18B13	F18B13-F gagtggttgcagctggagc	30201476bp	351bp	421bp	62°C
	F18B13-R gaacgggccgtacattgggc				
Chromosome 2 (19725468b) (95.73cM)					
nga1145	nga1145-F CCTTCACATCCAAAACCCAC	9.6cM 682624bp	213bp	217bp	56°C
	nga1145-R GCACATACCCACAACCAGAA				
ciw3	2U-F GAAACTCAATGAAATCCACTT	30cM 6351398bp	230bp	200bp	54°C
	2U-R TGAACTTGTTGTGAGCTTTGA				
nga1126	nga1126-F CGCTACGCTTTTCGGTAAAG	50.65cM	191bp	199bp	56°C
	nga1126-R GCACAGTCCAAGTCACAACC				
nga168	2L-F TCGTCTACTGCACTGCCG	73cM 16240385bp	141bp	209bp	58°C
	2L-R GAGGACATGTATAGGAGCCTCG				
Chromosome 3 (2356358bp) (101.45cM)					
nga162	3U-F CATGCAATTTGCATCTGAGG	20.56cM 4608281bp	107bp	89bp	58°C
	3U-R CTCTGTCACTCTTTTCCTCTGG				
AthGAPAb	AthGAPAb-F CACCATGGCTTCGGTTACTT	43.77cM	142bp	150bp	58°C
	AthGAPAb-RTCCTGAGAATTCAGTGAAACCC				
T16K5-TGF	3L-F TTGTCGAAATAAAAATTGACCGTTA	75cM 18441052bp	168bp	<col	59°C
	3L-R TGGATGTGGATTCTATTGTTTCTCA				
nga112	nga112-F TAATCACGTGTATGCAGCTGC	87.88cM 23177332bp	197bp	189bp	61°C
	nga112-R CTCTCCACCTCCTCCAGTACC				

Chromosome 4 (17549528bp) (119.09cM)					
nga8	4U-F GAGGGCAAATCTTTATTTCGG 4U-R TGGCTTTCGTTTATAAACATCC	26.56cM 4593289bp	154bp	198bp	56°C
ciw6	ciw6-F CTCGTAGTGCACTTTCATCA ciw6-R CACATGGTTAGGGAAACAATA	50cM 6857107bp	162bp	148bp	54°C
ciw7	4L-F AATTTGGAGATTAGCTGGAAT 4L-R CCATGTTGATGATAAGCACAA	70cM 10488849bp	130bp	123bp	51°C
nga1107	nga1107-F GCGAAAAAAACAAAAAAATCCA nga1107-R CGACGAATCGACAGAATTAGG	104.73cM 17060616bp	150bp	140bp	54°C
Chromosome 5 (26689408p) (140.3Cm)					
ciw14	5U-F CATGATCCATCGTCTTAGT 5U-R AATATCGCTTGTTTTTGC	15cM 2174596bp	179bp	120bp	47°C
nga106	nga106-F GTTATGGAGTTTCTAGGGCACG nga106-R TGCCCCATTTTGTTCTTCTC	33.35cM	157bp	123bp	58°C
AthSO262	AthSO262-F TTGCTTTTTGGTTATATTCGGA AthSO262-R ATCATCTGCCCATGGTTTTT	65.20cM	145bp	159bp	52°C
ciw9	5L-F CAGACGTATCAAATGACAAATG 5L-R GACTACTGCTCAAACTATTCGG	90cM 16757909bp	165bp	145bp	58°C
ciw10	ciw10-F CCACATTTTCCTTCTTTCATA ciw10-R CAACATTTAGCAAATCAACTT	115cM 24244776bp	140bp	130bp	49°C

Markers F5114 and MSAT1.13 are from the Versailles' QTL *Arabidopsis* Microsatellite page: http://www.inra.fr/qtlat/index.htm?PHPSESSID=523254d5abfc29f11fd0c7dcaecafdf9

Marker AthSO262 that was found on the website: http://cbil.humgen.upenn.edu:80/~atgc/SSLP_info/nga_sequences.html, which can no longer be accessed and was cited in Ponce *et al*, 1999.

Markers T23E18, F22K20, T14N5 and F18B13 were created from small insertions/deletions (INDELs) between the publicly available Columbia (Col) sequence and Landsberg *erecta* (Ler) sequence generated by Syngenta (Jander *et al*, 2002).

All other markers are from the TAIR SSLP marker pages: http://www.arabidopsis.org/servlets/Search?action=new_search&type=marker

5.2.6.4 SNP Primers

AGI ID/ Bac Name	PCR Primers	Tm	SNP Primer	SNP	MW SNP Primer (Da)	Position (bp)
T14N5 At1g77120	At1g77120-F ACTGTTGATAATGTCTACC At1g77120-R CGTGTTTCTGCGGTGGAG 247bp	56 56	At1g77120-SNP gGGATTCATAACAAAAAC 5524.71Da	t/c	Col: 5797 Ler: 5812	29042358
T32E8 At1g77720	At1g77720-F cgtcttcttcatcctcttc At1g77720-R ccatcagagaaacctagc 233bp	56 56	At1g77720.1-SNP CGACCCAGAAAGAGA 4604.09Da	g/a	Col: 4917 Ler: 4901	29277661
T32E8.2 At1g77800	At1g77800-F cggactcagctacaacatc At1g77800-R ccatcctctgaaacactag 273bp	58 56	At1g77800-SNP GGAAGTAGCACTGTCATC 5523.68Da	T/C	Col: 5796 Ler: 5810	29326477
F28K19.1 At1g78040	At1g78040-F gcaacgatagagtttgagg At1g78040-R ggctgcgtgtatgagtc 279bp	56 54	At1g78040-SNP TATCTGCTTATGTCAAA 5159.46	G/A	Col: 5472 Ler: 5456	29411406
YUP8H12R At1g79260	At1g79260-F AGTATTGCTTTGAGATGTGG At1g79260-R gtctctgtctctacacaca 218bp	56 65	At1g79260-SNP CTCATACGAACCACATA 5107.44Da	C/A	Col: 5380 Ler: 5404	29790064

5.2.7 SALK Lines

SALK lines found to have insertion events within candidate *SKS* genes were identified by searching the http://signal.salk.edu/cgi-bin/tdnaexpress webpage and only insert lines found to lie within exons or introns were selected for phenotypic analysis. The SALK insert lines below were supplied by the Nottingham *Arabidopsis* Stock Centre (http://nasc.nott.ac.uk/).

BAC Clone	AGI Identifier	Description	SALK Line
T11I11	At1g78090	Trehalose-6-phosphate phosphatase	Salk_037324 Salk_037310 Salk_137712 Salk_051229
T11I11	At1g78095	Mutator related transposase	Salk_082581 Salk_059419
T11I11	At1g78100	F-box protein	Salk_069429 Salk_022582 Salk_026385 Salk_006851
T11I11	At1g78110	Hypothetical protein	Salk_003000
T11I11	At1g78120	Tetratricopeptide repeat protein	Salk_056021 Salk_031913 Salk_114479
T11I11	At1g78130	Transporter-related protein	Salk_044158
T11I11	At1g78140	Expressed protein	Salk_123390 Salk_145002 Salk_027211 Salk_023909
T11I11	At1g78150	Expressed protein	No suitable Insert Lines
T11I11	At1g78160	Pumilio-family RNA-binding protein	No Suitable Insert Lines

5.3 RESULTS

5. 3.1 Sequencing of *Quasimodo* and Initiation of *sks* Mapping

In the October of 2002, Bouton *et al* published an *Arabidopsis* mutant known as *Quasimodo1* that bore remarkable phenotypical similarity to the *sks* mutant. *Quasimodo1* was reported to encode a putative membrane bound family 8 glycosyltransferase near the middle of chromosome 3 (At3g25140 on BAC clone MJL12). In the absence of mapping data for *sks*, it was decided to sequence this gene in the *sks* background to investigate whether the *QUASIMODO1* gene was allelic to *sks*.

A series of primers were designed as listed in section 5.2.6.1 and the *QUASIMODO1* gene was sequenced in three overlapping fragments using primers Quas-F1/R2, Quas-F3/R4 and Quas-F5/R6. The Quas-F1/R2 fragment was sequenced using the primers Quas-F1, Quas-F2 and Quas-R2. The fragment Quas-F3/R4 was sequenced using the primers Quas-F3, Quas-R3 and Quas-R4. The remaining fragment Quas-F5/R6 was sequenced using the primers Quas-R5, Quas-F5a and Quas-R6.

The sequencing results were BLAST searched against the whole *Arabidopsis* genome using NCBI BLAST2.0 at http://www.arabidopsis.org/Blast/ with BLASTN and AGI whole genome parameters to search for differences in the *sks* sequence compared to the Columbia sequence. No sequence differences were found in the *QUASIMODO* gene in the *sks* background and rough mapping of the *sks* mutation was initiated using SSLP mapping primers.

5.3.2 Rough Mapping of *sks* and Sequencing of At1g77130

SSLPs were used to rough map the *sks* mutation using DNA isolated from seedling displaying the *sks* phenotype in the *sks* x L*er* F2-1 mapping population. The approximate position of the SSLP markers used to localise the map the *sks* mutation to an arm of a chromosome are shown in figure 5.3.1 and further details can be found in section 5.2.4. The *sks* mutation exhibited linkage with the marker nga11 and hence mapped to the lower arm of chromosome 1 between 25, 000, 000 and 30, 000, 000bp.

Figure 5.3.2 (A-T) shows gel electrophoresis images of the PCR reactions of the SSLP markers used to rough map the *sks* mutation. Only one SSLP marker, nga111 (figure 5.3.2 D) showed a bias in amplification of Columbia PCR products over Landsberg *erecta* products indicative of linkage. *In silico* searching of the

Carbohydrate Active enZYme (CAZY) website http://afmb.cnrs-mrs.fr/CAZY/ identified two glycosyltransferase family 8 members localised near marker nga111 on chromosome 1. The first gene, At1g70090 was found on BAC clone F20P5 located at ~26, 000,000bp, the second gene, At1g77130 was found on BAC clone T14N5 at ~28, 575, 000bp. At1g70090 was immediately discounted as further analysis of the *sks* x Ler F2-1 mapping population using MSAT1.13, a marker upstream of nga111, indicated that the *sks* mutation lay further downstream towards At1g77130.

Sequencing primers (section 5.1.2.2) were designed for At1g77130 as this gene seemed to be a likely candidate for the *sks* mutation based on the SSLP mapping data. Sequencing of At1g77130 in the *sks* background revealed no sequence changes and further analysis with INDEL mapping primers T32E18, F22K20, T14N5, T5M16.1 and F28K19.1 indicted that the *sks* mutation lay further downstream of the At1g77130 gene.

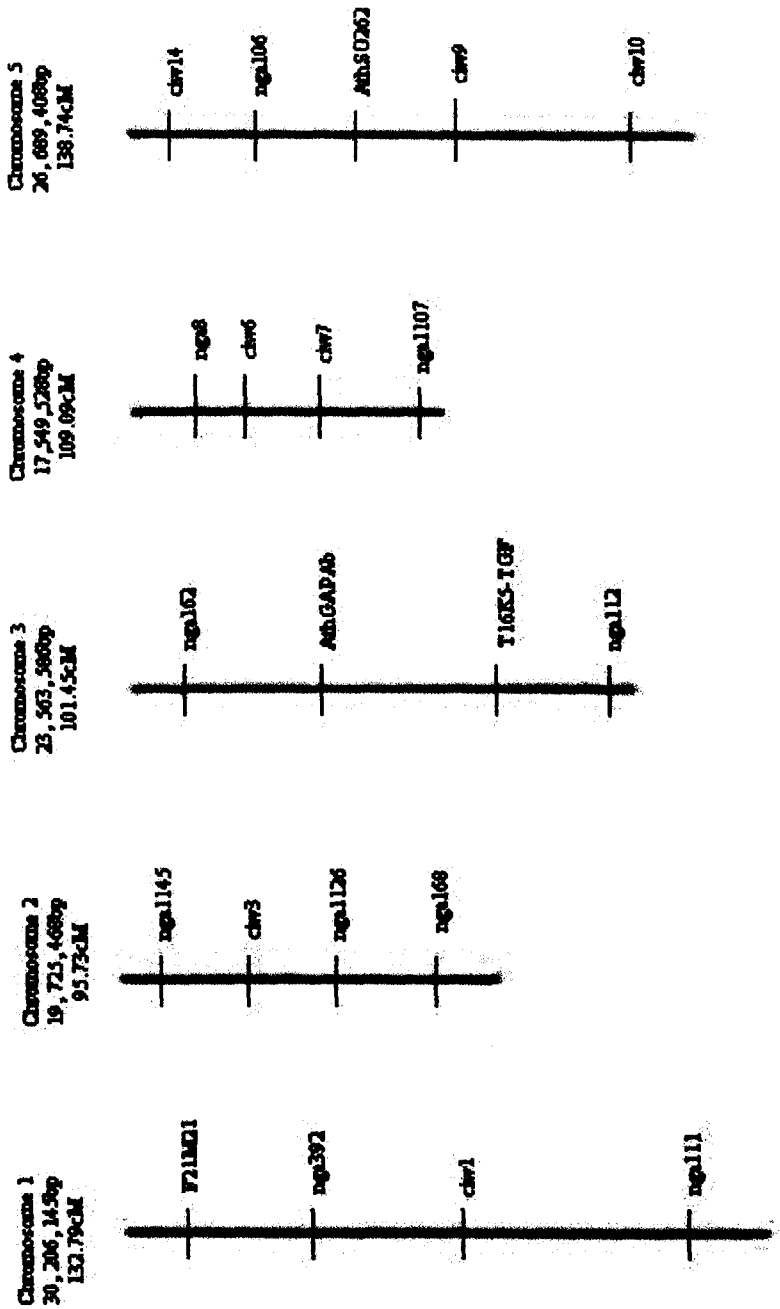

FIGURE 5.3.1: Map of the five *Arabidopsis* chromosomes showing the approximate location of the SSLP markers used to rough map the *SKS* locus.

Chromosome 1 -30, 206, 145bp (135cM)

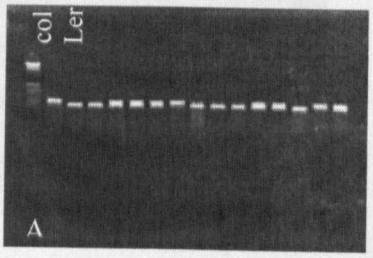

F21M12 –3, 212, 193 bp

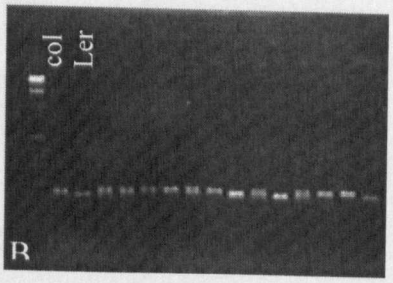

nga392- 9, 831, 900 bp

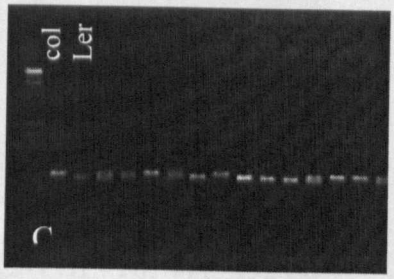

ciw1- 17, 951, 444 bp

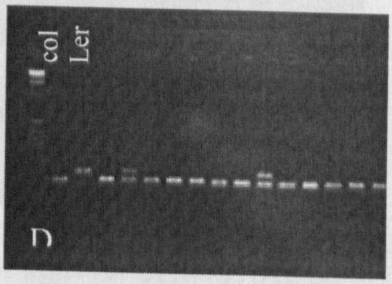

nga111- 27, 005, 122 bp

Chromosome 2 - 19, 725, 468bp (95.73cM)

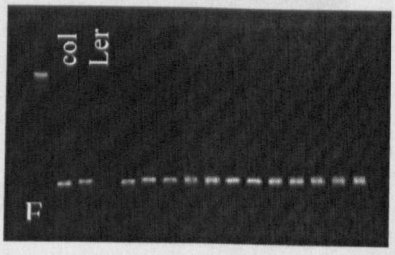

nga1145- 682, 624

ciw3- 6, 351, 398 bp

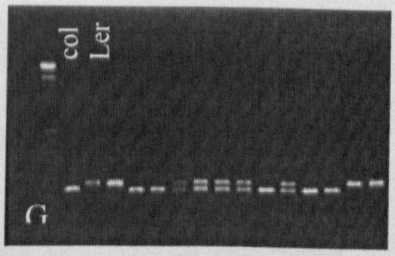

nga1126- 50.65cM

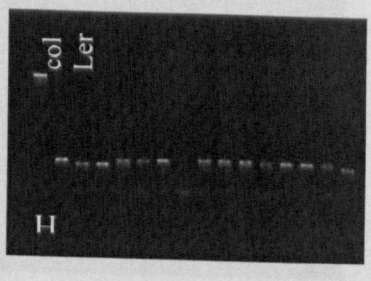

nga168- 16, 240, 385 bp

Chromosome 3- 23, 563, 586bp (101.45cM)

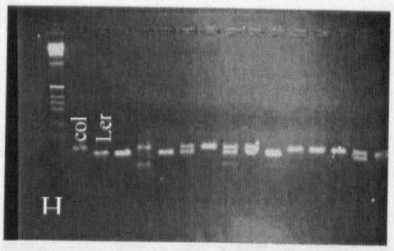

nga162- 4, 608, 281 bp

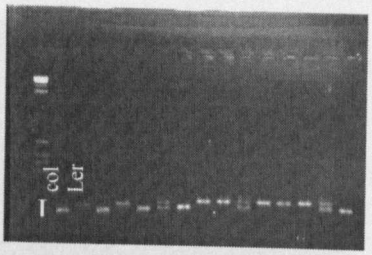

AthGAPAb- 43.77cM

T16K5-TGF- 18, 441, 052 bp

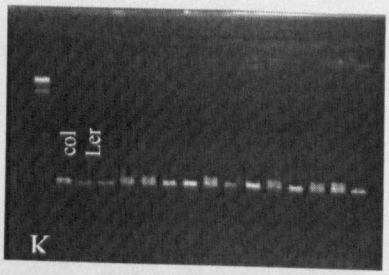

nga112- 23, 177, 332 bp

Chromosome 4- 17, 549, 528bp (125cM)

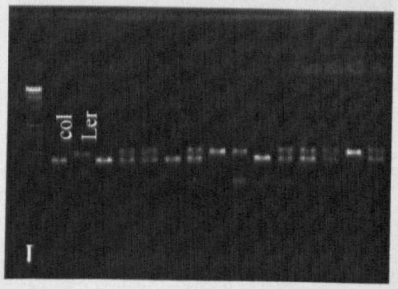

nga8- 4, 593, 289 bp

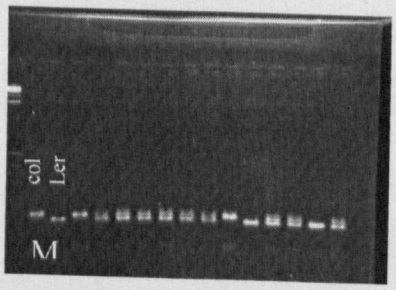

ciw6- 6, 857, 107 bp

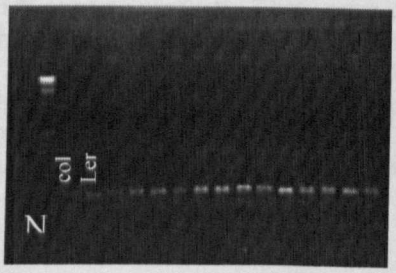

ciw7- 10, 488, 849bp

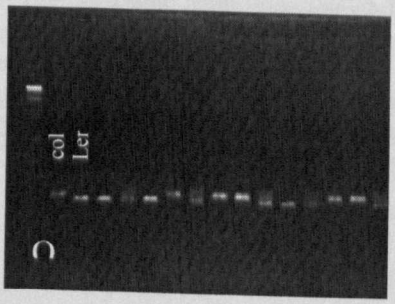

nga1107- 17, 060, 616bp

Chromosome 5- 26, 689, 408bp (140.3cM)

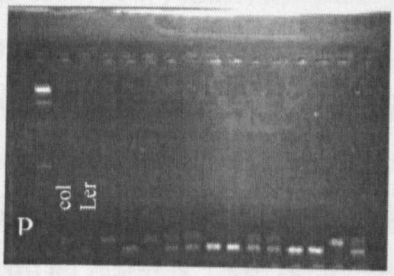

ciw14- 2, 174, 596 bp

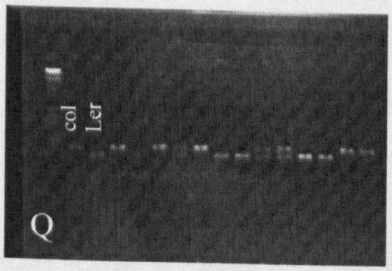

nga106- 33.35cM

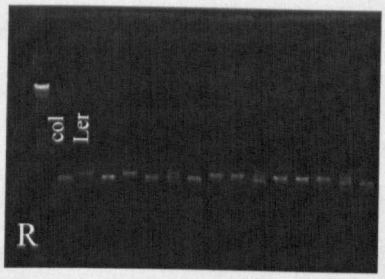

AthSO262- 65.20cM

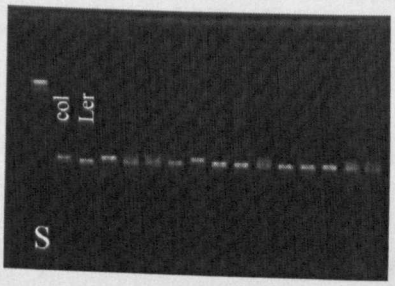

ciw9- 16, 757, 909bp

ciw10- 24, 244, 776bp

FIGURE 5.3.2: Gel electrophoresis pictures of the SSLP markers used for the initial rough mapping with Col, L*er* and *sks* x L*er* F2-1 DNA. The first two lanes are the Columbia and Landsberg *erecta* WT controls to indicate the product size expected for that DNA. The remaining lanes show the F2-1 DNA PCR reaction products. These products can either be Columbia size; L*er* size or two bands may have amplified indicating that the DNA came from a heterozygous plant.

The *sks* mutant was created in the Columbia background and marker nga111 (D) on the bottom arm of chromosome 1 showed bias towards amplification of Columbia PCR products. The remaining markers showed no obvious amplification of Columbia products to Landsberg *erecta* products indicating that the *sks* mutation was unlinked to those loci.

5.3.4 Further Mapping of the *sks* mutation using InDELs

DNA was isolated from 232 *sks* x L*er* F2-1 seedlings and 48 recombinant (heterozygous) individuals were identified by using markers nga111 and F18B13. All suitable InDel markers found between BAC clones T32E8 and F9K20 on chromosome 1 on the Syngenta (Cereon) database were utilised as markers and used for mapping. However, it was found that approximately one-half of all attempted InDel markers failed consistent with other reports (Jander *et al*, 2002).

InDel markers T32E18, F22K20 and T14N5 were found to behave consistently and recombinants could readily be identified (figure 5.3.3 and 5.3.4 A, B, C). The number of recombinants decreased the further down chromosome 1 each InDel marker was located indicating that the *sks* mutation lay near the bottom of chromosome 1 (figure 5.3.3).

Recombination frequencies were calculated by taking the: Total Number of Recombinants/ Total Number of DNA samples X 100, it was assumed that a 1% recombination frequency is equivalent to ~250Kb (Luckowitz *et al*, 2000). InDel T32E18 (figure 5.3.4 A), F22K20 (figure 5.3.4 B) and T1N45 (figure 5.3.4 C) had recombination frequencies of 4.31%, 3.87% and 3.45% respectively. These recombination frequencies led to the *sks* mutation being localised to a 400Kb region between BAC clones T5M16 and F9K20 (figure 5.3.3).

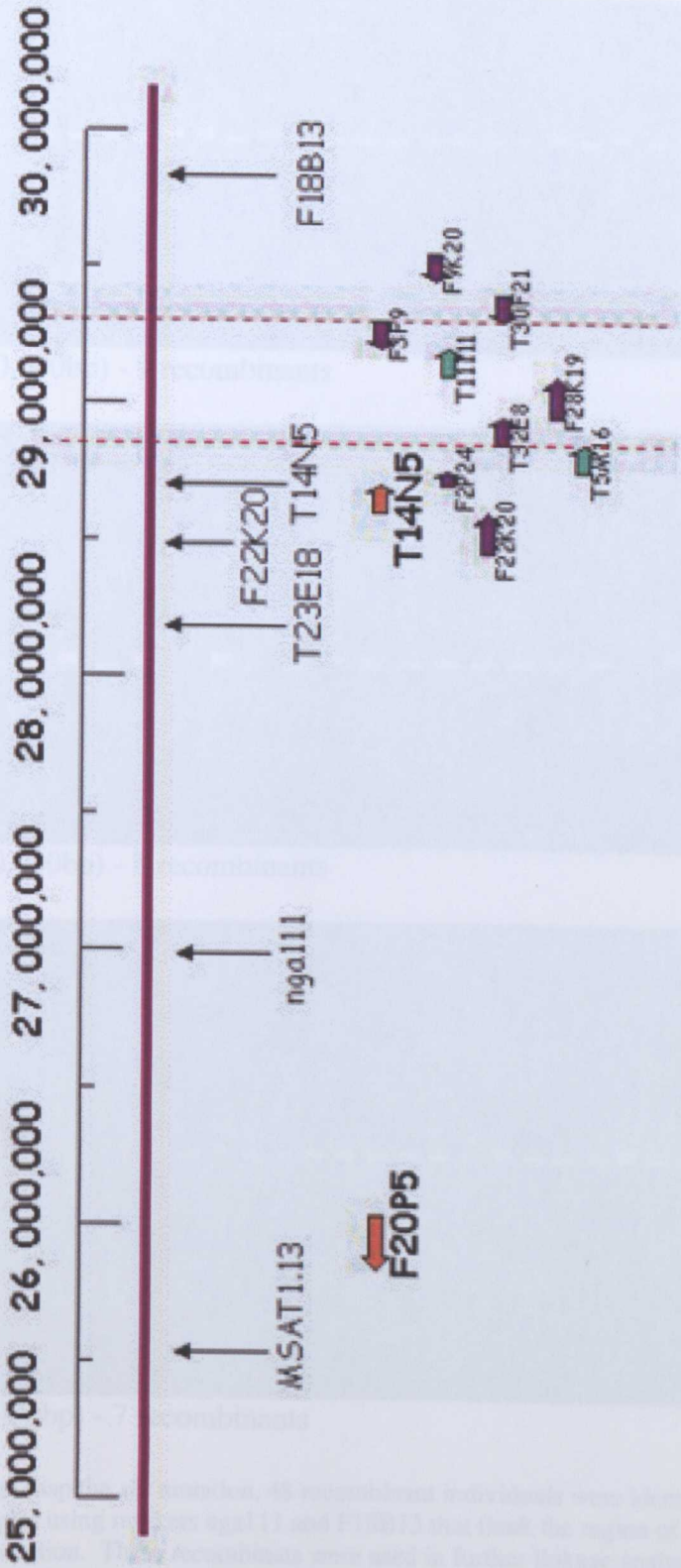

FIGURE 5.3.3: Map of the lower arm of chromosome 1 between 25, 000, 000bp and 30, 000, 000bp indicating the location of the principal SSLP and InDel markers that were used to further localise the *SKS* locus. BAC clones F20P5 and T14N5 are highlighted orange and show the location of initial candidate genes, both contain family 8 glycosyltransferase members of which the *quasimodo* mutant is a member (Bouton *et al*, 2002). Both, however, were discarded as mapping data indicated that the *sks* mutation lies further downstream between BAC clones T32E8 and T30F21 between 28, 700, 000bp and 29, 200, 000bp. BAC clones highlighted in purple (T32E8, F28K19 & F3F9) contain cell wall related genes.

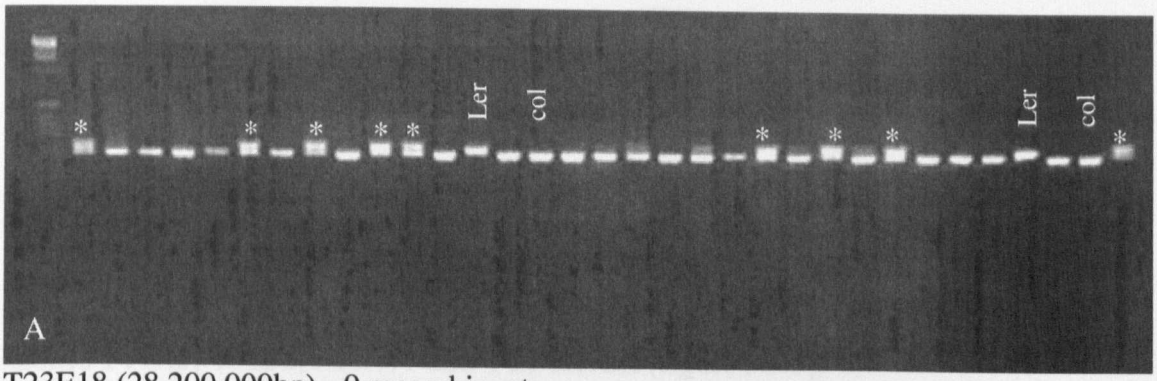

T23E18 (28,200,000bp) - 9 recombinants

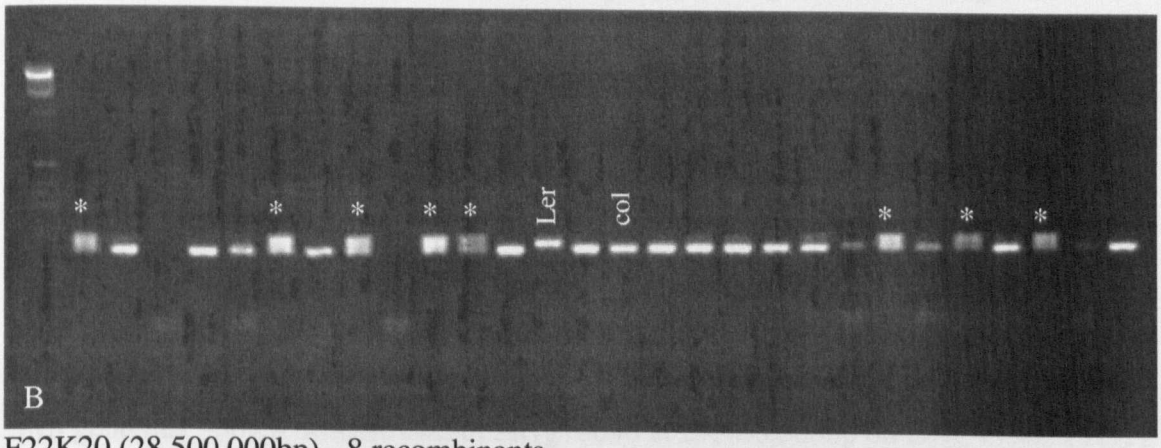

F22K20 (28,500,000bp) - 8 recombinants

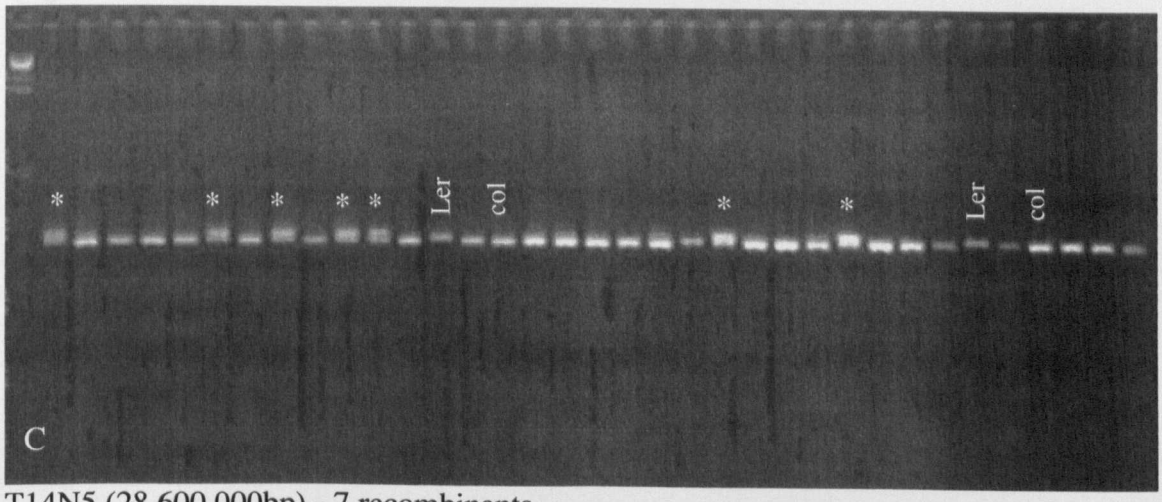

T14N5 (28,600,000bp) - 7 recombinants

FIGURE 5.3.4: To fine map the *sks* mutation, 48 recombinant individuals were identified from 232 *sks* x L*er* F2-1 DNA samples using markers nga111 and F18B13 that flank the region of chromosome 1 containing the *sks* mutation. These recombinats were used in further linkage analysis using INDEL markers T32E18 (A), F22K20 (B) and T14N5 (C) within the region of 27,000,000bp and 30,000,000bp on the lower arm of chromosome 1. From the recombination frequencies, the *sks* mutation was thought to lie in a 400Kb region between BAC clones T5M16 and F9K20 as shown in figure 5.1.3.

The Columbia (Col) and Landsberg *erecta* (Ler) WT controls are labelled and indicate the product size expected for that DNA. The remaining lanes show the recombinant *sks* x L*er* F2-1 DNA PCR reaction products. These products can either indicates a Col or L*er* homozygote or two bands may have amplified indicating that the DNA came from a heterozygous recombinant plant (asterisks).

5.3.5 Fine Mapping of the *sks* Mutation using SNPs

All InDels between BAC clones T5M16 and F9K20 that had been found to be suitable had already been used and so it was decided to turn to SNP markers to undertake fine mapping of the *sks* gene. The InDel marker F22K20 was used to isolate 43 recombinants from a further 924 samples of *sks* x Ler F2-1 DNA (figure 5.3.3 and section 5.3.4). These recombinants were used with a range of SNP markers on BAC clones T14N5, T32E8, F28K19 and YUP8H12R (figure 5.3.5).

SNP markers At1g77120, At1g77720, At1g77800, At1g78040 and At1g79260 had recombination frequencies of 2.38%, 1.62%, 1.3%, 0.5% and 4.54% respectively. A *xy* plot of the recombination frequency between them and their position along chromosome 1 reveals a linear relationship (figure 5.3.6). It can be postulated that regression of the relationship to intersect the *x*-axis would predict that the final position of the *SKS* gene lies at ~29, 460, 000bp. One can also calculate the approximate distance to the *SKS* gene by using the relationship between the recombination frequencies between pairs of markers and their physical location on the chromosome. This would indicate that the *SKS* gene lies ~60Kb downstream of At1g78040 at 29,460,000bp on BAC clone T11I11 (figure 5.3.7).

If the *SKS* gene is located at ~29,460,000bp on BAC clone T11I11 and one takes the 20Kb region either side i.e. 29,440,000 to 29, 480,000bp then there are nine predicted candidate genes (figure 5.3.7). SALK insert lines exist for seven of the nine genes (section 5.2.7), and if the *SKS* gene cannot be identified through phenotypic identification of SALK lines then sequencing of the entire region between 29,440,000 to 29, 480,000bp in the *sks* background will be instigated.

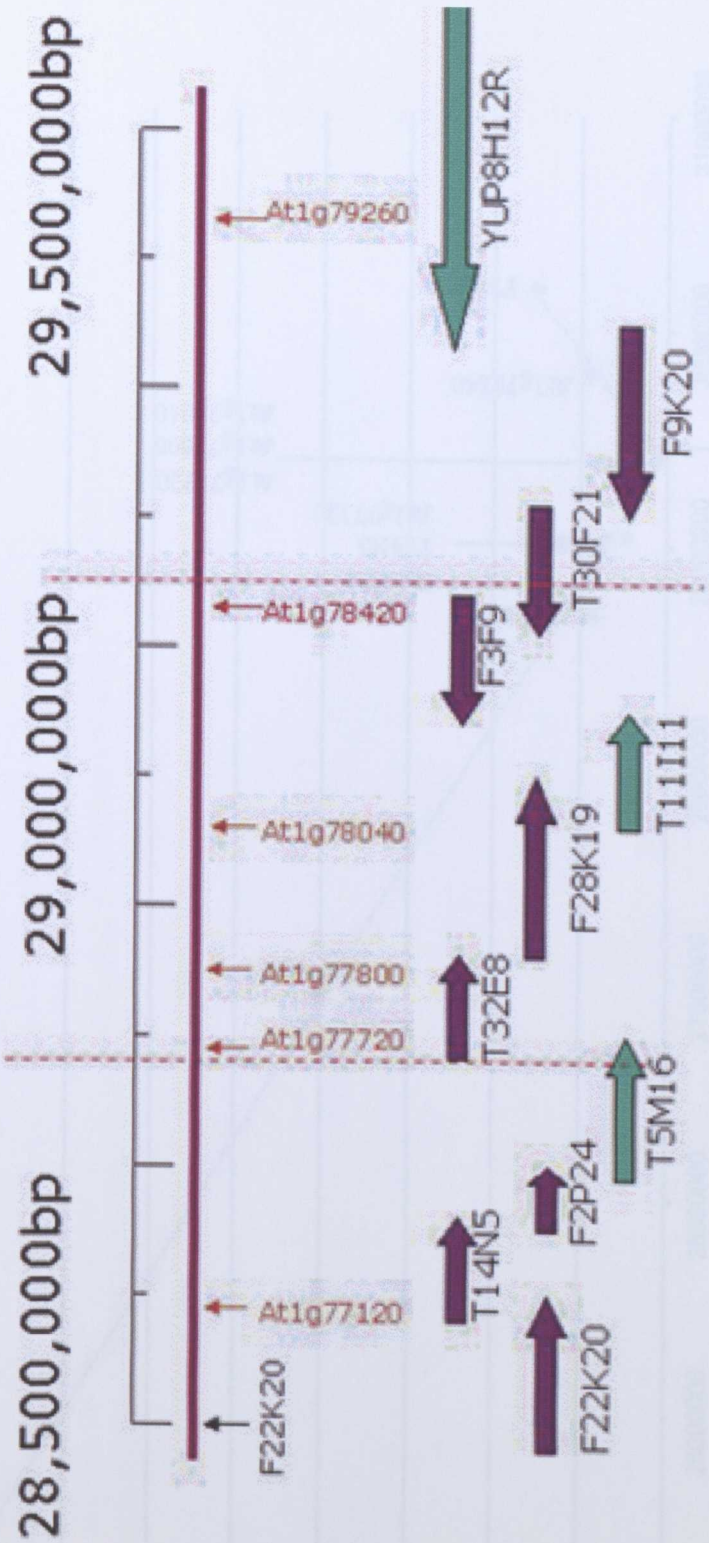

FIGURE 5.3.5: The InDel marker F22K20 was used to isolate 43 recombinants from 924 *sks* x L*er* F2-1 DNA samples for SNP analysis. SNP markers At1g77120, At1g77720, At1g77800, At1g78040 and At1g79260 were used to pinpoint the *sks* mutation to ~60Kb downstream of SNP marker At1g78040.

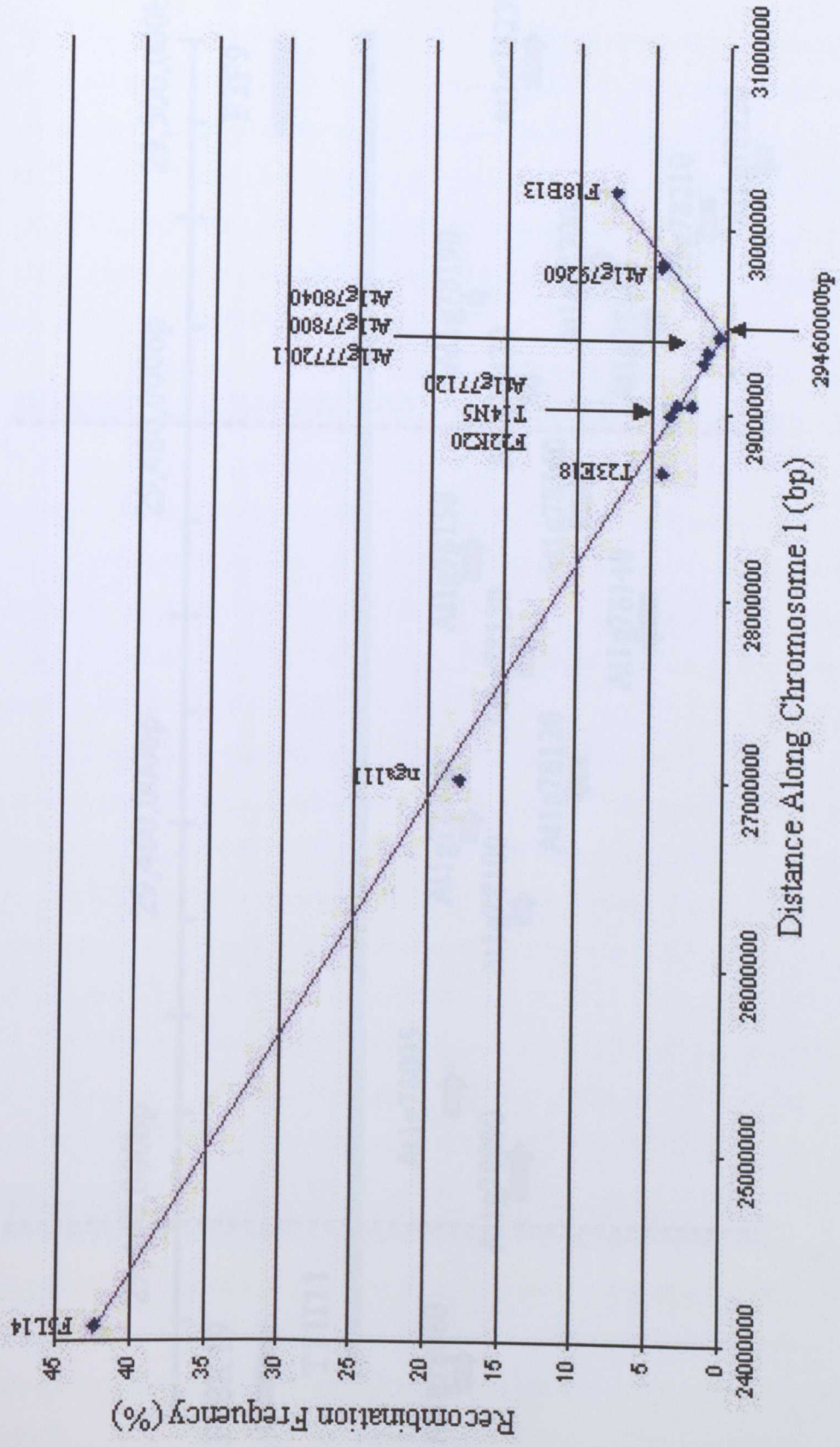

FIGURE 5.3.6: Linear *xy* plot of the recombination frequency of each marker against its position on chromosome 1. Regression of the linear relationship to intersect the *x*-axis leads to the *SKS* mutation being located at ~29, 460, 000bp on BAC clone T11I11.

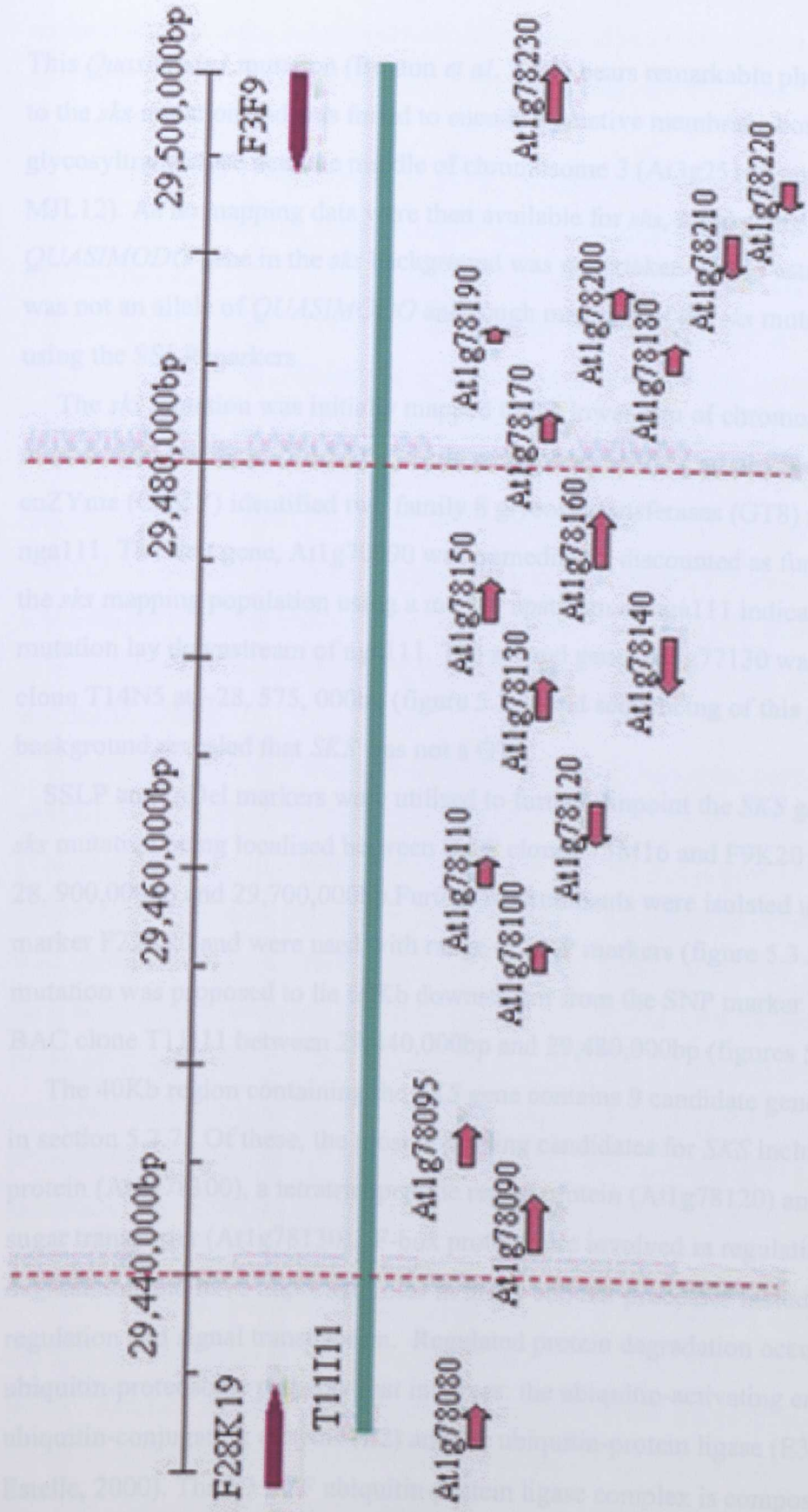

FIGURE 5.3.7: Map based cloning of the *SKS* gene has located this locus to BAC clone T11I11 between 29,440,000bp and 29,480,000bp at the very bottom of chromosome 1. There are nine genes in this region and SALK insert lines will be used to identify the *SKS* gene by phenotypic analysis and sequencing of BAC clone T11I11 will also be instigated.

5.4 DISCUSSION

This *Quasimodo1* mutation (Bouton *et al*, 2002) bears remarkable phenotypic similarity to the *sks* mutation and was found to encode a putative membrane bound family 8 glycosyltransferase near the middle of chromosome 3 (At3g25140 on BAC clone MJL12). As no mapping data were then available for *sks*, sequencing of the *QUASIMODO* gene in the *sks* background was undertaken. It was established that *sks* was not an allele of *QUASIMODO* and rough mapping of the *sks* mutation was initiated using the SSLP markers.

The *sks* mutation was initially mapped to the lower arm of chromosome 1, near marker nga111 (figure 5.3.2 D). *In silico* searching of the Carbohydrate Active enZYme (CAZY) identified two family 8 glycosyltransferases (GT8) near marker nga111. The first gene, At1g70090 was immediately discounted as further analysis of the *sks* mapping population using a marker upstream of nga111 indicated that the *sks* mutation lay downstream of nga111. The second gene, At1g77130 was found on BAC clone T14N5 at ~28, 575, 000bp (figure 5.3.3) and sequencing of this gene in the *sks* background revealed that *SKS* was not a GT8.

SSLP and InDel markers were utilised to further pinpoint the *SKS* gene and led to the *sks* mutation being localised between BAC clones T5M16 and F9K20 (figure 5.3.3) at 28, 900,000bp and 29,700,000bp.Further recombinants were isolated using InDel marker F22K20 and were used with range of SNP markers (figure 5.3.5). The *sks* mutation was proposed to lie 60Kb downstream from the SNP marker At1g78040, on BAC clone T11I11 between 29,440,000bp and 29,480,000bp (figures 5.3.4 and 5.3.5).

The 40Kb region containing the *SKS* gene contains 9 candidate genes that are listed in section 5.2.7. Of these, the most promising candidates for *SKS* include an F-box protein (At1g78100), a tetratricopeptide repeat protein (At1g78120) and a putative sugar transporter (At1g78130). F-box proteins are involved in regulating protein degradation and have important roles in many cellular processes including cell cycle regulation and signal transduction. Regulated protein degradation occurs via the ubiquitin-proteosome pathway that involves: the ubiquitin-activating enzyme (E1), the ubiquitin-conjugating enzyme (E2) and the ubiquitin-protein ligase (E3) (del Pozo and Estelle, 2000). The E3 SCF ubiquitin-protein ligase complex is composed of four subunits: cullin, SKP1, RBX1 and an F-box protein. F-box proteins contain a motif that interacts with SKP1 and also contain WD40 or leucine-rich repeats that are involved in

recognition of the protein to be degraded (del Pozo and Estelle, 2000). Mutations within F-box proteins have resulted in alterations in jasmonic acid response (Devoto and Turner, 2003), cell division (del Pozo *et al*, 2002) and regulation of circadian rhythm (Kim *et al*, 2003).

Tetratricopeptide repeat proteins (TPR) contain a 34-amino acid repeat present in multiple arrays that form antipathic α-helices that mediate protein-protein interactions (Vittorioso *et al*, 1998). Tetratricopeptide repeats are found in kinesin light chains (Ginhart and Goldstein, 1996), SNAP secretory proteins (Ordway *et al,* 1994) and clathrin heavy chains (Andrade *et al,* 2000), suggesting a link to vesicle formation, transport and fusion. TPRs have also been found to have a role in gibberellin response (Tseng *et al*, 2001) and in cell elongation and division. The PASTICCINO1 mutant encodes a protein with TPR repeats that has several phenotypic similarities to *sks* including a vitreous appearance and a loss of cell adhesion (Vittorioso *et al*, 1998). In addition, several other mutants with similar phenotypes to *sks* are known to have defects in their cytoskeleton network or in vesicle transport (Burk *et al*, 2001, Qiu *et al*, 2002 and Smith, 2003).

Sugar transporters are widespread throughout *Arabidopsis* not only for transporting photosynthetic assimilates throughout the plant (Gottwald *et al*, 2000, Buettner *et al*, 2000 and Barker *et al*, 2000) but they may also be involved in protection from environmental stresses (Kiyosue *et al*, 1998) and in the synthesis of non-cellulosic cell wall components (Norambuena *et al*, 2002 and Baldwin *et al*, 2001). Nucleotide sugars such as GDP-mannose and UDP-galactose are transported from the cytosol to the lumen of the golgi apparatus by nucleotide sugar transporters. Glycosyltransferases use these nucleotide-linked sugars for donation of the sugar moiety to synthesize non-cellulosic polysaccharides and glycoproteins (Baldwin *et al*, 2001). Alterations in either of these processes may affect the synthesis of cell wall components and result in changes to the cell wall architecture.

The *sks* mutant is known to have alterations in the cell wall and a defective sugar transporter could explain the phenotype. However, alterations in F-box proteins and tetratricopeptide repeat proteins could also result in the *sks* phenotype, especially if they are involved in the regulation of cell division and elongation or in the localization of cell wall components via the cytoskeleton. SALK insert lines (section 5.2.7) were ordered for seven of the nine candidate genes to try and isolate the *SKS* gene by

identification via its phenotype and sequencing of the 40Kb region will also be instigated.

5.4.1 Conclusions

SSLP, InDel and SNP markers were used to localise the *sks* mutation to BAC clone T11I11 between 29,440,000bp and 29,480,000bp at the bottom of chromosome 1. There are nine candidate genes within this region encoding a variety of proteins with known and unknown functions. Of these genes, the most promising candidates for *SKS* include an F-box protein (At1g78100), a tetratricopeptide repeat protein (At1g78120) and a putative sugar transporter (At1g78130). Changes within the coding sequence of any of these genes could potentially lead to a phenotype similar to *sks*. SALK insert lines have been ordered for phenotypic analysis for seven out of nine of the candidate genes and sequencing of the region will be undertaken.

6.0 CONCLUSIONS AND FUTURE PROSPECTS

Investigation into the role of the *SKS* gene in *Arabidopsis* has revealed complex links between the plant cell wall and cell expansion that when disrupted result in gross morphological changes. The *sks* mutant was originally isolated on the basis of its seedling phenotype from an *En*-element mutagenised population (Marchant and Bennett, unpublished results). The mutant is recessive and exhibits a seedling lethal phenotype. However approximately 36% of homozygous *sks* seedlings display a "wild type" phenotype. These "wild type" *sks* seedlings can survive in greenhouse conditions but display an altered phenotype when compared to wild type plants.

The mutation results in a complex and varied shoot and root phenotype incorporating epidermal cell separation and changes in epidermal cell architecture and distribution that becomes increasingly severe as seedling development progresses. The most apparent defect in *sks* seedlings is observed in epidermal pavement cells, which exhibit reduced cell expansion and the absence of characteristic jigsaw shaped epidermal cell lobes. There is also a progressive reduction in cell-to-cell adhesion between the pavement epidermal cells of *sks* seedlings. The epidermal layer may have defects in cell wall biosynthesis or expansion and the turgor pressure and mechanical stresses in the underlying cell layers could act to pull apart or initiate cell wall degradation between the pavement epidermal cells.

Hypocotyl epidermal cells of *sks* show irregular cell divisions and have reduced epidermal cell-to-cell adhesion similar to those of the foliar epidermis. Under normal growth conditions there are twice as many hypocotyl epidermal cells in *sks* but they are 2-fold shorter indicating that increased division is occurring due to reduced elongation. Increased epidermal cell division has been observed in the apex of the *sks* hypocotyls using *Cyclin B1*::GUS and *AtML1*::GUS markers. In addition, temperature induced hypocotyl elongation occurs primarily by cell elongation, and when *sks* seedlings are grown under conditions of stress hypocotyl elongation is limited.

A variety of mutants have been isolated in *Arabidopsis* that display similar epidermal cell phenotypes to *sks* in one or more of their organs and often have defects in their cell wall, the cytoskeleton or in cell division and include the *korrigan* mutant (His *et al*, 2001) and the *keule* mutant (Assad *et al*, 2001). The *SPIKE1-1 gene* encodes a protein that may mediate the reorganisation of the cytoskeleton in response to extracellular signals and the mutant displays defects in epidermal cell-cell adhesion and epidermal

cell expansion similar to that of *sks* (Qiu *et al*, 2002). There are no obvious changes in *spk1-1* cell wall composition and so it was suggested that the reduction in interdigitation of unlobed cells and subtle cell wall defects led to the failure of epidermal cells to withstand the forces of organ expansion (Qui *et al*, 2002).

The defects in *sks* epidermal pavement cell architecture also results in clusters of stomata and an increase in stomatal density and stomatal index. These changes may be due to the disruption of cell-cell signalling processes that govern stomatal patterning. However, stomatal divisions are also important for producing not only stomatal complexes but also the majority of cells in the foliar epidermis (Geisler *et al*, 2000). Both the *AtML1*::GUS and *CyclinB1*::GUS markers have been found to be up-regulated in *sks* indicating increased expression of L1 specific genes in conjunction with an increase in mitotic division. This results in an increased number of stomatal complexes and pavement epidermal cells that could partially compensate for limited expansion of *sks* epidermal cells. However, to confirm the *ATML1*::GUS expression data in *sks*, quantitative RT-PCRs need to be performed on the *AtML1* mRNA.

The trichomes of the *sks* mutant are unusual as they lack papillae and possess a smooth surface. Trichomes of the *tbr* mutant are similar to those of *sks* and are thought to lack a cellulosic secondary cell wall (Potikha and Delmer, 1995). Therefore, if the basis for *sks* trichomes lacking papillae is cell wall based then the reduced expansion of pavement epidermal cells may also be due to a cell wall defect. Both FT-IR and neutral sugar analysis have indicated that there is an increase in cellulose and XG within *sks* that could lead to a stronger and stiffer cell wall. An increasingly rigid cell wall would not be able to expand as easily and may therefore lead to the cell-cell separation observed in the epidermis of *sks* due to the pressure of the underlying cell layers.

FT-IR analysis and labelling of *sks* hypocotyl sections with the JIM5 antibody has indicated that de-esterified pectins are localised throughout the cell wall and not just at the intercellular junctions and middle lamella. If the de-esterified block structure is normal this could lead to strengthening of the cell wall. However, this has not been determined and if the block structure is altered it could equally lead to reduced cell-to-cell adhesion. Further cell wall analysis would be required to determine the extent and distribution of de-esterified pectin within *sks* cell walls and its likely role in cell-to-cell adhesion.

There is also a reduction in the xylosyl containing sidechains on RG-II leading to reduced intercellular attachment via borate-diol ester crosslinks. However, the

distribution of methyl-esterified pectin is unaltered indicating that linkages between methyesterified pectin and the hemicellulose-cellulose network and between HGA and RG-I pectin are normal. Arabinan-sidechains on RG-I also appear to have increased leading to strengthening of the crosslinks of RG-I to XG fibrils and this in association with a normal distribution of methyl-esterified HGA leads to the promotion of intercellular attachment.

Changes in cell wall composition can be due to defects in either cell wall biosynthesis or in the cytoskeleton and can disrupt the normal cell expansion processes that can lead to alterations in cell and organ morphology (Burk *et al*, 2001). For example, the morphogenesis of lobed epidermal pavement cells and trichomes, involves multi-directional cell expansion that depends on both microtubules and F-actin to co-ordinate cell wall deposition. As *sks* epidermal cells do not develop lobes and have cell wall defects further investigation into the distribution of F-actin and microtubules within these cells by immunolocalisation is required to investigate the cytoskeletal network and its role in cell wall expansion and cell morphology.

A variety of mutants that have defects in their cell wall or cytoskeleton, have altered epidermal cell morphology and/or reduced cell-to-cell adhesion have been identified including the *Arabidopsis* mutants *angustifolia* (Kim *et al*, 2002) and *fragile fiber2* (Burk *et al*, 2001) and the maize *brick* mutations (Frank *et al*, 2003). The *QUASIMODO1* gene encodes a family 8 glycosyltransferase that is thought to have a role in the synthesis of homogalacturonan and has alterations in its cell wall leading to a phenotype very similar to *sks* (Bouton *et al*, 2002).

To identify the gene responsible for the phenotype of the *sks* mutant, map based cloning was undertaken. The *SKS* gene was proposed to lie 60Kb downstream from the SNP marker At1g78040, on BAC clone T11I11 between 29,440,000bp and 29,480,000bp. This 40Kb region contains 9 candidate genes, of which the most promising candidates for *SKS* include an F-box protein (At1g78100), a tetratricopeptide repeat protein (At1g78120) and a putative sugar transporter (At1g78130) could have roles in cell wall biosynthesis, signal transduction or in vesicle transport.

Changes within the coding sequence of any of these genes could potentially lead to a phenotype similar to *sks*. The *sks* mutant is known to have alterations in the cell wall and a defective sugar transporter could result in changes to the cell wall architecture. However, alterations in F-box proteins and tetratricopeptide repeat proteins could also result in the *sks* phenotype, especially if they are involved in the regulation of cell

division and elongation or in the localization of cell wall components. SALK insert lines have been ordered for seven of the nine candidate genes to try and isolate the *SKS* gene by identification via its phenotype and sequencing of the 40Kb region will also be instigated.

Further work in this area involves identifying and cloning the *SKS* gene and investigating its function via localisation of the transcript and protein by immunolocalisation, quantitative RT-PCR and through GUS and GFP constructs. Following the isolation of the *SKS* gene it will also be possible to determine whether the *sks* mutant does possess an epidermal specific defect by undertaking tissue specific expression studies. Protein interaction studies could also be carried out to investigate whether the *SKS* gene product is closely associated with other proteins.

In summary, the *sks* mutant has defects in its cell wall composition that results in reduced cell elongation and increased cell division. These fundamental changes result in altered epidermal cell development and distribution and reduced epidermal cell-to-cell adhesion. Whilst the function of the *SKS* gene is as yet unknown, it has been mapped to a 40Kb region on the bottom of chromosome 1 that codes several candidate genes involved in regulating cell wall biosynthesis, the cytoskeleton or cell division.

7.0 ACKNOWLEDGEMENTS

I would like to thank the senior members of the Bennett lab especially Alan Marchant for their sensible and patient advice and help in times of need. To the remaining members of the Bennett, Roberts, Pyke and Wilson labs (especially Paula, Becky, Monica, Kamal and Gema), I would like them to know how much I appreciated their ability to make the lab a much more enjoyable and fun place to work and to thank them for listening to me moaning when things annoyed me that bit too much!

To my family and friends at home, thanks for believing in me and letting me come home, relax and then let me return to the deepest South. To Dan, for making me feel guilty enough to get out of bed in the morning, looking after me in times of need and for being my guiding light. And last, but not least, Malcolm, thank you for bombarding me with ideas some of which were actually fairly sensible and then letting me get on with it. I would also like to thank the BBRSC for funding my PhD, without which none of this work would have been possible.

8.0 BIBLOGRAPHY

Abe M, Katsumata H, Komeda Y and Takahashi T, (2003), Regulation of shoot epidermal differentiation by a pair of homeodomain proteins in *Arabidopsis*, *Development*, **130**: 635-643.

Alonso J.M, Stepanova A.N, Leisse T.J, Kim C.J, Chen H, Shinn P, Stevenson D.K, Zimmerman J, Barajas P, Cheuk R, Gadrinab C, Heller C, Jeske A, Koesema E, Meyers C.C, Parker H, Prednis L, Anasari Y, Choy N, Deen H, eralt M, Hazari N, Hom E, Karnes M, Mulholland C, Ndubaku R, Scmidt I, Guzman P, Aguilar-Henonin L, Schmid M, Weigal D, Carter D.E, Marchand T, Risseeuw E, Brogden D, Zeko A, Crosby W.L, Berry C.C, Ecker J.R, (2003), Genome-wide insertional mutagenesis of *Arabidopsis thaliana*, *Science*, **301**: 653-657.

Andrade M.A, Ponting C, Gibson T and Bork P, (2000), Identification of protein repeats and statistical significance of sequence comparisons, *Journal of Molecular Biology*, **298:** 521–537.

Assaad F.F, Huet Y, Mayer U and Jurgens G, (2001), the cytokinesis gene KEULE encodes a SEC1 protein that binds the syntaxin KNOLLE, *The Journal of Cell Biology*, **152**:531-543.

Atkinson R.G, Schroder R, Hallett I.C, Cohen D and MacRae E.A, (2002), Overexpression of polygalacturonase in transgeneic apple trees leads to a range of novel phenotype involving changes in cell adhesion, *Plant Physiology*, **129**:122-133.

Baldwin T.C, Handford M.G, Yuseff M-I, Orellana A, Dupree P, (2001), Identification and characterisation of GONST1, a Golgi-localised GDP-mannose transporter in *Arabidopsis, The Plant Cell*, **13**: 2283-2295.

Balzergue S, Dubreucq B, Chauvin S, Le-Clainche I, Le Boulaire F, de Rose R, Samson F, Biaudet V, Lecharny A, Cruaud C, Weissenbach J, Caboche M and Lepiniec L, (2001), Improved PCR-walking for large-scale isolation of plant T-DNA borders, *Biotechniques*, **30**: 496-498.

Barker L, Kuehn C, Weise A, Schulz A, Gebhardt C, Hirner B, Hellmann H, Schulze W, Ward J.M, Frommer W.B, (2000), SUT2, a putative sucrose sensor in sieve elements, *The Plant Cell*, **12**: 1153-1164.

Barlier I, Kowalczyk M, Marchant A, Ljung K, Bhalerao R, Bennett M, Sandberg G and Bellini C, (2000), The *SUR2* gene of *Arabidopsis* thaliana encode the cytochrome P450 CYP83B1, a modulator of auxin homeostasis, *Proceedings of the National Academy of Sciences*, **97**:14819-14824.

Berger D and Altmann T, (2000), A subtilisin-like serine protease involved in the regulation of stomatal density and distribution in *Arabidopsis thaliana, Genes and Development*, **14**:1119-1131.

Beemster G.T.S, Fiorani F, Inze D, (2003), Cell cycle: the key to plant growth control? *Trends in Plant Science*, **8**:154-158.

Bird S.M and Gray J.E, (2003), Signals from the cuticle affect epidermal cell differentiation, *New Phytologist*, **153**:9-23.

Bougourd S, Marrison J and Haseloff J, (2000), An aniline blue staining procedure for confocal microscopy and 3D imaging of normal and perturbed cellular phenotypes in mature *Arabidopsis* embryos, *The Plant Journal*, **24**: 543-550.

Bouton S, Leboeuf E, Mouille G, Leydecker M, Talbotec J, Granier F, Lahaye M, Hofte H and Truong H, (2002), *QUASIMODO1* encodes a putitive membrane bound glycosyl transferase required for normal pectin synthesis and cell adhesion in *Arabidopsis*, *The Plant Cell*, **14**:2577-2590.

Brownlee C, (2001), The long and the short of stomatal density signals, *Trends in Plant Science*, **6**:441-442.

Buettner M, Truernit E, Baier K, Scholz-Starke J, Sontheim M, Lauterbach C, Huss V.A.R, Sauer N, (2000), AtSTP3, a green leaf-specific, low affinity monosaccharide-H^+ symporter of *Arabidopsis thaliana*, *Plant Cell and Environment*, **23**: 175-184.

Burk D.H, Liu B, Zhong R, Morrison W.H, Ye Z-H, (2001), A katanin-like protein regulates normal cell wall biosynthesis and cell elongation, *The Plant Cell*, **13**:807-827.

Burton R.A, Gibeaut D.M, Bacic A, Findlay K, Roberts K, Hamilton A, Baulcombe D.C and Fincher G.B, (2000), Virus induced silencing of a plant cellulose synthase gene, *The Plant Cell*, **12**:691-705.

Cano-Delgado A.I, Metzlaff K and Bevan, M.W, (2000), The *eli1* mutation reveals a link between cell expansion and secondary cell wall formation in *Arabidopsis thaliana*, *Development*, **127**:3395-3405.

Carpita N.C and Gibeaut D.M, (1993), Structural models of primary cell walls in flowering plants: consistency of molecular structure with the physical properties of the walls during growth, *The Plant Journal*, **3**:1-30.

Carpita N, Tierney M and Campbell M, (2001), Molecular biology of the plant cell wall: searching for the genes that define structure, architecture and dynamics, *Plant Molecular Biology*, **47**:1-5.

Cascuberta E, Puigdomenech P and Monfort A, (2000) Distribution of microsatellites in relation to coding sequences within the *Arabidopsis thaliana* genome, *Plant Science*, **157**: 97-104.

Casimiro I, Marchant A, Bhalerao R.P, Beeckman T, Dhooge S, Swarup R, Graham N, Inze D, Sandberg G, Casero P.J and Bennett M, (2001), Auxin transport promotes *Arabidopsis* lateral root initiation, *The Plant Cell*, **13**:843-852.

Chen L.M, Carpita N.C, Reiter W.D, Wilson R.W, Jeffries C and McCann MC (1998) A rapid method to screen for cell wall mutants using discriminate analysis of Fourier transform infrared spectra, *The Plant Journal*, **16:** 385-392.

Cosgrove D.J, (1997), Assembly and Enlargement of the primary cell wall in plants, *Annual Review of Cellular and Developmental Biology*, **13**:171-201.

Cosgrove D.J, (2001), Wall structure and wall loosening. A look backwards and forwards, *Plant Physiology*, **125**: 131-134.

Dale, J.E, (1988), The control of leaf expansion, *Annual Review of Plant Physiology and Plant Molecular Biology*, **39**:267-295.

del Pozo J.C and Estelle M, (2000), F-box proteins and protein degradation: An emerging theme in cellular regulation, *Plant Molecular Biology*, **44**:123-128.

del Pozo J.C, Boniotti M.B, Gutierrez C, (2002), *Arabidopsis* E2Fc functions in cell division and is degraded by the ubiquitin-SCFAtSKP2 pathway in response to light, *The Plant Cell*, **14**: 3057-3071.

Dellaporta S.L, Wood J and Hicks J.B (1983), A plant DNA minipreparation: Version II, *Plant Molecular Biology Reporter*, **1**: 19-21.

Desnos T, Orbovic V, Bellini C, Kronenberger J, Caboche M, Traas J and Hofte H, (1996), *Procuste1* mutants identify two distinct genetic pathways controlling hypocotyl cell elongation, respectively in dark- and light-grown *Arabidopsis* seedlings, *Development*, **122**:683-693.

Devoto A, Turner J.G, (2003), Regulation of jasmonate-mediated plant responses in *Arabidopsis*, *Annals of Botany*, **92**: 329-337.

Drenkard E, Richter B.G, Rozen S, Stutius L.M, Angell N.A, Mindrinos M, Cho R.J, Oefner P.J, Davis R.W and Ausubel F. M, (2000), A simple procedure for the analysis of single nucleotide polymorphisms facilitates map-based cloning in *Arabidopsis*, *Plant Physiology*, **124**:1483-1492.

Englyst H.W, Wiggins H.S and Cumming J.H, (1982), Determination of the non-starch polysaccharides by gas liquid chromatography of constituent sugars as alditol acetates, *Analyst*, **107**:307-318.

Feminia A, Rigby N.M, Selvendran and Waldron K.W, (1999), Investigation of the occurrence of pectic-xylan-xyloglucan complexes in the cell walls of cauliflower stem tissues, *Carbohydrate Polymers*, **39**:151-164.

Fernie A.R, Willmitzer L and Trethewey R.N, (2002), Sucrose to starch: a transition in molecular plant physiology, *Trends in Plant Science*, **7**:35-41.

Ferreira P.C.G, Hemerly H.S, de Almeida Engler J, Van Montagu M, Engler G and Inze D, (1994), Developmental expression of the *Arabidopsis* cyclin gene *cyclAt*, *The Plant Cell*, **6**: 1763-1774.

Folkers U, Kirik V, Schobinger U, Falk S, Krishnakumar S, Pollock M.A, Oppenheimer D.G, Day I, Reddy A.R, Jurgens G and Hulskamp M, (2002), The cell morphogenesis gene *ANGUSTIFOLIA* encodes a CtBP/BARS-like protein and is involved in the control of the microtubule cytoskeleton, *The EMBO Journal*, **21**:1280-1288.

Frank M.J and Smith L.G, (2002), A small, novel protein highly conserved in plants and animals promotes the polarized growth and division of maize leaf epidermal cells, *Current Biology*, **12**:849-853.

Frank M.J, Cartwright H.N and Smith L.G, (2003), Three *Brick* genes have distinct functions in a common pathway promoting polarised cell division and cell morphogenesis in the maize leaf epidermis, *Development*, **130**:753-762.

Freeman S (2002), Land Plants. In *Biological Sciences*, New Jersey, US, Prentice Hall, pg 540-560.

Fry S.C, (1983), Feruloylated pectins from the primary cell wall: their structure and possible functions, *Planta*, **157**: 111-123.

Fry S.C, (1989), The structure and functions of xyloglucan, *Journal of Experimental Botany*, **40**: 1-11.

Fu Y, Li H and Yang Z, (2002), The ROP2 GTPase controls the formation of cortical fine F-actin and the early phase of directional cell expansion during *Arabidopsis* organogenesis, *The Plant Cell*, **14**:777-794.

Gardiner J.C, Taylor N.G and Turner S, (2003), Control of cellulose synthase complex localisation in developing xylem, *The Plant Cell*, **15**: 1740-1748.

Geisler M, Yang M and Sack F.D, (1998), Divergent regulation of stomatal initiation and patterning in organ and suborgan regions the *Arabidopsis* mutants *too many mouths* and *four lips, Planta*, **205**:522-530.

Geisler M, Nadeau J, Sack F.D, (2000), Orientated asymmetric divisions that generate the stomatal spacing pattern in *Arabidopsis* are disrupted by the *too many mouths* mutation, *The Plant Cell*, **12**:2075-2086.

Geisler M.J, Deppong D.O, Nadeau J.A and Sack F.D, (2003), Stomatal neighbour cell polarity and division in *Arabidopsis*, *Planta*, **216**:571-579.

Gelineo-Albersheim I, Darvill A, Albersheim P, (2001), Book of Abstracts of the Ninth International Cell Wall Meeting, September 2-7th, Toulouse, France, CNRS/INRA, Toulouse, p183.

Gendreau E, Traas J, Desnos T, Grandjean O, Caboche M and Hofte H, (1997), Cellular basis of hypocotyl growth in *Arabidopsis thaliana, Plant Physiology*, **114**:295-305.

Gindhart J.G Jr. and Goldstein L.S, (1996) Tetratrico peptide repeats are present in the kinesin light chain, *Trends Biochemical Science*, **21**: 52–53.

Glover B.J, (2000), Differentiation in plant epidermal cells, *Journal of Experimental Biology*, **51**:497-505.

Gottwald J.R, Krysan P.J, Young J.C, Evert R.F, Sussman M.R, (2000), Genetic evidence for the *in planta* role of phloem-specific plasma membrane sucrose transporters, *Proceedings of the National Academy of Sciences*, **97**: 13979-13984.

Grace J and van Gardingen P.R, (1996), Plant cuticles under challenge. In Kersteins G, ed. *Plant Cuticles: an integrated functional approach*, Oxford, UK, Bios Scientific Publishers, 319-329.

Gray W.M, Ostin A, Sandberg G, Romano C.P and Estelle M, (1998), High temperature promotes auxin mediated elongation in *Arabidopsis*, *Proceedings of the National Academy of Sciences USA*, **95**:7197-7202.

Gray J.E, Holroyd G.H, van der Lee F.M, Bahrami A.R, Sijmons P.C, Woodward F.I, Schuch W and Hetherington A.M, (2000), The HIC signalling pathway links CO_2 perception to stomatal development, *Nature*, **408**:713-716.

Ha M.A, Apperley D.C and Jarvis M.C, (1997), Molecular rigidity in dry and hydrated onion cell walls, *Plant Physiology*, **115**: 593-598.

Hauser M.T and Bauer E, (2000), Histochemical analysis of root meristem activity in *Arabidopsis thaliana* using a *cyclin*::GUS (β-glucuronidase) marker line, *Plant and Soil*, **226**:1-10.

Hawes M.C and Lin H-J, (1990), Correlation of pectolytic enzyme activity with the programmed release of cells from root caps of pea (*Pisum sativum*), *Plant Physiology*, **94**:1855-1859.

Heredia A, (2003), Biophysical and biochemical characteristics of cutin, a plant barrier biopolymer, *Biochimica et Biophysica Acta*, **1620**:1-7.

His I, Driouich A, Nicol F, Jauneau A and Hofte H, (2001), Altered pectin composition in primary cell walls of *korrigan*, a dwarf mutant of *Arabidopsis* deficient in a membrane bound endo-1, 4-β-glucanase, *Planta*, **212**:348-358.

Hulskamp M, Misera S and Jurgens G, (1994), Genetic dissection of trichome cell development in *Arabidopsis*, *Cell*, **76**:555-566.

Ilgenfritz H, Bouyer D, Schnittger A, Mathur J, Kirik V, Schwab B, Chua N.H, Jurgens G and Hulskamp M, (2003), The *Arabidopsis STICHEL* gene is a regulator of trichome branch number and encodes a novel protein, *Plant Physiology*, **131**:643-655.

Ilyama K, Lam T.B-T and Stone B, (1994), Covalent cross-links in the cell wall, *Plant Physiology*, **104**: 315-320.

Iwai H, Ishii T and Satoh S, (2001), Absence of arabinan in the side chains of the pectic polysaccharides stongly associated with cell walls of *Nicotiana plumbaginifolia* non-organogenic callus with loosely attached constituent cells, *Planta*, **213**: 907-915.

Iwai H, Masaoka N, Ishii T and Satoh S, (2002), A pectin glucuronyltransferase is essential for intercellular attachment in the plant meristem, *Proceedings of the National Academy of Sciences USA*, **99**:16319-16324.

Jander G, Norris S.R, Rounsley S.D, Bush D.F, Levin I.M, Last R.L, (2002), *Arabidopsis* Map-Based Cloning in the Post-Genome Era, *Plant Physiology*, **129**:440-450.

Jarvis M.C, (1984), Structure and properties of pectin gels in plant cell walls, *Plant Cell and Environment*, **7**:153-164.

Jarvis M.C, (1998), Intercellular separation forces generated by intracellular pressure, *Plant, Cell and Environment*, **21**:1307-1310.

Jeffree C.E, (1996), Structure and ontogeny of plant cuticles. In Kersteins G, ed. *Plant Cuticles: an integrated functional approach*, Oxford, UK, Bios Scientific Publishers, 33-82.

Jin P, Guo T and Becraft P.W, (2000), The maize CR4 receptor-like kinase mediates a growth factor-like differentiation response, *Genesis*, **27**:104-116.

Jung G and Wernicke W, (1990), Cell shaping and microtubules in developing mesophyll of wheat (*Tritium aestivum* L.), *Protoplasma*, **153**:141-148.

Kerstiens G, (1996), Signalling across the divide: A wider perspective of cuticular structure –function relationships, *Trends in Plant Science*, **1**: 125-129.

Kikuchi A, Edashige Y, Ishii T, Fujii T and Satoh S, (1996), Variations in the structure of neutral sugar chains in the pectic polysaccharides of morphologically different carrot calli and correlations with the size of cell clusters, *Planta*, **198**: 634-639.

Kim G-T, Shoda K, Tsuge T, Cho K-H, Uchimiya H, Yokoyama R, Nishitani K and Tsukaya H, (2002a), The *ANGUSTIFOLIA* gene of *Arabidopsis*, a plant CtBP gene, regulates leaf-cell expansion, the arrangement of cortical microtubules in leaf cells and expression of a gene involved in cell-wall formation, *The EMBO Journal*, **6**:1267-1279.

Kim W-Y, Geng R and Somers D.E, (2003) Circadian phase-specific degredation of the F-box protein ZTL is mediated by the proteasome, *Proceedings of the National Academy of Sciences USA*, **100**: 4933-4938.

Kiyosue T, Abe H, Yamaguchi-Shinozaki K, Shinozaki K, (1998), *ERD6*, a cDNA clone for an early dehydration-induced gene of *Arabidopsis*, encodes a putative sugar transporter, *Biochimica et Biophysica Acta*, **1370**: 187-191.

Knox J.P, Linstead P.J, King J, Cooper C and Roberts K, (1990), Pectin esterification is spatially regulated both within cell walls and between developing tissues of root apices, *Planta*, **181**:512-521.

Knox J.P, (1992), Cell adhesion, cell separation and plant morphogenesis, *The Plant Journal*, **2**:137-141.

Kobayashi M, Nakagawa H, Asaka T and Matoh T, (1999), Borate-rhamnogalacturonan II bonding reinforced by Ca^{2+} retains pectic polysaccharides in higher-plant cell walls, *Plant Physiology*, **119**:199-203.

Larkin J.C, Young N, Prigge M and Marks M.D, (1996), The control of trichome spacing and number in *Arabidopsis*, *Development*, **122**: 997-1005.

Larkin J.C, Marks M.D, Nadeau J and Sack F, (1997), Epidermal cell fate and patterning in leaves, *The Plant Cell*, **9**:1109-1120.

Levy S, York W.S, Stuike-Prill R, Meyer B and Staehelin L.A, (1991), Simulations of the static and dynamic molecular conformations of xyloglucan. The role of the fucosylated sidechain in surface-specific sidechain folding, *The Plant Journal*, **1**:195-215.

Levy S, Maclachlan G and Staehelin L.A, (1997), Xyloglucan sidechains modulate binding to cellulose during in vitro binding assays as predicted by conformational dynamics simulations, *The Plant Journal*, **11**: 373-386.

Li Y, Rosso M.G, Strizhov N, Viehoever P, and Weisshaar B, (2003), GABI-Kat SimpleSearch: a flanking sequence tag (FST) database for the identification of T-DNA insertion mutants in *Arabidopsis thaliana*, *Bioinformatics*, **19**: 1441-1442.

Lu P, Porat R, Nadeau J.A and O'Neill S.D, (1996), Identification of a meristem L1 layer-specific gene in *Arabidopsis* that is expressed during embryonic pattern formation and defines a new class of homeobox genes, *The Plant Cell*, **8**:2155-2168.

Lukowitz W, Gillmor C.S and Scheible W.R, (2000), Positional cloning in *Arabidopsis*. Why it feels good to have a genome initiative working for you, *Plant Physiology*, **123**: 795-805.

Lunn J.E and MacRae E, (2003), New complexities in the synthesis of sucrose, *Current Opinion in Plant Biology*, **6**:208-214.

Malamy J.E and Benfey P.N, (1997), Organisation and cell differentiation in lateral roots of *Arabidopsis thaliana*, *Development*, **124**:33-44.

Manrique G.D and Lajolo F.M, (2002), FT-IR spectroscopy as a tool for measuring degree of methyl esterification in pectins isolated from ripening papaya fruit, *Postharvest Biology and Technology*, **25**:99-107.

Mathur J and Chua N-H, (2000), Microtubule stabilisation leads to growth reorientation in *Arabidopsis* trichomes, *The Plant Cell*, **12**:465-477.

Mathur J, Mathur N, Kernebeck B and Hulskamp M, (2003a), Mutations in actin-related proteins 2 and 3 affect cell shape development in *Arabidopsis*, *The Plant Cell*, **15**:1632-1645.

Mathur J, Mathur N, Kirik V, Kernebeck B, Srinivas B.P and Hulskamp M, (2003b), *Arabidopsis CROOKED* encodes for the smallest subunit of the ARP2/3 complex and controls cell shape by region specific fine F-actin formation, *Development*, **130**: 3137-3146.

Marks D, (1997), Molecular genetic analysis of trichome development in *Arabidopsis*, *Annual Review of Plant Physiology and Plant Molecular Biology*, **48**:137-163.

McCann M.C, Wells B and Roberts K, (1990), direct visualization of cross-links in the primary cell wall, *Journal of Cell Science*, **96**: 323-334.

McCann M.C, Hammouri M, Wilson R, Belton P and Roberts K, (1992), Fourier transform infrared microspectroscopy is a new way to look at plant cell walls, *Plant Physiology*, **100**:1940-1947.

McCann M.C, Shi J, Roberts K and Carpita N.C, (1994), Changes in pectin structure and localisation during the growth of unadapted and NaCl-adapted tobacco cells, *The Plant Journal*, **5**; 773-785.

McManus M.T, Thompson D.S, Merriman C, Lyne L and Osborne D.J, (1998), Transdifferentiation of mature cortical cells to functional abscission cells in bean, *Plant Physiology*, **116**:891-899.

McQueen-Mason S.J, (1995), Expansin and cell wall expansion, *Journal of Experimental Botany*, **46**: 1639-1650.

Nadeau J.A and Sack F.D, (2002), Control of stomatal distribution on the *Arabidopsis* leaf surface, *Science*, **296**:1697-1700.

Nicol N.T, (1998), *Apparent metabolisable energy values of wheat in chick diets*, PhD Thesis University of Nottingham.

Norambuena L, Marchant L, Berninsone P, Hirschberg C.B, Silva H, Orellana A, (2002), Transport of UDP-galactose in plants, identification and functional characterisation of AtUTr1, an *Arabidopsis* thaliana UDP-galactose/UDP-glucose transporter, *Journal of Biological Chemistry*, **277**: 32923-32929.

Ordway R.W, Pallanck L and Ganetzky B, (1994), A TPR domain in the SNAP secretory proteins, *Trends Biochemical Science*, **19**:530–531.

Orfila C, Huisman M.M.H, Willats W.G.T, Van Alebeck G-J.W.M, Schols H.A, Seymour G.B and Knox J.P, (2002), Altered cell wall disassembly during ripening of *Cnr* tomato fruit: implications for cell adhesion and fruit softening, *Planta*, **215**: 440-447.

Panteris E, Apostolakos P and Galatis B, (1993), Microtubules and morphogenesis in ordinary epidermal cells of *Vignia sinensis* leaves, *Protoplasma*, **174**:91-100.

Panteris E, Apostolakos P and Galatis B, (1994), Sinuous ordinary epidermal cells: behind several patterns of waviness, a common morphogenetic mechanism, *New Phytologist*, **127**:771-780.

Parinov S and Sundarasen V, (2000), Functional genomics in *Arabidopsis*: large scale insertional mutagenesis complements the genome sequencing project, *Current Opinion in Biotechnology*, **11**:157-161.

Parker C.C, Parker M.L, Smith A.C and Waldron K.W, (2001), Pectin distribution at the surface of potato parenchyma cells in relation to cell-cell adhesion, *Journal of Agricultural and Food Chemistry*, **49**:4364-4371.

Peters J.L, Cnudde F and Gerats T, (2003), Forward genetics and map-based cloning approaches, *Trends in Plant Science*, **8**:484-491.

Picart J.A and Morgan D.G, (1984), Pod development in relation to pod shattering, *Aspects of Applied Biology*, **6**:101-110.

Ponce M.R, Robles P and Micol J.L, (1999), High throughput Mapping in *Arabidopsis thaliana*, *Molecular and General Genetics*, **261**: 408-415.

Potikha T and Delmer D.P, (1995), A mutant of *Arabidopsis thaliana* displaying altered patterns of cellulose deposition, *The Plant Journal*, **7**:453-460.

Pyke K and Lopez-Juez E, (1999), Cellular differentiation and leaf morphogenesis in *Arabidopsis, Critical Reviews in Plant Sciences*, **18**:527-546.

Qiu J-L, Jilk R, Marks M.D and Szymanski D.B, (2002), The *Arabidopsis SPIKE1* gene is required for normal cell shape control and tissue development, *The Plant Cell*, **14**:101-118.

Reiter WD, (1998), The molecular analysis of cell wall components, *Trends in plant Science*, **3**:27-32.

Ridley B.L, O'Neill M.A and Mohnen D, (2001), Pectins: Structure, biosynthesis, and oligonucleotide-related signalling, *Phytochemistry*, **57**: 929-967.

Roberts J.A, Whitelaw C.A, Gonzalez-Carranza Z.H and McManus M.T, (2000), Cell separation processes in plants-Models, mechanisms and manipulation, *Annals of Botany*, **86**:223-235.

Roberts J.A, Elliott K.A and Gonzalez-Carranza Z.H, (2002), Abscission, dehiscience and other cell separation processes, *Annual Review of Plant Biology*, **53**:131-158.

Ross P, Hall L, Smirnov I and Haff L, (1998), High level multiplex genotyping by MALDI-TOF mass spectrometry, *Nature Biotechnology*, **16**: 1347-1351.

Ryden P, Sugimoto-Shirasu K, Smith A.C, Findlay K, Reiter W-D and McCann M.C, (2003), Tensile properties of *Arabidopsis* cell walls depend on both a xyloglucan cross-

linked microfibrillar network and rhamnoglacturonan II-borate complexes, *Plant Physiology*, **132**:1033-1040.

Schindelman G, Morikami A, Jung J, Baskin T.I, Carpita N.C, Derbyshire P, McCann M.C and Benfey P.N, (2001), COBRA encodes a putative GPI-anchored protein, which is polarly localized and necessary for orientated cell expansion in *Arabidopsis, Genes and Development*, **15**:1115-1127.

Serna L and Fenoll C, (2000a), Stomatal development in *Arabidopsis:* how to make a functional pattern, *Trends in Plant Science*, **5**:458-460.

Serna L and Fenoll C, (2000b), Stomata development and patterning in *Arabidopsis* leaves, *Physiologia Plantarum*, **109**:351-358.

Serna L, Torres-Contreras J and Fenoll C, (2002), Specification of stomatal fate in *Arabidopsis*: evidences for cellular interactions, *New Phytologist*, **153**:399-404.

Sessions A, Weigel D and Yanofsky M.F, (1999), The *Arabidopsis* thaliana MERISTEM LAYER 1 promoter specifies epidermal expression in meristems and young primordia, *The Plant Journal*, **20**:259-263.

Sessions A, Burke E, Presting G, Aux G, McElver J, Patton D, Dietrich B, Ho P, Bacwaden J, Ko C, Clarke J.D, Cotton D, Bullis D, Snell J, Miguel T, Hutchison D, Kimmerly B, Mitzel T, Katagiri F, Glazebrook J, Law M, and Goff S.A, (2002), A High-Throughput *Arabidopsis* Reverse Genetics System, *The Plant Cell*, **14**: 2985-2994.

Smith L.G, (2003), Cytoskeletal control of plant cell shape: getting the fine points, *Current Opinion in Plant Biology*, **6**:63-73.

Szymanski D.B, Lloyd A.M and Marks M.D, (2000), Progress in the molecular genetic analysis of trichome initiation and morphogenesis in *Arabidopsis*, *Trends in Plant Science*, **5**:214-219.

Talbott L.D and Ray P.M, (1992), Molecular size and separability features of pea cell wall polysaccharides implications for models of primary wall structure, *Plant Physiology*, **92**:357-368.

Tanaka H, Onouchi H, Kondo M, Hara-Nishimura I, Nishimura M, Machida C and Machida Y, (2001), A subtilisin-like serine protease is required for epidermal surface formation in *Arabidopsis* embryos and juvenile plants, *Development*, **128**:4681-4689.

The *Arabidopsis* Genome Initiative, (2000), Analysis of the genome sequence of the flowering plant *Arabidopsis thaliana*, *Nature*, **408**: 769-815.

Tseng T-S, Swain S.M, Olszewski N.E. (2001), Ectopic expression of the tetratricopeptide repeat domain of SPINDLY causes defects in gibberellin response, *Plant Physiology*, **126**:1250-1258.

Turner S.R, Taylor N and Jones L, (2001), Mutations of the secondary cell wall, *Plant Molecular Biology*, **47**:209-219.

Tzfira T and Citovsky V, (2002), Partners-in-infection: host proteins involved in the transformation of plant cells by *Agrobacterium, Trends in Cell Biology*, **12**:121-129.

Vinken J-P, Schols HA, Oomen R.J.F.J, McCann M.C, Ulvskov P, Voragen A.G.J and Vsser R.G.F, (2003), If homogalacturonan were a side chain of rhamnogalacturonan I. Implications for cell wall architecture, *Plant Physiology*, **132**:1781-1789.

Vittorioso P, Cowling R, Faure J-D, Caboche M and Bellini C, (1998), Mutation in the *Arabidopsis PASTICCINO1* gene, which encodes a new FK506-binding protein-like protein, has a dramatic effect on plant development, *Molecular and Cellular Biology*, **18**: 3034-3043.

Wei M, Kwok S.F, von Arnim A.G, Lee A,McNellis T.W, Piekos B and Deng X, (1994), *Arabidopsis COP8, COP10*, and *COP11* genes are involved in repression of photomorphogenic development in darkness, *The Plant Cell* **6**:629-643.

Wells B, (1985), Low temperature box and tissue handling device for embedding biological tissue for immunostaining in electron microscopy, *Micron and Microscopica Acta*, **16**: 49-53.

Whitney S.E.C, Gothard M.G.E, Mitchell J.T and Gidley M.J, (1999), Roles of cellulose and xyloglucan in determining the mechanical properties of primary plant cell walls, *Plant Physiology*, **121**:657-663.

Willats W.G.T, Limberg G, Buchholt H.C, van Alebeek G.J, Benen J, Christensen T.M.I.E, Visser J, Voragen A, Mikkelsen J.D and Knox J.P, (2000), Analysis of pectic epitopes recognised by hybridoma and phage display monoclonal antibodies using defined oligosacchartides, polysaccarides and enzymatic degradation, *Carbohydrate Research*, **327**:309-320.

Wilson R.H, Smith A.C, Kacurakova M, Saunders P.K, Wellner N and Waldron K.W, (2000), The mechanical properties and molecular dynamics of plant cell wall polysaccharides studied by Fourier-transform infrared spectroscopy, *Plant Physiology*, **124**: 397-405.

Yang M and Sack F, (1995), The *too many mouths* and *four lips* mutations affect stomatal production in *Arabidopsis*, *The Plant Cell*, **7**:2227-2239.

Yephremov A, Wisman E, Huijser P, Huijser C, Wellesen K and Saedler H, (1999), Characterisation of the *FIDDLEHEAD* gene of *Arabidopsis* reveals a link between adhesion response and cell differentiation in the epidermis, *The Plant Cell*, **11**:2187-2201.

Zablackis E, Huang J, Muller B, Darvill A.G and Albersheim P, (1995), Characterisation of the cell-wall polysaccharides of *Arabidopsis thaliana* leaves, *Plant Physiology*, **107**:1129-11.